**August 2015**

**Ph.D. Dissertation**

# Study on spectral features of electromagnetically induced absorption in degenerate two-level system of $^{85}$Rb atoms

Graduate School of Chosun University

**Department of Photonic Engineering**

**Hafeez-Ur- Rehman**

# Study on spectral features of electromagnetically induced absorption in degenerate two-level system of $^{85}$Rb atoms

축퇴된 이준위 시스템 루비듐 원자의
전자기적으로 유도된 흡수 분광선 특성 연구

**August 25, 2015**

Graduate School of Chosun University

**Department of Photonic Engineering**

**Hafeez-Ur- Rehman**

# Study on spectral features of electromagnetically induced absorption in degenerate two-level system of $^{85}$Rb atoms

**Advisor: Prof. Jin-Tae Kim**

*This dissertation is submitted to the Graduate School of Chosun University in partial fulfillment of the requirements for the degree of Doctor of Philosophy in Science*

**April 2015**

Graduate School of Chosun University

**Department of Photonic Engineering**

**Hafeez-Ur- Rehman**

This is to certify that the PhD thesis of **Hafeez-Ur-Rehman** has successfully met the dissertation requirements of Chosun University**.**

Chairman (Chosun Univ.) : Prof. Jong-Rak Park .....

Member (Chosun Univ.) : Prof. Jin-Tae Kim .....

Member (Chosun Univ.) : Prof. Hyun Su Kim .....

Member (Chosun Univ): Prof. Tae-Jung Ahn .....

Member (Chonnam Univ):Prof. Heung-Ryoul Noh.....

**June 2015**

Graduate School of Chosun University

# Contents

# List of figures

# 초록

# 축퇴된 이준위 시스템 루비듐 원자의 전자기적으로 유도된 흡수 분광선 특성 연구

Hafeez-Ur- Rehman

Advisor: Prof. Jin-Tae Kim

Graduate School of Chosun University

Department of Photonic Engineering

결합광과 조사광의 편광, 파워, 방향에 따른 축퇴된 상온 셀내에 있는 루비듐 원자의 기저준위와 여기준위 D2 사이의 초미세 구조에서 약한조사빔의 투과 신호의 분광선에 대한 실험적, 이론적 고찰을 본 논문에서 연구한다. 조사광은 $F_g$ =3→$F_e$ =4 에 주파수 잠금되고, 결합광은 기저준위 $F_g$ = 2와 3에서 여기준위 $F_e$= 1, 2, 3, 4 사이를 주사 한다. 축퇴된 이원자 준위에서 조사광과 결합광의 편광은 여기준위로부터의 밀도 이전,EIA 혹은 EIT 신호 의 분광선 모양 등에 중요한 역할을 한다. 약한 조사광과 강한 결합광의 경우에 닫혀진 계에서 좁은 선폭과 넓은 선폭을 가지는 이중 구조 분광선이 광펌핑에 의해 얻어진다. 이러한 광펌핑 효과 등이 광 밀도 방정식에 의해 얻어진 분광선과 실험적으로 얻어진 분광선과 비교되었다.

또한, 상온에서 매우 좁은 분광선 선폭을 가지는 EIA 신호가 얻어졌

다. 이러한 매우 좁은 선폭을 가지는 분광선이 같은 편광 ($\sigma^+$-$\sigma^+$, $\pi \parallel \pi$) 과수직 편광 ($\sigma^+$-$\sigma^-$,$\pi \perp \pi$) 구도에서 연구되었다. 같은 편광의 경우 ~90 kHz 정도의 EIA 신호가 처음으로 실험적, 이론적으로 확인되었다. 이러한좁은 선폭을 가지는 EIA 신호를 연구하기 위해 파워와 편광이 일반화된 광 밀도 방정식의 해의 결과와 실험적으로 얻은 결과와 비교한 결과, 매우 잘 일치함을 확인하였다.

# ABSTRACT

## Study on spectral features of electromagnetically induced absorption in degenerate two-level system of $^{85}$Rb atoms

Hafeez-Ur- Rehman

Advisor: Prof. Jin-Tae Kim

Graduate School of Chosun University

Department of Photonic Engineering

We present experimental and theoretical studies on spectral profile variations of weak probe beam transmission signal from hyperfine level between the ground 5 $S_{1/2}$ and excited 5 $P_{3/2}$ D2 lines of $^{85}$Rb atom at room temperature with degenerate magnetic sublevels in the case of polarization configurations, powers, and directions of control and probe beams. The probe laser frequency is fixed and locked at the $F_g = 3 \rightarrow F_e = 4$ degenerate two level system of $^{85}$Rb atom while the control beam is scanned through F" = 2 and 3 → F" = 1, 2, 3, and 4. In degenerate two-level system polarizations of probe and control laser fields play important roles to transfer of population from excited states. Consequently variation in absorption and transmission signal profiles including EIA and EIT-like signal have been observed when the polarization state of control and probe lasers fields were changed. In case of weak probe and strong coupling laser field we observed double structure transmittance spectrum, a narrow due to

coherence and broad due to optical pumping in cycling transition. The experimental results are compared with the results calculated by solving time-dependent density-matrix equations including the optical and Zeeman coherences connected via multi-photon interactions process between magnetic levels and match well with the calculated signal profiles.

We also present theoretical and experimental study of EIA for different hyperfine transitions of $^{85}$Rb-D2 line. The calculated result in case of cycling transition of $^{85}$Rb show that EIA signal have ultra-narrow feature in low power of coupling beam in both stationary and thermal atoms. In case of thermal atom the ultra-narrow EIA signal due to high coupling power beam still remained in ultra-narrow state in the same polarization configuration. Ultra-narrow EIA spectral features of thermal $^{85}$Rb atom with respect to coupling Rabi frequencies in a degenerate Zeeman multiplet system have been unraveled in the cases of same ($\sigma^+$-$\sigma^+$, $\pi \parallel \pi$) and orthogonal ($\sigma^+$-$\sigma^-$, $\pi \perp \pi$) polarization configurations. The EIA signals with subnatural linewidth of ~ 90 kHz even in the cases of same circular and linear polarizations of coupling and probe laser have been obtained for the first time theoretically and experimentally. In weak coupling power limit of orthogonal polarization configurations, time-dependent transfer of coherence plays major role in the splitting of the EIA spectra while in strong coupling power, Mollow triplet-like mechanism due to strong power bring into broad split feature. The experimental ultra-narrow EIA features using one laser combined with an AOM match well with simulated spectra obtained by using generalized time-dependent optical Bloch equations

# Chapter 1

## Introduction

Many applications such as slowing light, quantum information processing, high-resolution spectroscopic measurements, sensitive magnetometery, atomic clocks, lasing without inversion, and light information storage [1- 23] have been developed using changes of the refractive index and nonlinear susceptibility of atoms. Electromagnetically induced absorption (EIA) [1-7] and transparency (EIT) [8-10] have been nice methods to investigate effects on the atoms due to quantum interference and coherences between atomic quantum states, which leads to the abrupt changes of the refractive index and nonlinear susceptibility, *etc*. The EIA involves two laser fields such as strong coupling and weak probe beams interacting with properly selected three quantum states [15, 20-21] and enhances probe absorption due to quantum coherence effects through three different quantum states connected with the coupling and probe lasers. EIT also occurs in three-level atomic systems which interacts with two lasers fields similarly as the EIA under proper required conditions. However, destructive quantum coherences between the quantum states in the EIT differently from the EIA cases make probe laser beams transparent to the atoms. Simple three level atomic systems [4-6, 24-26] and degenerate multilevel configuration system have been used to investigate such quantum coherence effects. Compared to non-degenerate simple three levels, degenerate two level configurations is much more complex than three level systems in reality.

The spectral profiles of the EIA and EIT are also dependent on directions, polarizations, intensities, beam sizes of the coupling and probe laser beams. The spectral profiles of the EIA and EIT show peculiar behaviors depending on directions, polarizations, intensities, beam sizes of the coupling and probe laser beams. In this work the EIA phenomena in degenerate two level system (DTLS) of rubidium atom have been investigated instead of simple three level quantum systems. Previous EIA works done in the degenerate quantum system and goals of this work have been introduced in this chapter. In this chapter previous works due to velocity selective optical pumping (VSOP) effects have also been introduced.

## 1.1 Previous EIA works in DTLS

In pump-probe experimental setup two independent laser sources or one laser combined with AOMs can be used to observe pump-probe absorption spectra of atomic samples. The advantage of one laser instead of two laser beams overcomes limit of laser beam linewidth in observed spectral width so that much narrower spectral linewidth can be obtained. Although there are many subnatural experimental observations of EIA in DTLS, the observed linewidths are still close to laser linewidths. Early previous EIA works of DTLS have focused on subnatural lineshape using two different pump and probe lasers because it brought out subnatural linewidth.

Prepared samples can be in thermal or cold state depending on how the samples have been prepared. Recent progresses in atomic cooling and

trapping have provided cold atomic samples. Also atomic beam experiments can prepare cold samples. Thermal atomic samples with large velocity distributions can also be used to do EIA experiments. Moving atoms in a cell provide velocity dependent distributions interacting with laser beams so that steady state solution cannot be applied to the system and interaction region of the atoms with the laser beam should be considered. However, most of previous works have not considered those effects. Thus thermal averaging effects occurred in hot sample have been overlooked considering only atomic samples with cold internal temperatures.

There have been number of experimental and theoretical reports [1-3, 27-42] to observe sub-natural EIA signals in DTLS depending on powers and polarizations of pump and probe laser beams. Lezama *et al*. [1] observed for the first time EIA in DTLS and reported experimental observation of narrow spectral features in the presence of two laser fields which interacts with common ground state of Rb atom. Lezama *et al*. [2] explained also that EIA occur due to transfer of coherence between interacting degenerate system in which (i) $F_g \rightarrow F_e = F_g + 1$, where $F_g$ and $F_e$ are the hyperfine quantum number of ground and excited states respectively (ii) the ground state must be degenerate ($F_g > 0$ ) and (iii) the system should be closed. Under this situation the two photon resonance conditions will populate to those Zeeman sub-levels which are coupled to that laser field.

However, Kim *et al*. [30] observed EIA signal in an open system using an orthogonal linear polarization configuration of coupling and probe laser beams with co-propagating beam directions differently from expected results of Lezama *et al*. [2]. Chou *et al*. [31] interpreted that the anomalous EIA

signal in [30] is due to splitting of the EIA signals in an open system with $F_e = F_g - 1$ using a dressed atomic picture and qualitative perturbation methods employing different power-dependence of the coupling laser. They have provided comprehensive detail to explain probe absorption spectra in DTLS on the basis of dressed-atom multiphoton spectroscopy (DAMS).

There are few experimental works using one laser to investigate EIA in DTLS. Y. C. Chen [39] used similar experimental scheme using one laser to observe the EIA single in cold $^{87}$Rb atoms. But he [39] could not observe the splitting of EIA at moderate high power of pump beam. Instead of two independent lasers experiment the author of [30] performed also one laser experiment using linear and orthogonal polarized pump and probe beams to observe ultranarrow EIA signal in Cs atom. They investigated that how the intensity of pump laser bean effect the line shape of observed ultra-narrow EIA signals.

One of other interesting features in the coherence experiments, conversion from EIA to EIT or EIT to EIA. K. Dahl *et al*. [41] presented the pump laser absorption profile for four different polarization configurations in DTLS of Cs atom. In case of circular and orthogonal polarization of pump and probe beams, the absorption within transparency and transparency within transparency were detected when the power of probe laser exceeded from power of pump beam. Absorption with in transparency was observed in case of linear and circular polarization combination of pump and probe laser fields. Z. Y. Ting *et al*. [42] observed pump power dependent EIA spectra in DTLS using linear and perpendicular polarized pump and probe laser fields. Conversion of EIA to EIT is also studied. At low power of pump beam EIA

dip signal show sub-natural line width but when the power of pump beam increase to 650 mW then EIA-dip become broader and EIT appear at the central area.

Theoretical works to understand EIA in real DTLS, especially multi-oscillation effects of pump and probe beams make the system more complex because of more sub-Zeeman levels are involved in the contribution of EIA. A. D. W-Gordon *et al*. [43] theoretically investigated the ultra-narrow extra resonant anti-hole and its origin in an open atomic two level system in which relaxation rate of excited state is less than that of ground state. Origins of EIA signal in DTLS in the same and orthogonal polarizations have not been revealed. Obviously pure two-level system cannot provide EIA signal if there is no external population or coherence input to the two levels. If we use two pump and probe lasers, N type connections cannot be provided so that EIA cannot be formed. The EIT and EIA have been explained by using V and N type of connections between two levels. However, one can expect that V or N type system cannot be formed in the case of the same polarization configuration of pump and probe laser beams so that EIA cannot occur in this case.

One of very intuitive way to understand EIA origin was investigated by A. V. Taichenachev *et al*. [45]. They used this four-level system and interpreted that decay from TOC could create EIA signal which was similar to the case of perpendicular polarization combination. In the DTLS differently from this simple 4-levels system, the polarizations of the pump and probe laser beams play vital role in Zeeman coherences of the ground and excited states, transfer of the coherence from the excited states,

contribution to optical coherences between the ground and excited states because the polarizations connect magnetic sublevels of the ground state with those of the excited states. C. Goren *et al*. [46] predicted and explained that the ultranarrow EIA-TOP can be observed in DTLS even in case of same polarization configuration of pump and probe laser beams. For observing EIA-TOC, they used double two-level system which was later compared with four-level N-type system. In each model Doppler broadening increases the width of dip. In double two level system EIA peak become narrower on Doppler broadening but in contrast N-type system, does not devolved a dip at line center. In case of same polarization configuration of pump and probe lasers fields, the time dependent TOP can also be observed at sufficient low powers of pump beam in the absence of inelastic collision. C. Goren *et al*. [47] presented EIA-TOP and EIA-TOC models and show that at low power the both model give EIA peaks at the line center, whereas at high intensity the double two level system has the same spectrum as a simple two level system. T. Zigdon *et al*. [48] used circular- orthogonal and linear-perpendicular polarized pump-probe spectroscopy in cycling transition of $F_g = 2 \rightarrow F_e = 3$ of $^{87}$Rb to explained that the TOC played important role in splitting of narrow signals in such case when pump power is greater than decay rate of upper excited state and lower than probe power. To calculate absorption spectra, the stationary case with phenomenal parameter was taken into account which is quite different form that calculation which presented in [23].

In Hanle configuration the ultranarrow EIA resonance in absorption and transmission signal can be measured by scanning magnetic field, either

orthogonal to the direction of propagation of radiation field or parallel to the direction of propagation of optical field instead of pump or probe scanning. However, these origins of the ultranarrow Hanle signals are different from ours which are from TOC and time-dependent TOP, *etc*.

In our one laser experiment we produced ultranarrow EIA signal differently from the case of Hanle configuration by scanning pump laser beam. In our case no magnetic field has been applied to observe ultranarrow EIA signals.

To observe the ultranarrow EIA signal experimentally we made major changes in conventional two lasers pump-probe experimental setup and used single laser coupled with an Acousto-optic modulator (AOM) to observe TOP and TOC effects for such ultra-narrow EIA resonances where relative linewidth is limited to AOM scanning resolution. In this way we observed these ultranarrow signals successfully not only in orthogonal polarization configuration case but also in same polarization combination of pump and probe laser beams.

Polarization and power dependent ultra-narrow and split EIA signal inside the broad probe transmission spectra are still to be investigated. We performed several experiments using Rb vapor cell at room temperature. In case of circular and orthogonal polarization configuration we observed that these ultranarrow EIA signals are split into two even at low pump powers. The pump laser power plays a major role in the splitting due to TOC effects. This splitting occurs even at the relatively lower power of the pump laser differently from the orthogonal case of linear polarization as performed by [39]. In EIA experiments usually two independent laser beams have been

used for pump and probe beams. Each of these two lasers can have linewidth approximately equal to 1 MHz and together these two lasers produce linewidth of 2 MHz. That is why in our two lasers experimental results which are presented in chapter 4, we could notable to produced ultra-narrow EIA signal because of the large combined linewidths of the two different lasers. The observed EIA signal is slightly wider and shallower than we expected in the case of orthogonal polarization.

## 1.2 Velocity selective optical pumping

In the pump-probe experiment, multilevel atomic system prepared with strong pump laser beams can be probed by a weak probe beam. Pump beam frequency is fixed and locked to specific atomic transition and probe beam is scanned over wide frequency range. The probe transmission signal changes when probe laser also comes into resonance with same or other hyperfine transitions for atoms with zero velocity. Atomic coherences and optical pumping effects on atomic samples with hyperfine components due to laser interaction have been investigated. Hyperfine splittings in the alkali atoms are less than the Doppler width so that optical pumping effects between the hyperfine transitions due to Doppler profiles occurs including atomic coherence effects depending on the conditions of polarizations, intensities, *etc*. of pump and probe laser beams. When strong pump beam counter-propagating or co-propagating with weak probe beam in a vapor cell, a set of velocity selective resonance peaks can be observed at different velocities.

Doppler-free experiments with counter-propagating pump-probe geometry can provide nice Doppler free spectra. However, in the co-propagating case Doppler shifted resonance lines can be observed. Because EIA and EIT signals depend on the directions, polarizations and powers of pump and probe lasers. Thus broad Doppler and sharp coherence spectra can be obtained [49-51] together. The sharp interference spectra come from EIT or EIA depending on signal shapes while the broad spectrum resulting from optical pumping by pump laser field called VSOP. The sharp interfered spectra can be affected by the optical pumping. However, the effects are limited because of small coherence effect in the case of large detuning of the probe laser.

The VSOP can be used as a sensitive technique for precise measurements using a relationship between atomic velocity and internal parameters of the atoms in the ground or metastable state [50]. S. J. Park *et al*. [51] used co-propagating pump and probe laser beams to demonstrate VSOP spectroscopy on Rb atom and explained the position and magnitude of absorption spectra with respect to frequencies of both beams. S. Chakrabarti *et al*. [52-53] explained the experimentally observed EIT dip signal along with five extra peaks in probe transmission spectra transition line of $^{87}$Rb atoms. Also they studied the effect of co-propagation and counter propagation of pump beam on the absorption spectra of Rb atoms. In both case a set of extra resonance dips are observed A. J. Krmpot et al. [54] explained the pump transmission spectra by using rate equation. These results were obtained in wide scanning range of probe laser while pump laser is locked to particular transition. In co-propagating beams experiment they [54] observed several lines as a result of

contribution from laser absorption on atoms in different velocity groups. S. Mitra *et al*. [55] did both, theoretical and experimental investigation on EIT-dip signal with respect to pump Rabi frequency along with existence of VSOP peaks in probe transmission profiles by using V, Λ and V+Λ type atomic system.

D. Bhattacharyya *et al*. [56] developed theoretical model to describe the occurrence of seven transmission peaks due to VSOP in case of co-propagating and six peaks in case of counter-propagating pump and probe beam but experimentally they could not observed all peaks due to Doppler broadened background. S. Chakrabarti *et al*. [57] demonstrated the VSOP resonances in probe absorption spectra of both isotopes of rubidium D2 transitions in their experimental investigation. They used strong pump and weak probe beam which co-propagates through Rb vapor cell and explained the size of dips based on population depletion for different velocity groups. A. Krasteva *et al*. [58] used linear and orthogonal polarized pump and probe laser beam to investigate the pump-probe spectra of Cs atom in thin cell without buffer gas. Their theoretical model is based on optical Bloch equation. On the basis of this theoretical model they explain experimentally observed sharp EIT peaks and enhanced VSOP resonances for probe absorption and transmission spectra.

Most of the results from these VSOP experiments have been explained using a simple rate equation model. Stationary cases have been considered instead of generalized time-dependent OBEs. Arbitrary intensity and polarization effects of probe absorption spectra including EIA and EIT due to adjacent hyperfine levels and velocity groups of atom in cell have not

been investigated well both theoretically and experimentally.

Here we present pump-probe transmission spectra in the case when co-propagating pump beam scanned frequency in wide range and fixed frequency of probe laser transmission is observed. The spectral broad spectral profiles due to VSOP and sharp coherence effects have been investigated in the cases of arbitrary polarizations and intensities of the probe and pump lasers in $^{85}$Rb and $^{87}$Rb vapor cell at room temperature. In this research a theoretical method without phenomenal parameters is developed by H. R. Noh [23] for obtaining pump-probe absorption spectra from generalized solutions such as populations, optical coherences, transfer of the coherences from the excited states to the ground state and Zeeman coherences of the ground and excited states. The density matrix considering arbitrary polarization, power combinations of the pump and probe laser beam, time dependences of velocity groups of the atoms in a cell instead of steady state, and high-order Zeeman and optical coherence terms due to multi-order mixings of the pump and probe, by themselves, *etc*. have been applied to DTLS between 5 $S_{1/2}$ to 5 $P_{3/2}$ multi-level transitions of both isotopes of the Rb atom. The experimentally observed signal profiles are compared with probe transmission signals calculated from the generalized time-dependent density matrix equations and match well with the calculated signal profiles. Peculiar behaviors of coherence signals depending on powers and polarizations have been investigated in detail.

## 1.3 Motivation

In pump-probe experiments when both beams, which derive from two separate laser sources co-propagates through vapor cell with probe frequency fixed and locked to specific transition line and the pump laser tuned across the same transition line. Then in probe absorption spectra extra transmission peaks can be observed due velocity selective optical pumping effects with arbitrary polarizations and intensities of pump and probe lasers in closed and open system.

To investigate spectral features of ultra-narrow EIA signals experimentally we used two independent lasers systems for pump and probe laser beams but ultra-narrow EIA signal was not observed in the experiment. Because two different lasers with linewidth of 1 MHz produce together 2 MHz linewidth so the observed EIA signals are wider than calculated value of EIA signal. So we made major advance to observe these ultra-narrow signals using one laser combined with two AOMs.

The motivation behind our research work is also to understand the thermal averaging effects on spectral features of EIA and to investigate origin of formation of ultra-narrow and split EIA signal unknown previously in case of same and orthogonal polarization configuration with one laser discussed above.

.

## 1.4 Summary of this work

This work describes the experimental and theoretical investigation of rubidium vapor-cell EIA and EIT in a DTLS. Polarization and power dependent experimental and theoretical EIT and EIA spectra of both isotopes of rubidium are presented.

In chapter 2 we explain theoretically EIA and EIT spectra. Different atomic system and conditions which are necessary for occurrence EIA are also discussed.

The EIT mainly observed in three-level Λ-type system. DTLSs also provide possible way to analyze coherent effects in light-matter interaction. These systems are not only suitable for observation of coherent effects predicted and observed in three-level configurations, but also use for another opposite effect such as EIA. As each level of degenerate consists of multiple magnetic sublevel so EIA and EIT can also be observed in two level $F_g \rightarrow F_e$ transition. in degenerate two leve system EIA mainly occure due TOP and TOC. The occurrence of EIA due to TOC needs a particular type of system which consists of at least four degenerate states. Two of these states should be ground state and two excited state.

Theoretical calculation for spectral features of EIA in case of two independent laser sources with respect to power of pump beam is presented. Calculation for ultra-narrow and split EIA signal in case of same and orthogonal polarization configuration of pump and probe beam using single laser are also explained in this chapter.

In chapter 3 we describe theoretical and experimental detail of probe absorption spectra due to VSOP depending on polarization, power and direction of pump-probe lasers beam. We explain that due to VSOP effect the occurrence of transmittance peaks in spectra. We demonstrate EIA experiment for both closed and open system of $^{85}$Rb and $^{87}$Rb atom in D1 and D2 transition line. We describe different polarization configuration of pump and probe beam EIA spectra. Pump laser power dependent EIA spectra are also presented. We present our experimentally observed EIA spectra in DTLS of Rb atoms. The experiments were performed in both closed and open atomic system in D1 and D2 transition lines. As polarization combination of pump and probe laser beams play vital role in degerate magnetics sub levles for redistibution of atomic population abmong these levels and variation in polarization of pump and probe beams bring a noticeable change in spectral profile and intensity of EIA dip signal. So we explaine complet ploarzation dependent EIA spectra of $^{85}$Rb in this chapter.

In chapter 4 we describe theoretical and experimental pump-probe EIA spectra in general case of arbitrary polarization and powers of pump and probe beams of $^{85}$Rb atom. Spectral features of EIA in case of different polarization configurations also discussed. Thermal averaging effects on spectral features such as extra ultra-narrow and split spectral profiles of EIA implanted in broad sub-natural EIA have also been studied with respect to powers of pump beam.

In chapter 5 we describe in detail introduction about the features and ultra-narrow-EIA signal in case of all possible polarization configurations of pump and probe laser fields. By using single laser for both pump and probe

laser experiment the observe results in DTLS of $^{85}$Rb atom are also shown. Theoretical and experimental details are also presented.

Two different experimental schemes using one laser combined with an AOM have been used to investigate theoretical predictions for TOESC and TOP in cycling transitions of TSZMD of thermal $^{85}$Rb atoms. The general transient treatments are used to solve optical Bloch equations (OBEs) with full considerations of magnetic sublevels without phenomenal parameters in the arbitrary polarizations and arbitrary powers.

In chapter 6 we present the conclusin of the entire research work done in this thesis.

# Chapter 2
# Theoretical calculation of electromagnetically induced absorption (EIA)

## 2.1 Introduction

A simple two-level model for the atom can explain many light-atom interaction phenomena, while the three-level systems are compulsory to get coherent processes involving two optical transitions. In three-level system a medium which is initially absorbing for a weak probe tuned to one of the transitions becomes transparent when the other transition is irradiate with an intense coupling field.This transparency is a phenomenon of reducing the absorption of weak probe beam passing through a medium in the presence of second relative strong coupling beam. The occurrence of EIT in three-level atomic systems is common in which two lasers fields interacts with properly selected transition lines of atom and the quantum interference causes the ground state population to disappear the medium become transparent to probe laser field.

Two separate lasers fields named pump (strong) and probe (weak) couples to each arm with common excited level of Λ-type system. So absorption of probe laser field in the medium is reduces and very narrow spectral profile can be observed [19]. CPT and EIT are the examples of such dark states. CPT is well known both in three levels Λ-type system and DTLSs [15].

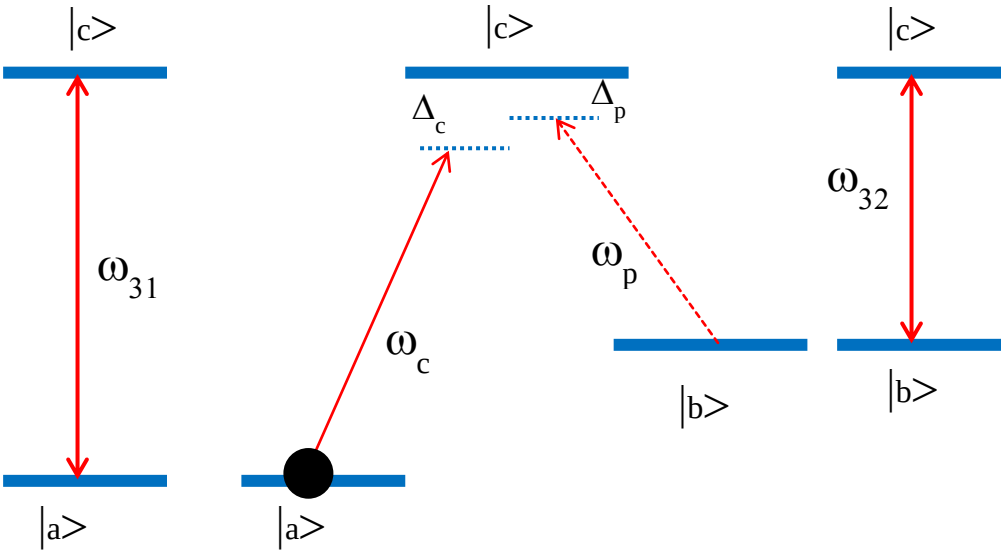


Fig. 2.1 Three levels Λ-type system with dipole allowed transition |a> → |c> and |b> → |c>.

The basic arrangement of Λ-types three levels atomic system is shown in Fig. 2.1 and we label the level as |a>, |b> and |c>. The system consists of two grounds (|a>, |b>) and one common excited states (|c>). $\omega_{31}$ and $\omega_{32}$are the transition frequencies of control and probe laser fields respectively. EIT requires two dipole allowed transitions (|a> → |c> and |b> → |c>) and one forbidden transition (|a>→|b>). In Λ-types three levels atomic system the state |b> being a metastable state has particular importance to produce long lived coherence between state |a> and state |b> which is very important condition for observing EIT in this system. According to quantum mechanics, when there are multiples excitation pathway exists, interference between their probability amplitude will occur. From Fig. 2.1 one possible way to get EIT is the interference between transition path way. Initially the atoms are

accumulated in the lowest ground state (|a>). When we turn on laser field of frequency of $\omega_{31}$then atoms in ground state can absorb energy and makes transition to state |c>. Meanwhile, when an electromagnetic field resonant with |b> → |c> transition is also turned on, now there are two transitions path ways through which atom can make transition from ground state to excited state. Either an atom can make transition in the way from |a> → |c> or it can follow the path to reach the excited state through |a> → |c> → |b> → |c>. Under certain conditions these two transitions path can show zero probe absorption at resonance peak due destructive interfere. EIT resonance can be several orders of magnitude narrower than the natural linewidth of the atomic transition. The interesting effect of EIT is includes large dispersion effect at the atomic resonance especially a very steep linear dispersion relation could be found at the point of minimal absorption.

.

## 2.2 EIA in degenerate two level atomic system of Rb atom

Electromagnetically induced absorption (EIA) [7] is an enhanced absorption of weak probe beam in the presence of strong pump beam. EIA is an absorption due to atomic coherences between the states via coherent laser photons [37]. For this enhanced absorption, there should be additional enhancement supports for a state which is probed absorption externally through transfer of population or transfer of coherence, *etc*. To observe EIA in different atomic system we should have a particular atomic system. For example in DTLS EIA can occur under two different procedures to prepare

induced absorption. One is known as EIA due to transfer of coherence (TOC) while the other is called as transfer of population (TOP). The enhanced absorption based on TOP can occur when both pump and probe laser beams have same polarization configuration. Similarly to observe EIA due to TOC the polarization of both beams must be orthogonal. Generally the occurrence of EIA due to TOC requires a special type of system which consists of at least four degenerate states. Two of these states should be ground state and two excited state. This system is usually known as N-type system which is shown in Fig. 2.2. It is important to note that there should be sufficient amount of population in degenerate excited state which leads to establish coherence and spontaneous emission from excited state to ground state leads the transfer of coherence. As it can be seen from Fig. 2.2 that N-type system is closed system and if pump beam derive to this closed transition then reasonable amount of population can be obtained. In Fig. 2.2 the |b> → |d> transition is closed path which is just similar as $F_g = 3 \rightarrow F_e = 4$ in case of $^{85}$Rb atom and $F_g = 2 \rightarrow F_e = 3$ in case of $^{87}$Rb

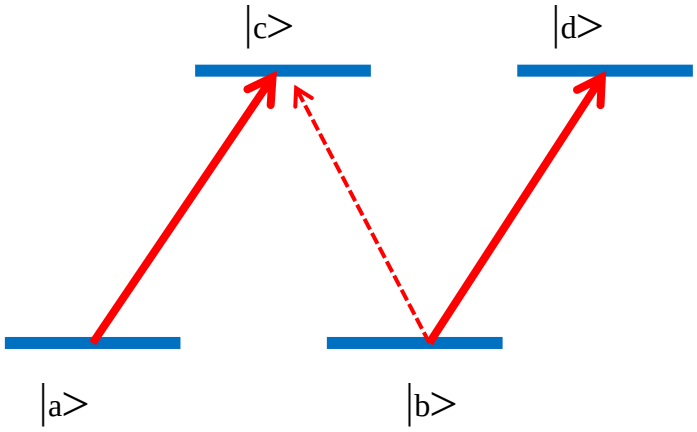


Fig. 2.2 The N-type atomic system in DTLS. Two heavy arrow show the Pump transition and dotted line arrow show probe transition.

Compared to non-degenerate three-level systems, degenerate two-level configurations are much more complicated and it more complex to describe pump-probe system due to many sublevels. Thus, the fundamental origins of EIA in DTLSs have not been investigated well, in contrast to those in three level atomic systems. Both, EIT and EIA occur due to optical pumping and coherence [15]. We present theoretical model for solving the generalized time dependent density matrix equation to explain complete polarization dependence of experimentally observed EIA signals for two rubidium isotopes at room temperature in vapor cell. A simple N-type model which is commonly used to clarify the theoretical explanation of EIA signal under certain polarization configuration of pump and probe laser beam is shown in Fig. 2.3.

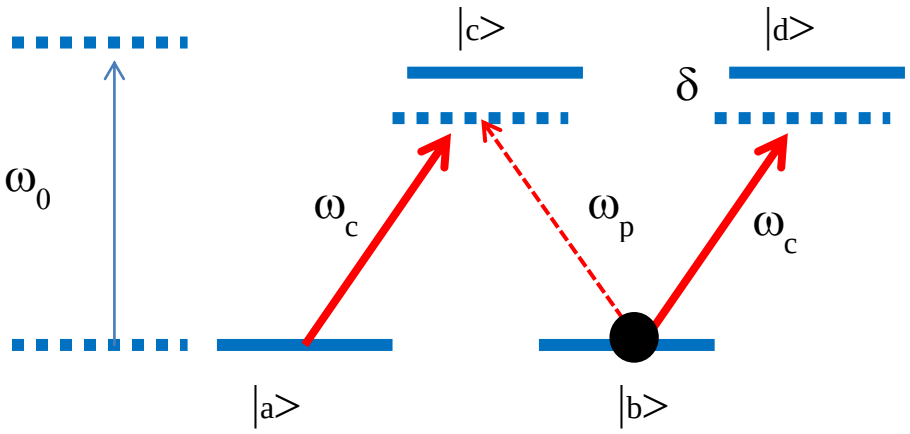


Fig. 2.3 The N-type atomic system in DTLS.

Suppose $\omega_0$ is the resonance frequency between ground and excited sub-level and $\delta$ show the detuning from resonance line. $\omega_c$ is the frequency of coupling beam which derive $|a\rangle \rightarrow |c\rangle$ and $|b\rangle \rightarrow |d\rangle$ transitions while $\omega_p$ is the frequency of weak probe beam which derive the $|b\rangle \rightarrow |c\rangle$ transition. In case of circular and orthogonal polarization configuration of pump and probe laser the population will be pumped into right most or left most ground state Zeeman sublevel. Compare to circular and orthogonal polarization, linear and perpendicular polarization case is more complex and complicated and make many sets of N-type system

## 2.3 Theoretical calculation of pump probe spectra

In case of two independent lasers sources for pump and probe beams, we performed two sets of experiments to observe the spectral features of EIA

signal profile. These experiments were designed to check the effect of different polarization configuration of both beams on spectral features of EIA because the role of polarizations combination in degenerate atomic systems becomes decisive. The polarization combinations can be classified into orthogonal and circular case and same-circular case of both beams. Here we explain the theoretical calculation to describe the line shape of observed EIA signal profile. To explain the procedure used for calculating the pump-probe spectra in straightforward way, we take the general case of an arbitrarily polarized pump beam. Let us consider pump and probe beams having optical frequencies $\omega_c$ and $\omega_p$ respectively co-propagates through vapor cell. Similarly we suppose that $\Omega_1$ and $\Omega_2$ are the Rabi frequencies of pump and probe laser beams respectively. As mentioned earlier that we take the case of cycling transition $F_g = 3 \rightarrow F_e = 4$ of the $^{85}$Rb D2 line. The energy level diagram of this cycling transition line is shown in Fig. 2.4. We have neglected the effect of other transition in calculation because of large hyperfine energy difference.

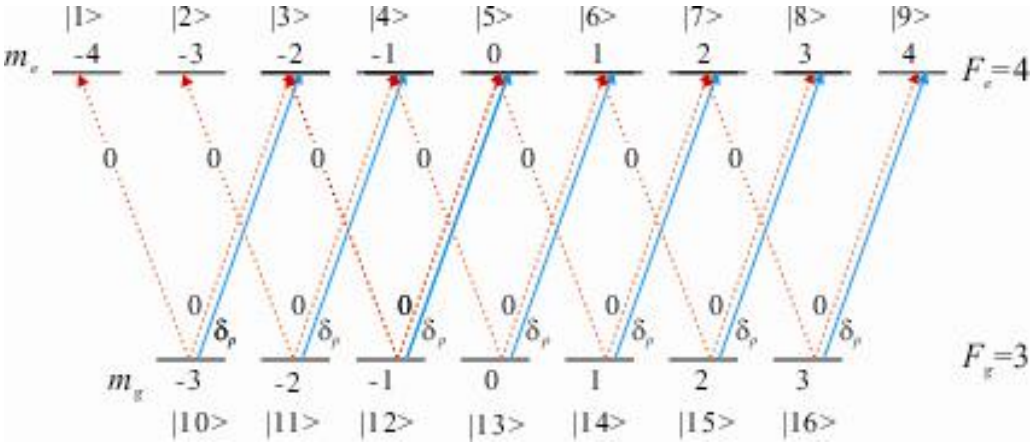


Fig. 2.4 Energy level diagram for the $F_g = 3 \rightarrow F_e = 4$ transition of $^{85}$Rb-D2 line.

In Fig 2.4 the solid line represents the probe beam while the dotted line denotes the pump laser beam. The magnetic sub levels in excited sate are labeled as $|m_e = -4\rangle = |1\rangle, |m_e = -3\rangle = |2\rangle, \ldots | m_e = 4\rangle = |9\rangle$ and magnetic level in ground state ( $F_g = 3$) are label as $|m_g = -3\rangle = |10\rangle, |m_g = -2\rangle = |11\rangle, \ldots. |m_g = 3\rangle = |16\rangle$.

The atoms of the gas are randomly moving in all directions inside the vapor cell. One portion of these atoms is moving in opposite direction of co-propagating pump and probe beams with velocity v. the laser frequencies of these pump and probe beams as observed by an atom are written as. $\omega_1 = \omega_p - kv$ and $\omega_2 = \omega_c - kv$ respectivily, where k ($=2\pi/\lambda$) is the wave vector and $\lambda$ is the wavelength of the coupling or probe beam we define the detuning $\delta_2$ ( $\equiv \omega_2 - \omega_0 = d_c - kv$ ) and $\delta_p$ ( $\equiv \omega_1 - \omega_2 = d_p - d_c$) where $\omega_0$ is the resonance frequency and $d_{p(c)} = \omega_{p(c)} - \omega_0$ is the detuning of the probe (coupling) beam.

When the absorption coefficient is calculated by solving the density matrix equation, all the quantities are expressed in terms of $\delta_2$ and $\delta_p$. The behavior of the internal dynamics of the $^{85}$Rb atom is described by a density matrix equation in the rotating frame with frequency $\omega_{2:}$

$$\dot{\rho} = \frac{i}{\hbar}[H_0 + v, \rho] + \dot{\rho}_{sp} \qquad (2.1)$$

where $\rho$ is the density operator and $H_0$ is the bare atomic Hamiltonian as given by

$$H_0 = \sum_{j=1}^{9} h\,\delta_2 \langle j|j\rangle \qquad (2.2)$$

$\dot{\rho}_{sp}$ denotes the spontaneous emission term. We consider that there is no collisional dephasing in atomic coherence due to pure Rb vapor inside the cell. There will be collisions between atom and wall of the container which can affect the coherence and can induce the dephasing in atomic coherence. But this effect is negligible small so can be neglected in theoretical calculations. Therefore, the decay rate of the optical coherence in $\dot{\rho}_{sp}$ is set to $\Gamma/2$ where $\Gamma$ is the decay rate of the excited state.

The interaction Hamiltonian in equation (1), V, is given by

$$V = \frac{\hbar}{2}\sum_{j=0}^{6}\{C_{10+j}^{3+J}\,\Omega 1 e^{-i\delta pt}|3+j\rangle\langle 10+j| + C_{10+j}^{1+J} a_{-}\Omega 2\,|1+j\rangle\langle 10+j| + C_{10+j}^{3+J} a_{+}\Omega 2\,|3+j\rangle + h.c \qquad (23)$$

where h.c denotes the Hermitian conjugate and $C_u^v$ is the normalized transition strength between the states |v> and |$\mu$> In equation (3), $a_{\pm}$ are the coefficient of the $\sigma\pm$ components of the coupling beam, as given by

$$a_{\pm} = \pm 1/2(1\pm \sin 2e) \pm i/2 \cos 2\varepsilon$$

where c is the angle between the incident electric field of probe beam and optic axis of quarter wave plat. We take two different arrangements for polarization configuration of pump and probe laser fields, the same ($\sigma+ - \sigma+$) polarization case and orthogonal ($\sigma- - \sigma+$) polarization case. In both cases, ε = $\pi/4$ and ε = $-\pi/4$, respectively. To obtained a series of linear differential equation for the density matrix elements, we substitute equations (2.2) and (2.3) in equation (2.1). It can be seen that there is exists obvious time dependence on right side of equation (2.1) so it necessary to expand the density matrix element into terms oscillating at different frequencies [59, 60]. To calculate non vanishing terms of density matrix element, we consider the interaction of two photons for population and Zeeman coherence. Similarly for optical coherence three photons were taken into account. In Fig. 2.4, we see that the oscillation frequencies for the $\sigma+$ transition are {0, $\delta_p$}, whereas that for $\sigma-$ transitions is 0. The oscillation frequencies for the populations can be determined by {0, $-\delta_p$} + {0, $\delta_p$}, and are finally given by 0, $-\delta_p$, and $\delta_p$. Therefore, the populations are expressed clearly as follows:

$$\rho_{jj} = \rho_{jj}^{(1)} + \left(\rho_{jj}^{(2)} + i\rho_{jj}^{(3)}\right) e^{-i\,\delta_p t} + ((\left(\rho_{jj}^{(2)} - i\rho_{jj}^{(3)}\right) e^{i\,\delta_p t} \qquad (2.4)$$

where, j = 1, 2, ⋯, 16. In equation (2.4), $\rho_{jj}^{(1)}$ are real for l = 1, 2, 3.The oscillation frequencies for Zeeman coherences are given by $\{0, \delta_p\}$ for $\rho_{1+j,3+j}$ ( $j$ = 0, 1, ⋯, 6) and $\rho_{10+j,12+j}$ ($j$ = 0, 1, ⋯, 4). The oscillation frequencies for the optical coherences are given by $\{0, -\delta_p, -2\delta_p, \delta_p\}$ for $\rho_{3+j,10+j}$ ( $j$ = 0, 1, ⋯, 6), $\{0, -\delta_p, \delta_p\}$ for $\rho_{1+j,10+j}$ ( $j$ = 0, 1, ⋯, 6),$\{0, -\delta_p, -2\delta_p\}$ for $\rho_{5+j,10+j}$ ( $j$ = 0, 1, ⋯, 4), and $\{0, \delta_p\}$ for $\rho_{1+j,12+j}$ ( $j$ = 0, 1, ⋯, 4). The oscillation frequencies of $\rho_{\mu v}$ are the negative of the oscillation frequencies of $\rho_{v\mu}$ for $\mu > v$. We neglected Zeeman coherences and optical coherences that are connected via interactions greater than three photons. The coherences can be written explicitly. As an example, the optical coherences with $\Delta m = 1$ are given by

$$\rho_{3+j,10+j} = \rho_{3+j,10+j}^{(1)} + \rho_{3+j,10+j}^{(2)} e^{-i\delta pt} + \rho_{3+j,10+j}^{(2)} e^{-2i\delta pt} + \rho_{3+j,10+j}^{(4)} e^{-i\delta pt} \tag{2.5}$$

where $j$ = 0, 1, ⋯, 6. Putting the coherences and populations described in the form of equations (2.4) and (2.5) in equation (2.1), we obtain a set of coupled differential equations for the components of the density matrix elements. These equations are then solved numerically as functions of time, $\delta_2$, and $\delta_p$. The absorption coefficient is given by

$$a_0(\delta_2, \delta_P, t) = \frac{N_{at} 3\lambda^2}{2\pi} \frac{\Gamma}{\Omega_1} \sum_{j=0}^{6} \mathrm{Im}[C_{10+j}^{3+j} \rho_{3+j,10+j}^{(2)}] \tag{2.6}$$

where Γ is the decay rate of the excited state and $N_{at}$ is the atomic number density in the vapor cell. The absorption coefficient is then averaged over the

transverse and longitudinal velocity distributions, and the final results are given by

$$a = 1/t_{av} \int_0^I dt \int_{-\infty}^{\infty} dv \frac{e^{-(\frac{v}{u})^2}}{\sqrt{\pi}\, u} a_0(d_c - j = kv, d_p - d_c, t) \qquad (2.7)$$

where u (=$(2k_BT/M)^{1\,2}$) is the most probable speed (T: temperature of the cell, M: mass of an atom) and $t_{av}$ (=$(\sqrt{\pi}/\ 2)d/u$) is the average transit time traversing a laser beam with a diameter d [61]. The restricted interaction time of the atoms with the laser beam is usually measured by assuming a decay rate of the ground state coherence and solving the steady-state solutions of the density-matrix equations [29, 47]. However, this method is not quite accurate because the included decay rate is a phenomenological constant. Instead of using such a phenomenological constant, we solve time dependent density-matrix equations and averaged the absorption coefficients over the distribution of finite transit times of the atoms crossing the laser beam. Since our method does not need any phenomenological constants differently from other previous calculation methods, the method of calculation is able to predict accurate line shapes of the EIA spectra. It is essential to examine time-dependent solutions of the density-matrix equations instead of stationary solutions to determine accurate EIA line shapes like previously investigated CPT system [62]. Although our system is not CPT system, our time-dependent solutions of the OBEs also give accurate line profiles because of time-dependent consideration in our calculation.

## 2.4 Theoretical backgrounds of ultra-narrow EIA signal

Fig. 2.5 shows the energy level diagram of $^{85}$Rb D2 for cycling transition line. Here in this case we consider the linearly polarized pump and probe beams in perpendicular direction. The procedure adopted for calculating EIA spectra in case of same-linear polarization configuration of both beams is quite similar to that which is used for same-circular polarization condition of both beams.

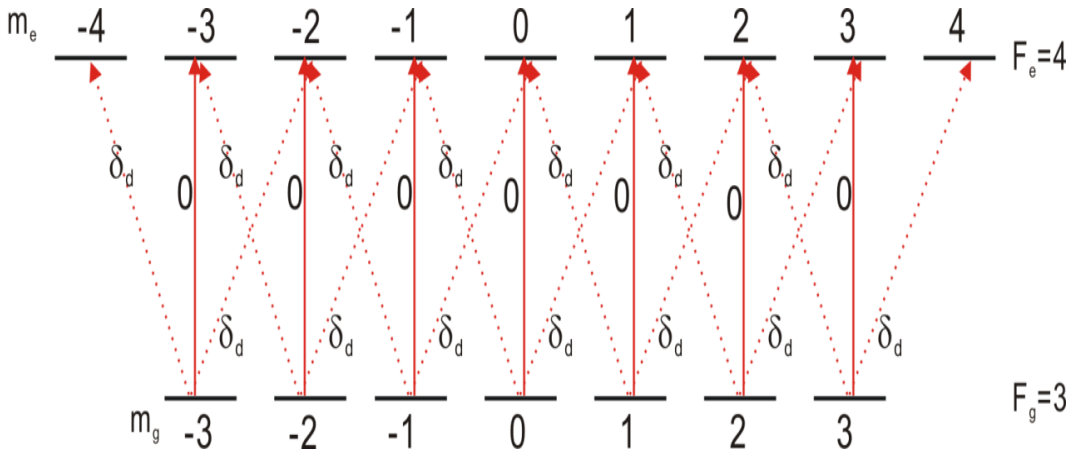


Fig. 2.5 The energy level diagram for the $F_g = 3 \rightarrow F_e = 4$ transition of $^{85}$Rb-D2 line.

In Fig. 2.5 “0” is the frequency of pump beam and “$\delta_d$” is the frequency of probe beam with respect to pump beam frequency $\omega_2$.

The Hamiltonian is given by

$$
\begin{aligned}
H = &-\sum_{m=-4}^{4} \hbar\delta_2 \left|F_e = 4, m\right\rangle\left\langle F_e = 4, m\right| \\
&+ \frac{\hbar}{2}\sum_{q=\pm 1} a_q \sum_{m=-3}^{3} C_{3,m}^{4,m+q}\Omega_1 \left|F_e = 4, m+q\right\rangle\left\langle F_g = 3, m\right| \\
&+ \frac{\hbar}{2}\sum_{m=-3}^{3} C_{3,m}^{4,m}\Omega_2 \left|F_e = 4, m\right\rangle\left\langle F_g = 3, m\right| + \text{h.c.},
\end{aligned}
\tag{2.8}
$$

In Eq. (2.1), $\dot{\rho}_{sp}$ represents the spontaneous emission term, which is given by

$$
\begin{aligned}
\dot{\rho}_{\text{sp}} = &-\Gamma \sum_{m=-4}^{4}\sum_{m'=-4}^{4} \left|F_e = 4, m\right\rangle\left\langle F_e = 4, m'\right| \\
&-\frac{\Gamma}{2}\sum_{m_e=-4}^{4}\sum_{m_g=-3}^{3}\left(\left|F_e = 4, m_e\right\rangle\left\langle F_g = 3, m_g\right| + \left|F_g = 3, m_g\right\rangle\left\langle F_e = 4, m_e\right|\right) \\
&+\Gamma \sum_{m=-3}^{3}\sum_{m'=-3}^{3}\sum_{q=-1}^{1} C_{3,m}^{4,m+q} C_{3,m'}^{4,m'+q} \left|F_e = 4, m+q\right\rangle\left\langle F_e = 4, m'+q\right|,
\end{aligned}
\tag{2.9}
$$

where $\Gamma$ is the decay rate of the excited state.

We consider the decay process from upper excited degenerate level, where TOP between the magnetic sublevels of the ground and excited states generates ultra-narrow absorption. The density matrix elements have large number of Fourier oscillation component in case of circular polarization, so the interaction of two photons will be consider for population and Zeeman coherences while three photons for optical coherence.

Here we describe density matrix elements for simplicity as

$\langle F_e, m'|\rho|F_g, m\rangle = \rho_{e_{m'}, g_m}$ $\langle F_e, m'|\rho|F_e, m\rangle = \rho_{e_{m'}, e_m}$ and Then, the expanded matrix elements of optical coherences are clearly written as $\rho_{e_m, g_m} = \rho^{(1)}_{e_m, g_m} + \rho^{(2)}_{e_m, g_m} e^{-2i\delta_d t}$ $\rho_{e_{m\pm1}, g_m} = \rho^{(1)}_{e_{m\pm1}, g_m} e^{-i\delta_d t} + \rho^{(2)}_{e_{m\pm1}, g_m} e^{i\delta_d t}$ $\rho_{e_{m\pm2}, g_m} = \rho^{(1)}_{e_{m\pm2}, g_m} + \rho^{(2)}_{e_{m\pm2}, g_m} e^{-2i\delta_d t}$ and $\rho_{e_{m\pm3}, g_m} = \rho^{(1)}_{e_{m\pm3}, g_m} e^{-i\delta_d t}$ for all the relevant values of m. Those of Zeeman coherences are given by $\rho_{e_m, e_{m+1}} = \rho^{(1)}_{e_m, e_{m+1}} e^{-i\delta_d t} + \rho^{(2)}_{e_m, e_{m+1}} e^{i\delta_d t}$ $\rho_{e_m, e_{m+2}} = \rho^{(1)}_{e_m, e_{m+2}}$ $\rho_{g_m, g_{m+1}} = \rho^{(1)}_{g_m, g_{m+1}} e^{-i\delta_d t} + \rho^{(2)}_{g_m, g_{m+1}} e^{i\delta_d t}$ and $\rho_{g_m, g_{m+2}} = \rho^{(1)}_{g_m, g_{m+2}}$ for all the relevant values of m. Finally each population has one constant term. We can have a series of linear differential equations by substituting the expanded density matrix elements in equation (2.1). After solving these equations, the matrix elements essential for the probe absorption can be derived. Finally, the absorption coefficient is averaged over the longitudinal velocity distribution and finite transit time distribution as follows [23]

$$\alpha = -\frac{3\lambda^2}{2\pi}\frac{N_{\text{at}}}{\Omega_1}\int_0^{t_{\text{av}}}\frac{dt}{t_{\text{av}}}\int_{-\infty}^{\infty}\frac{dv}{\sqrt{\pi}u}\ \text{Im}\left[\sum_{q=\pm1}\sum_{m=-3}^{3} a_q^* C_{3,m}^{4,m+q}\rho^{(1)}_{e_{m+q}, g_m}\right] \tag{2.10}$$

where $N_{at}$ is density of atoms in the cell, $t_{av}$ is the average time crossing a laser beam, and u is the most possible speed in the cell.

## 2.5 Saturated absorption spectroscopy

Saturated absorption spectroscopy (SAS) is frequently used for locking the laser to a specific hyperfine transition. With simple saturated

spectroscopy we can observe the decrease in probe absorption caused by strong pump beam which depletes the population.

Schematic of experimental setup which we used in our experiment is shown in Fig. 2.6

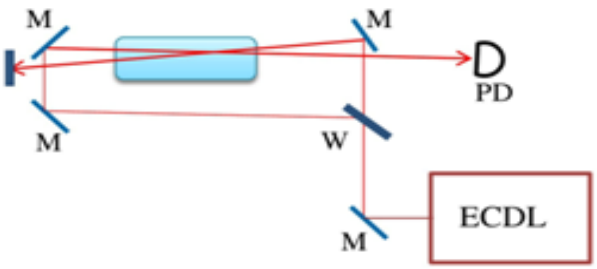


Fig. 2.6 Schematic of experimental setup of saturation absorption spectroscopy

Laser beam from external cavity diode laser (ECDL) is divided into two beams by using window. The transmitted beam, which is stronger and can be used as a pump and the reflected beam from window, is weaker and used as probe. These two counter propagating beam passes through gas cell which contains both rubidium isotopes in natural abundance overlap at the center cell. In off resonance condition when these two beams interact with atoms, one of them will excite the velocity group of $v_z$ and the other will excite the velocity group - $v_z$. When we tuned the laser to on resonance, both pump and probe beams will excite the same zero velocity group $v_z = 0$. As mentioned

the strong pump beam will excite most of the population to the excited state so the intensity of probe will pass through the cell without absorbing by atom. When we detect this probe beam by photodetector, we observe an increase in transmission of probe intensity. This decrease in absorption of probe beam caused by pump beam will result a dip in absorption profile and called as Lamb dip. When laser frequency is exactly similar to atomic transition frequency than one can observe saturated absorption spectroscopy signal. By looking at the spectra of SAS signals of Rb atoms one can observe six probe transmission peaks. Three of them are called principal hyperfine while the others three are known as crossover resonances. The occurrence of these crossover resonances can be explained as follow. As atoms inside the cell are always in random motion and we consider a group of atoms are moving with velocity $v_z$ in opposite direction to the prorogation of pump laser of frequency $\nu_{laser}$. So due to Doppler's effect the red-shifted resonant frequency for pump beam can be written as

$$\nu_{pump} = \nu_{laser}(1- v_z/c) \tag{2.12}$$

As mentioned above that pump and probe laser beams inside the cell are propagating in opposite direction. So at the same time for probe laser beam the blue shifted frequency can be of the form

$$\nu_{probe} = \nu_{laser}(1+ v_z/c) \tag{2.13}$$

by adding Eq. (2.12) and (2.13) we can have equation of the form

$$\nu_{laser} = (\nu_{pump} + \nu_{probe})/2 \quad (2.14)$$

Eq. (2.14) shows that the crossover resonance occurs at the middle of two transitions peaks.

# Chapter 3
# Optical pumping spectroscopy of Rb atoms

## 3.1 Introduction

Compared to non-degenerate three-level systems, degenerate two-level configurations [1-2, 15] are much more complicated and it is more complex to describe pump-probe system due to many sublevel and high order optical and Zeeman coherences. In case of D2 transition line of $^{85}$Rb and $^{87}$Rb atoms there are four closely-spaced excited state levels. The off resonance strong pump beam can cause non resonant excitation from ground level to all possible excited state levels and consequently the probe transmission shows the additional VSOP peaks [19]. In optical pumping mechanism, the Zeeman sub-levels plays vital role in response of light-matter interactions and as a result of this interaction not only there is population redistributions between magnetic sub-levels but also it creates coherence among the ground state Zeeman sublevels.

In pump-probe experiments when atoms are resonant with these two fields, the strong coupling laser beam creates dress states due to AC Stark shift and strong probe laser causes pump absorption dependent on the probe laser so that solution of the two-level system can be derived differently from the case of the weak probe beam. However the coupling laser can cause the populations to redistributes among the states by optical pumping. The population of one state can be optically pumped to another state which

affects the absorptions and transmissions spectrum profile of probe laser beam.

In the DTLS, the polarizations of the pump and probe laser beams play very important role in Zeeman coherences of the ground and excited states, transfer of the coherence from the excited states, contribution to optical coherences between the ground and excited states because the polarizations connect magnetic sublevels of the ground state with those of the excited states. In case of cycling transitions of both isotopes of rubidium atom, the probe transmittance peaks which results from atomic coherence is dominant because of transition selection rule the population of any ground state of cycling transition cannot optically pumped into any other or non- resonant states.

In this chapter we have applied for this solutions to understand the spectra of the EIT-like and EIA including the pump and probe absorption spectra due to adjacent hyperfine levels and velocity groups of the atoms. The observed signal profiles are compared with probe transmission signals calculated from the generalized time-dependent density matrix equations and match well with the calculated signal profiles. Thermal averaging of velocities of atoms in the cell is taken into account and complete analysis of arbitrary polarization change of the probe beam. Then, we have obtained the transition coefficient by averaging the calculated density matrix elements over a Maxwell-Boltzmann velocity distribution.

## 3.2 Experimental setup for same-circular and linear-linear polarization configuration

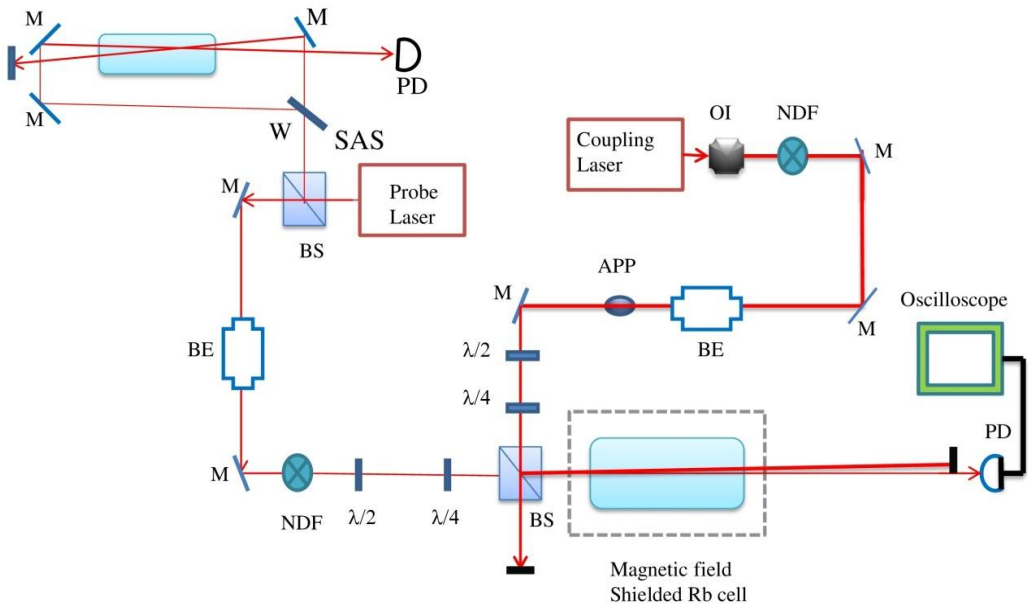


Fig. 3.1 Schematic diagram with two home-made External cavity diode lasers for same-circular and linear and parallel polarizations of both pump and probe beams. Figure keys**:** M-mirror, OI-optical isolator, W-window, APP-aperture, BE-beam expander, λ/2- half wave plate, λ/4-quarter wave plate, NDF- neutral density filter, PBS-polarizing beam splitter, PD-photodiode.

The Experimental setup is described schematically in above Fig. 3.1. Two separate 780 nm homemade external cavity Diode lasers (ECDL) are used for both pump and probe beams. The frequency of probe beam is fixed and locked on $F_g = 3 \rightarrow F_e = 4$ of $^{85}$Rb D2 transition line by using home-made lock-in amplifier. As shown in Fig, the vertically polarized coupling laser

beam after passing through optical isolator is sent into one of the beam expander to expand this beam up to 6 mm in diameter. An aperture is inserted in the path of coupling laser beam which control the size of beam used for experiment. Before mixing with weak probe laser beam at beam splitter (BS) which is placed just before the magnetic field shielded rubidium vapor cell, this coupling beam has to pass through half wave plate (HWP) and quarter wave plate (QWP). A neutral density filter (NDF) and these two plates contribute to control the variations in power and polarizations of coupling laser beam respectively. At BS the transmitted coupling beam is useless and is blocked while the reflected beam is used in cell experiment. Similarly another vertically polarized beam from probe laser is first divided into two parts by using another BS. The reflected beam from this BS is further divided by window to use for saturation absorption spectroscopy (SAS) setup to lock the laser frequency on desire hyperfine transition line. After window 90% of the total power of laser beam is transmitted while the remaining 10% will be reflected. These transmitted and reflected beams are used as pump and probe for SAS setup to observe the spectra. On the other hand the transmitted beam from second BS is sent to another beam expander to expand it up to required diameter. This expanded probe laser beam mixed with coupling beam at BS after passing through HWP and QWP. As mentioned that both lasers beams are vertical polarized but after passing through many optics the polarization state of these beams may be changed up to some extent so that the polarizations of the pump and probe lasers beams are made vertical polarizations just before a BS by using two HWPs once more. This experimental setup can be used for two different polarization

configurations of probe and coupling lasers beams. One of them is linear and parallel case while the other is same-circular polarization configuration For same-circular polarization configurations, two separate QWPs with optics axis angle ε = 45 with respect to y-axis for the pump and probe lasers are used to have same right circular polarizations just before the BS where two beam are combined. Both slightly deviated beams are overlapped well near the center of a magnetic shielded rubidium vapor cell for the pump and probe experiments. At long distance from the cell these two beams are separated and the pump beam is blocked while the probe beam is focused on a photodiode to measure the transmission of the probe beam through the cell. In case of linear and parallel polarization configurations of pump and probe lasers beams, two QWPs before BS for the coupling and probe experiment from the setup with same-circular polarization configuration are removed. In this way both the coupling and probe beams are vertically polarized.

## 3.3 Experimental setup for orthogonal-circular and linear-perpendicular polarizations configuration

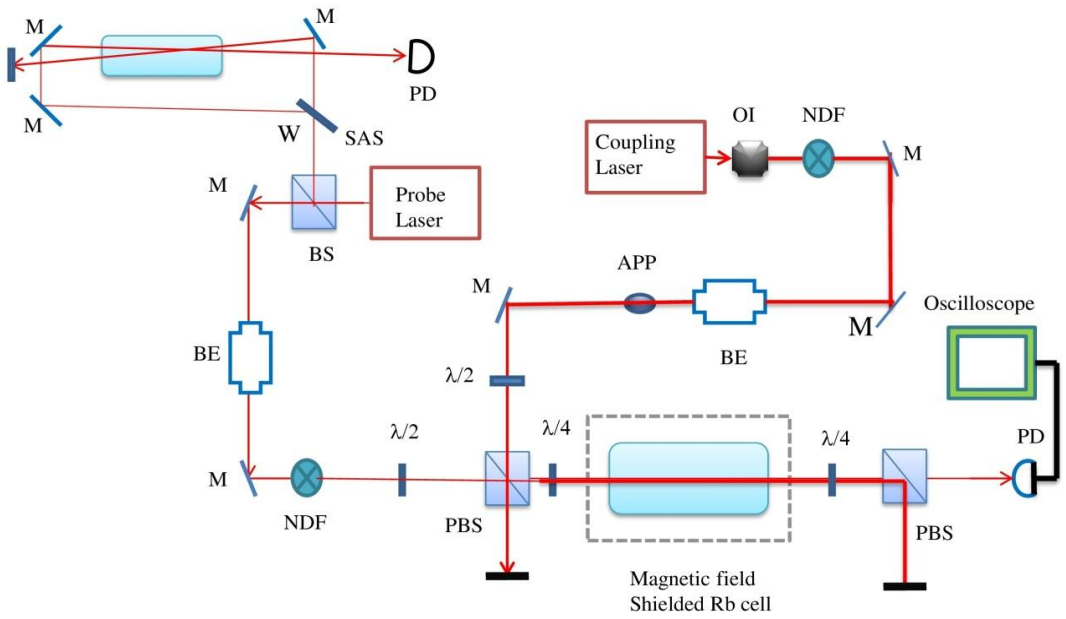


Fig.3.2 Schematic diagram with two home-made External cavity diode lasers for circular- orthogonal and linear - perpendicular polarizations of both pump and probe beams. Figure keys**:** M-mirror, OI-optical isolator, W-window, APP-aperture, BE-beam expander, λ/2- half wave plate, λ/4-quarter wave plate, NDF- neutral density filter, PBS-polarizing beam splitter, PD-photodiode.

By making some modifications in Fig. 3.1 and converting it into Fig. 3.2, we can use this setup for circular and orthogonal polarization configuration of coupling and probe lasers experiment in vapor cell. Further some changes in this setup will able us to use this experimental setup for liner and perpendicular polarization experiment of coupling and probe lasers beams.

For the experimental case of circular and orthogonal polarizations of the coupling and probe beams, one need to replace BS by PBS and inserting two quarter wave plates just before and after Rb vapor cell in Fig. 3.1 Finally one PBS should be inserted before the photodiode. As mentioned both beams are vertically polarized. The polarization state of probe beam is changed to horizontal polarization by changing the optic axis HWP. Now this beam transmits from PBS which is inserted before Rb cell. The vertically polarized coupling beam and horizontally polarized probe beam are mixed at PBS and very well overlapped in the throughout the rubidium vapor cell. When the polarization angle of QWP inserted before cell is set at $\varepsilon$ = -45 degree with respect to y-axis, then This arrangement prepared pump beam as left circularly polarized and at the same time initially horizontally polarized probe beam will be right circularly polarized. These two circular and orthogonal polarized beams interact with randomly moving atoms in the cell and emerged out to second QWP which is set at $\varepsilon$ = - 45 degree with respect to y-axis after the cell makes again the coupling beam as vertical polarized and probe beam horizontal polarized, respectively. When these two well overlapped beams reached at $2^{nd}$ PBS placed after vapor cell, the vertical pump beam reflected at 90 degree and horizontally polarized probe beam is transmitted. The reflected beam is blocked while the transmitted beam is detected by photodiode and monitored by oscilloscope.

In case of linear and perpendicular polarization configuration we need to remove both QWPs from the setup which are inserted before and after rubidium vapor cell. In this situation after $1^{st}$ PBS the coupling beam is vertically polarized while the probe beam is horizontally polarized. When

these two well overlapped beams reached at 2nd PBS after passing through Rb vapor cell, the vertical coupling beam reflected and horizontally polarized probe beam is transmitted. The reflected beam is blocked while the transmitted beam is detected by photodiode. The intensities of both beams were controlled by two separate neutral density filters (NDF).

## 3.4 Circular and orthogonal polarization dependences of the velocity dependent probe transmission signal

We have investigated theoretically and experimentally probe transmission profiles due to thermal velocities of atoms and scanning strong coupling laser frequency from $F_g = 3$ to $F_e = 2, 3, 4$ with weak probe laser resonant on $F_g = 3 \rightarrow F_e = 4$ of $^{85}$Rb atoms with respect to polarization. We have calculated the transmission and absorption spectra of $^{85}$Rb between hyperfine-level $F_g = 3 \rightarrow F_e = 4$ with degenerate magnetic sublevels when polarization coupling beam is changed from right circular polarized to left circularly polarized with fixed probe beam polarization. In DTLS polarization of probe and control lasers fields plays significant role to transfer of population from excited states and consequently variation in absorption and transmission signal profile is observed when the polarization state of control and probe lasers fields were changed. The experimental results matched well with those results which were calculated from density matrix equation. As probe and control lasers co-propagates through cell, detuning for control and probe lasers which atom feel are $\delta_{control} = \delta_c - kv$ and $\delta_{probe} = \delta_p - kv$, respectively where $\delta_c$ and $\delta_p$ are control and probe laser detuning from $F_g = 3 \rightarrow F_e = 4$ resonance line respectively. Fig. 3.3(a) and

(b) shows spectral change between frequency region including $F_e$ = 2, 3, and 4 hyperfine components with reference to fixed laser frequency of $F_g$ = 3 → $F_e$ = 4 and for theoretical calculation and experimental observation, respectively. Here polarizations of control beam are changed from right circular polarization to left circular polarization while the polarization of probe laser is right circularly polarized

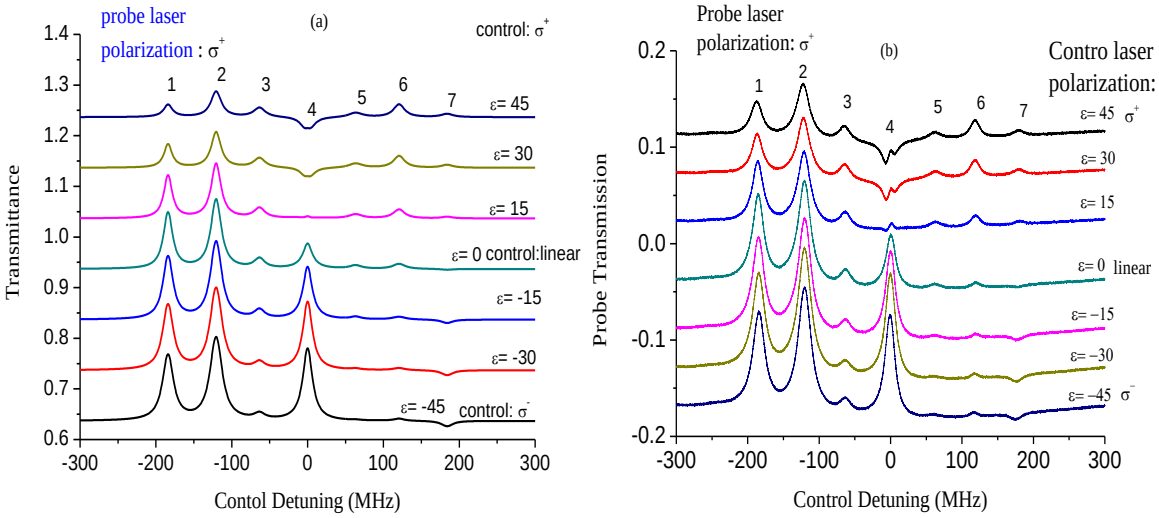


Fig. 3.3 Transmission spectra of $F_g = 3 \rightarrow F_e = 4$ of $^{85}$Rb (a) theoretically calculated from density matrix equation (b) experimentally observed spectra. Probe laser is right circularly polarized and the polarization of control laser is change from right circular polarization to left circular polarization. Shape and size of signal is changed due to redistribution of atomic population for different polarization state of control laser field.

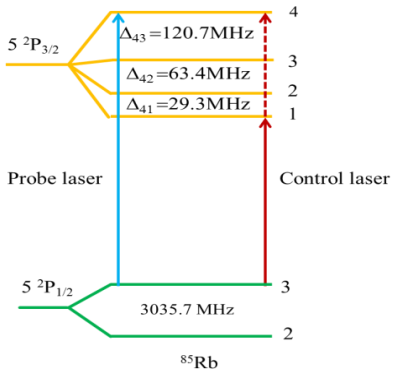


Fig. 3.4 Energy level diagram of $^{85}$Rb showing the hyperfine structure of the $5S_{1/2}$ and $5P_{3/2}$ levels.

Here we describe some detail about occurrence of seven peaks at different frequency domain. As the frequency of probe laser beam is fixed and locked between $F_g$ = 3 and $F_e$= 4 hyperfine of $^{85}$Rb D2 transition line. The pump beam is scanning between ground ($F_g$ = 3) and excited hyperfine components ($F_e$ = 2, 3, 4). As we have selected $F_e$ = 4 as a zero point, then possible velocity groups on resonant to the hyperfine components due to the pump beam can be 0 - kv = 0, $-\Delta_{43}$(= 120.64 MHz), and $-\Delta_{42}$(= 184.041 MHz) as shown in Fig. 3.4 (as pump beam scanning between hyperfine components $F_e$ = 2, 3, 4) ) and possible velocity groups on resonant to the hyperfine components due to probe laser beam scanning can be $\delta_c$- kv = 0, $-\Delta_{43}$(= 120.64 MHz), and $-\Delta_{42}$(= 184.041 MHz). Thus detuning $\delta_c$ which an atom feels for pump and probe laser can be obtained from kv = 0, 120.64 MHz, 184.041 MHz. Thus $\delta_c$ = -184.041 MHz, -120.64 MHz, -63.401 MHz, 0 MHz, 63.401 MHz 120.64 MHz, 184.041 MHz. Thus we observe seven resonances peaks when the pump laser is scanned through hyperfine

components between $F_e$ = 4 and $F_e$ = 2 as shown in Fig. 3.3a (theoretical calculated) and 3.3b (experimentally observed). As mentioned that the polarization of probe beam is fixed at right circular polarization while the polarization of coupling laser is changed from right circular to left circular polarization by changing the angle between optics axis of the quarter wave plate and vertically polarized probe beam with an increment of 15 degree. A vertically polarized coupling beam is passed through quarter wave plate with optic axis angle of +45 degree with respect to y-axis to make it as right circularly polarized coupling beam. Than the optic axis angle (ε) of the quarter waveplate with respect to the y-axis is rotated in anti-clockwise direction by +15 degree. The polarizations of the pump beam at ε = 0 and ε =15 are vertically linear polarization and elliptically polarizations. Finally the polarization of the coupling laser beam becomes left circular polarization at ε = -45. For each polarization of the probe laser beam, transmission signal of the probe beam are measured theoretically and experimentally. In Fig. 3.3 we have seven calculated and observed resonance peaks in between -300 MHz to 300 MHz control laser detuning frequency range. We can see that the signal for cycling transition $F_g$ = 3 to $F_e$ = 4 (fourth peak from left to right in the Fig. 3.3) is significantly changing as the polarization of coupling laser is changes. In case of $\sigma^+$–$\sigma^+$ –polarization (both coupling and probe lasers are right circularly polarized) the doublet structure (EIT-like) can clearly be observed which is the main difference from case of $\sigma^+$–$\sigma^-$ -polarization of probe and coupling lasers in the spectrum. According to transition selection rule $\Delta m_F$ = 0, ±1, the right circularly polarized probe beam is consider to be

taken as $m_F$ = +1 and coupling laser as $m_F$ = -1. In this particular condition, the two photon transition probability is lowest then all other polarization configuration of coupling and probe lasers beams. The atomic populations decay into dark state through optical pumping process by control laser and due to high saturation effect the transmission increase. Similarly if we look at other peaks of the spectrum it can be seen that first and second peaks continuously increasing as the polarization of control laser changes from right circular polarization to left circular polarization. Intensity of third, fifth and sixth peak is gradually decreasing while the 7$^{th}$ peak of the spectrum is totally upside down with orthogonal polarization state of probe and coupling lasers fields due to redistribution of atomic population in magnetic sub levels.

## 3.5 Linear-linear polarization dependences of the velocity dependent probe transmission signal

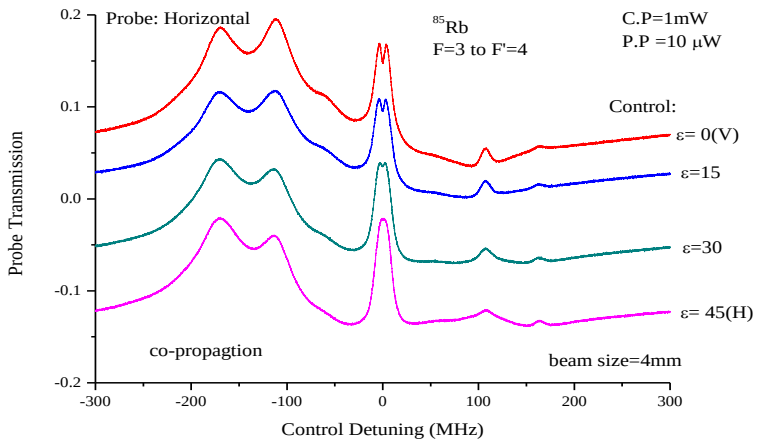


Fig. 3.5 Experimentally obtaind probe beam transmission spectra in case of linear and orthogonal polarization configuraltion.

We have observed experimentally probe transmission profiles due to thermal velocities of atoms in coupling-probe experiment from hyperfine level between the ground $5S_{1/2}$ and excited $5P_{3/2}$ D2 transition line of $^{85}$Rb atom with degenerate magnetic sub-level with respect to changes of polarization of coupling beam We have calculated the transmission and absorption spectra of $^{85}$Rb between hyperfine-level $F_g = 3 \rightarrow F_e = 4$ with degenerate magnetic sublevels when polarization coupling beam is changed from vertically polarized to horizontally polarized by changing the angle between optics axis of the half wave plate and vertically polarized coupling beam with an increment of 15 degree while the polarization of probe laser is fixed as horizontal linear polarized.

As explained earlier in detail the occurrence of probe transmission peaks in case of circular polarization configuration of coupling and probe laser fields. Similarly in case of liner polarization configuration of coupling-probe fields, one can explain these probe transmission peaks exactly similar way. Fig. 3.5 show transmission profile variation with respect to scanning of coupling laser beam between-300MHz to 300 MHz in closed system with zero detuning at $F_g = 3$ and $F_e = 4$ of $^{85}$Rb atom. The probe and coupling powers were kept fixed as 10 μW and 1mW respectively. The probe laser frequency is fixed and locked to transition between $F_g = 3$ ground and $F_e = 4$ excited state while the frequency of control laser is scanning. In case of linear and parallel polarization configuration of coupling and probe laser beams, the level configuration consists of separate two-level system which is connected through spontaneous emission. Each two-level system compose of

a two Zeeman sublevel with equal magnetic quantum number in ground and excited state $m_g = m_e$. A narrow transmission peak in linear and parallel case can be observe as the population transfer due spontaneous emission between pairs of level connected by these fields. As coupling-probe laser cannot form N-type or V-type atomic system in case of linear and parallel polarization configuration, that is why we cannot observe EIA-dip in lowest peak of Fig. 3.5.

In linear-linear configuration, the most interesting and most complex case is linear and orthogonal polarizations of coupling and probe beams. Linear and orthogonal polarization configuration provides almost similar probe transmission signal as in case of circular and orthogonal polarizations of coupling and probe laser because each of linear polarization consist of right and left circular polarizations with more transitions lines in DTLS. In Fig. 3.5 the top most curve show the result for case when coupling and probe laser fields are linear and perpendicular polarized. The main difference between circular-orthogonal and linear-orthogonal case is the optical pumping effect. Optical pumping is linear phenomenon for spontaneous decays and compare to linear polarization configurations the optical pumping effect in circular polarization configuration of coupling and probe laser is much stronger. When the polarization coupling and probe beams are linear and orthogonal, the strong coupling beam will transfer all the atomic populations to Zeeman sub-level through optical pumping mechanism and as result probe transmission decrease down at zero detuning regions. In DTLS polarization of probe and control laser fields plays significant role to transfer of population from excited states and consequently variation in absorption

and transmission signal profile is observed when the polarization state of control and probe lasers fields were changed.

## 3.6 Power dependent probe transmission spectra in case of linear and perpendicular polarizations.

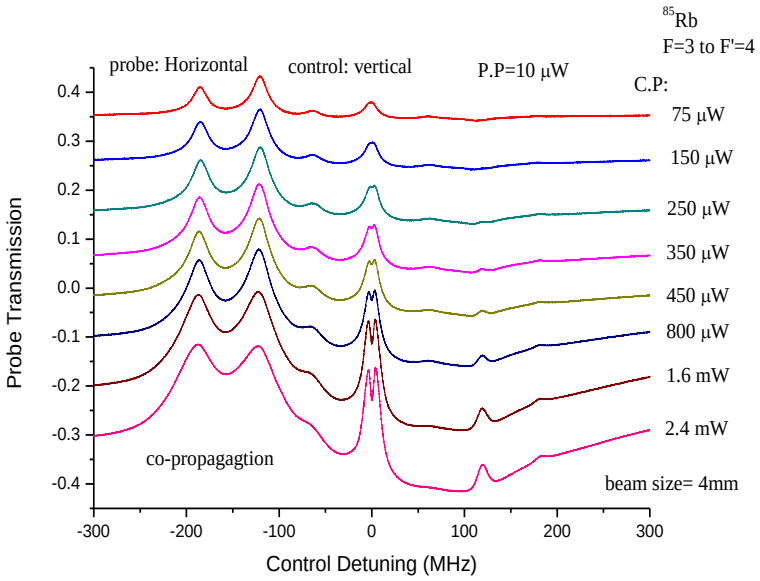


Fig 3.6 Experimentally obtaind coupling power dependent probe transmission spectra in case of linear and orthogonal polarization configuraltion between -300 MHz and 300 MHz.

In Fig. 3.6 we show obtained coupling power dependent transmission spectra of $F_g = 3 \rightarrow F_e = 4$ D2 transition line of $^{85}$Rb atom in rubidium vapor cell. Probe laser is horizontally polarized while the control laser is linear vertically polarized. The intensity of probe laser is fixed at 10 μW while the

intensity of coupling beam is changes from 75 μW to 2.4 mW. Probe laser is locked to $F_g = 3 \rightarrow F_e = 4$ while the coupling laser is scanned through hyperfine $F_g = 2$ and $3 \rightarrow F_e = 1,2,3,4$ of $^{85}$Rb. In linear and perpendicular polarization configuration, all ground state magnetic sub-levels are coupled to strong coupling laser beam and atomic population is distributed among all these ground state sub level. The size of these seven peaks depends upon the power of lasers beam. As shown in Fig. 3.6, when power of coupling laser is very weak, the optical pumping effect is lower and we observe smaller sized transmission spectra. However as power of coupling laser is gradually increased, the transmission peaks become clearer because the intensity of coupling laser is directly related to atomic coherence and in cycling transition one can observe very interesting phenomenon of probe absorption at zero detuning. It is already explained in detail in case of circular-circular polarization configuration that why and how these seven peaks appears when coupling laser scanned between -300 MHz and 300 MHz frequency range. Due to optical pumping effect the shape and size of transmitted peaks are changes due to redistribution of atomic population.

## 3.7 Probe Transmission spectra in an open system

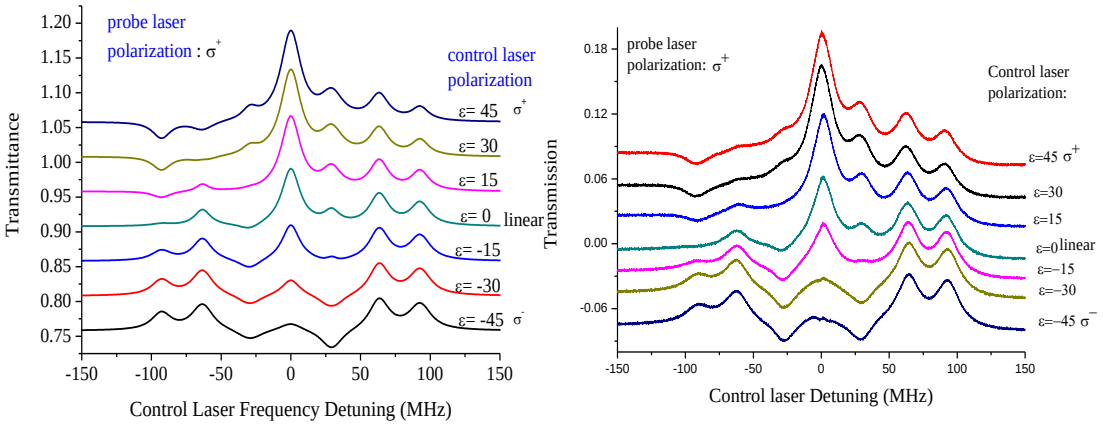


Fig. 3.7 Probe transmission spectra of $F_g = 2 \rightarrow F_e = 3$ of $^{85}$Rb at (a) theoretically calculated from density matrix equation (b) experimentally observed spectra. Probe laser is right circularly polarized and the polarization of control laser is change from right circular polarize to left circularly polarized.

This set of experiment was performed using co-propagating coupling and probe laser beams in an open system of $^{85}$Rb atom D2 line. Theoretically calculated and experimentally observed probe transmission spectra are shown in Fig. 3.7 the intensities of coupling and probe lasers were 90 μW and 9 μW respectively. The frequency of probe laser beam is fixed and locked between $F_g = 2$ and $F_e = 3$ hyperfine of $^{85}$Rb D2 transition line and coupling beam is scanning between ground $F_g = 2$ and excited hyperfine components $F_e = 1, 2, 3$. As probe laser is tuned to hyperfine level $F_g = 2 \rightarrow F_e = 3$ for zero velocity atoms, the transmission of probe laser is increases

when the coupling laser tuned to $F_g = 2 \rightarrow F_e = 1, 2, 3$ also for zero velocity atoms. The additional peaks appears in the spectrum can be explain by Doppler effects. For atoms moving in opposite direction to the propagation direction of laser beam with some particular velocities which correspond to the shifts of 63.4 MHz and 92.7 MHz shown in Fig. 3.4. It is clear that the atoms with velocities which can provide a shift of 63.4 MHz interacting with probe laser beam. The probe laser couple the transition $F_g = 2 \rightarrow F_e = 3$. One can observe the probe transmission peak if the coupling beam is tuned same transition for the same velocity group. This means the peak at 92.7 MHz is not only because of laser interactions with zero velocity atoms but also interaction of atoms in 63.4 MHz shifted velocity group. As coupling and probe laser co-propagates through vapor cell detuning for coupling and probe lasers which atom feel are $\delta_{control} = \delta_c - kv$ and $\delta_{probe} = \delta_p - kv$, respectively where $\delta_c$ and $\delta_p$ are coupling and probe laser detuning from $F_g = 2 \rightarrow F_e = 3$ resonance line respectively. Fig. 3.7(a) and (b) show spectral change between frequency region including $F_e = 1$, 2, and 3 hyperfine components with reference to fixed laser frequency of $F_g = 2 \rightarrow F_e = 3$ and for theoretical calculation and experimental observation, respectively. Because of Doppler's effect, the additional peaks in the spectrum can be observed. From energy level diagram shown in Fig. 3.4, one can predict the exact position of these peaks by looking at frequency shifts due to the Doppler's effect as energy shifts of excited level. As we have taken $F_e = 3$ as a zero point, then possible velocity groups on resonant to the hyperfine components due to the pump beam can be $0 - kv = 0$, $-\Delta_{23}$(= 63.4 MHz), and $-\Delta_{31}$(= 92.7 MHz) as shown

in Fig. 4 (as pump beam scanning between hyperfine components $F_e$ = 1, 2, 3) ) and possible velocity groups on resonant to the hyperfine components due to probe laser beam scanning can be $\delta_c$- kv = 0, -$\Delta_{32}$(= 63.4 MHz), and -$\Delta_{31}$(= 92.7 MHz). Thus detuning $\delta_c$ which an atom feels for pump and probe laser can be obtained from kv = 0, 63.4 MHz, 92.7 MHz. Thus $\delta_c$ = -92.7 MHz, -63.4 MHz, -29.3 MHz, 0 MHz, 29.3 MHz 63.4 MHz, 92.7 MHz. It is observed that the population distribution of among the ground sub-levels are affected by polarization configuration and intensities of laser filed so the magnitude of the transmitted peaks showing different behavior at different polarizations of coupling and probe lasers beams. The experimental results matched very well with those theoretical results which were calculated from density matrix equation.

## 3.8 Probe absorption and transmission spectra in an open system

It has been believed that in open system EIA signal could not be occur. However, Kim *et al*. [30] observed EIA signal in an open system using an orthogonal linear polarization configuration of coupling and probe laser beams with co-propagating beam directions Here we describe the experimentally observed narrow EIA-dip signal in open system of $^{85}$Rb and $^{87}$Rb D1 and D2 transitions line.

The experimentally observed EIA signal in D2 transition line of both isotopes of rubidium atoms for circular and orthogonal polarized coupling and probe lasers with coupling power of 3 mW and probe laser power of 10

μW are shown in Fig. 3.8 (a) and (b).

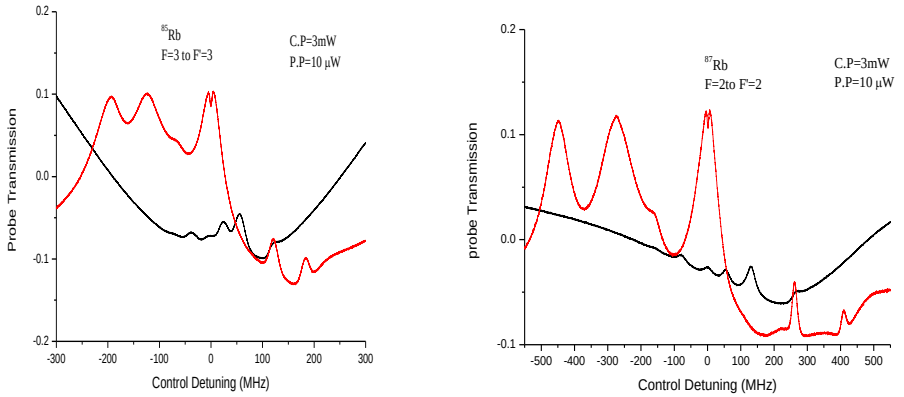


Fig. 3.8: Experimentally observed EIA signal when control laser is right circularly polarized and probe laser is left circularly polarized. The power of control laser is 3 mW while the power of probe beam is 10 μW. (a) Probe laser is locked to $F_g = 3 \rightarrow F_e = 3$ while the coupling laser is scanned through hyperfine $F_g = 2$ and $3 \rightarrow F_e = 1,2,3,4$ of $^{85}$RB (b) probe beam is locked to $F_g = 2 \rightarrow F_e = 2$ and coupling laser is scanned through hyperfine $F_g = 1$ and $2 \rightarrow F_e = 0,1,2,3$ of $^{87}$Rb D2 transition line in an open system. The bottom curve show the SAS signals of respective rubidium isotopes.

By using saturation absorption spectroscopy (SAS), the probe beam is locked to hyperfine components $F_g = 3 \rightarrow F_e = 3$ and scanning of control beam between -300 MHz and +300 MHz between frequency region including $F_g = 2$ and $3 \rightarrow F_e = 1,2,3,4$ of $^{85}$Rb and similarly in case of $^{87}$Rb, probe beam is locked to $F_g = 2 \rightarrow F_e = 2$ and coupling laser is scanned through hyperfine $F_g = 1$ and $2 \rightarrow F_e = 0,1,2,3$. As mentioned [2] that to observe EIA the atomic system must be closed but in case of $F_g = 3 \rightarrow F_e = 3$

of $^{85}$Rb and $F_g = 2 \rightarrow F_e=2$ of $^{87}$Rb atom system are open because of selection rule excited stat atoms can decay back to both of ground state sub levels and does not obey one of the three conditions for observing EIA dip signal so one can expect EIT because control laser is pumping atomic population in to those ground levels which are not coupled to probe laser (dark state) so the number of atoms in original ground state are reducing down. These dark states coupled coherently with control and probe laser fields but the probability of transfer of coherence from excited state to ground state reduced down so we observed decreased EIA dip signal compared with a closed system. The structure near frequency +121MHz, +194 MHz *etc*. in upper trace of Fig. 3.8 (a) and similarly the structure near frequency +267 MHz and +410 MHz in upper trace of Fig. 3.8 (b) are due to velocity selective optical pumping.

## 3.9 Absorption and transmission spectra in D1 line (open system)

In case of D1 line, we obtained EIA signal along with VSOP peaks for all possible allowed optical transitions. Fig. 3.9 show the schematic diagram of energy levels for both isotopes of Rb atom and each isotope separately compose of four allowed transition lines between $5S_{1/2}$ and $5P_{1/2}$ level.

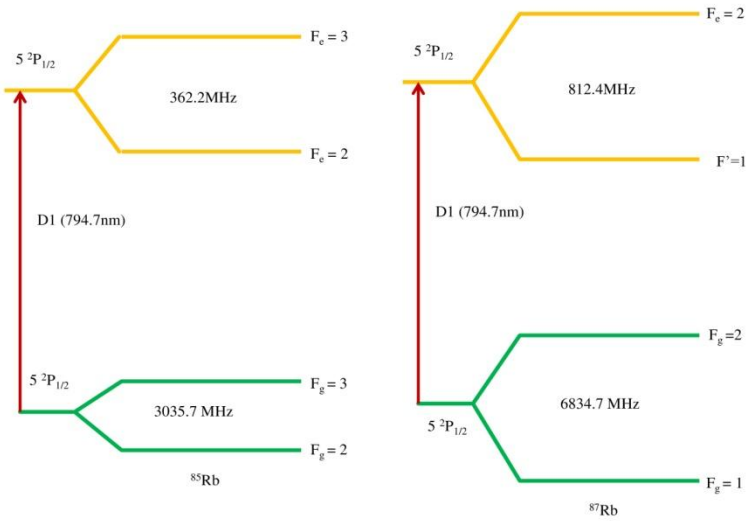


Fig. 3.9 Energy level diagram of $^{85}$Rb and $^{87}$Rb atoms D1 line showing hyperfine structure of the $5S_{1/2}$ and $5P_{1/2}$ level. Energy values are in MHz.

Experimentally observed probe absorption spectra for various values pump power with fixed probe intensity at 30 μW is shown in Fig. 3.10. The probe beam frequency is fixed and locked to the transition between $F_g$ = 2 and $F_e$ = 3 hyperfine D1 transition line of $^{85}$Rb atom while pump beam frequency is scanning around the same transition. Probe laser is horizontally polarized while the control laser is vertically polarized

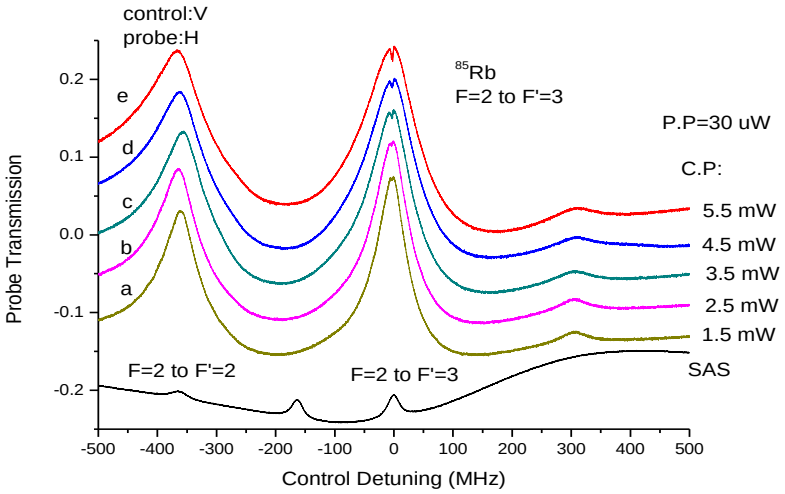


Fig. 3.10 Experimentally observe probe absorption spectra for $F_g = 2$ to $F_e = 3$ D1 transition line of $^{85}$Rb atom for various coupling powers with fixed probe laser power of 30 μW. The bottom curve is SAS signal for calibration.

By looking at the spectra shown in Fig. 3.10, we can observe the transmission peak on left side of EIA-dip signal near -362 MHz which is quite similar separation as shown in Fig. 3.9 between $F_g = 2 \rightarrow F_e = 3$ of $^{85}$Rb atom. This transmission peak is due to velocity selective structure with broad linewidth (FWHM). We could not observed EIA dip-signal up to 1 mW of coupling laser field but as the intensity of coupling field is increased we observe clear EIA signal which stated with 1.5 mW and signal become more clears with high coupling power of 5.5 mW. Compare to closed system much power is needed to observe EIA signal in an open system.

Fig. 3.11 show the absorption spectra observed in open system ($F_g = 3$ to $F_e = 2$) of $^{85}$Rb D1 transition line as a function of pump laser detuning frequency depending upon the intensity of coupling laser field. The pump laser is vertically polarized and probe laser is horizontally polarized. The

probe laser frequency is locked to transition between $F_g = 3$ ground and $F_e = 2$ excited state while the frequency of pump laser is scanning. The intensity of probe laser is fixed to 15 μW and the power of pump laser field is changing from 1mW to 8.5mW with an interval of 1 mW. The bottom curve shows SAS spectrum. We can see two transmittance peaks at $F_g = 3 \rightarrow F_e = 2$ and $F_g = 3 \rightarrow F_e = 3$ respectively, at coupling laser power of 1 mW. These peaks occur when control laser depletes population in open system by optical pumping. Most of the atoms in $F_e = 2$ state decay spontaneously to ground stat $F_g = 3$ and remaining atoms transfer to other ground state $F_g = 2$.

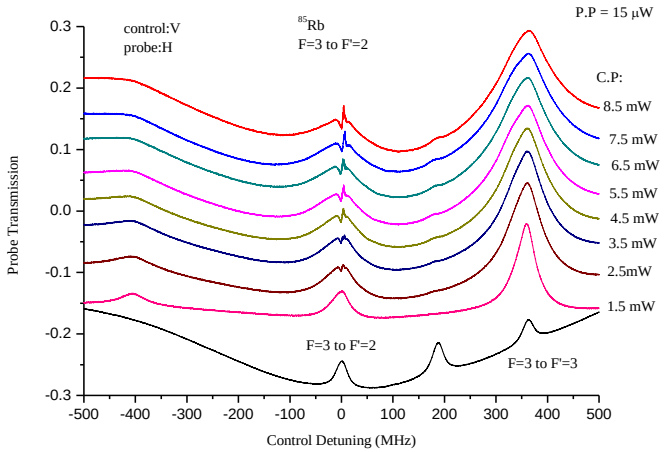


Fig. 3.11 Experimentally obtained probe absorption spectra of $F_g = 3$ to $F_e = 2$ , 3 D1 transition line as a function of control laser frequency while the probe laser frequency is locked to $F_g = 3$ to $F_e = 2$. Probe laser is horizontally polarized while control laser is vertically polarized. The power of probe laser is fixed to 15 μW. The power of control laser is increasing from 1 mW to 8.5 mW. The lowest curve indicates the SAS spectra of D1 line of $^{85}$Rb.

Since this system is an open system and absorption spectra should show transmission because strong coupling laser optically pumped the atomic population to other sub-levels which are not coupled with weak probe laser. Up to 1mW of coupling beam power we only observe the transmission peaks as the power of coupling laser field increases, EIA dip start to appear near 3.5 mW. Furthermore, an increase in control laser power breaks up EIA into two dips and convert it to EIT based on CPT into dark state. But we observe EIA signal although these observed signals are very small compare to those signals which we obtained in a closed atomic system of both isotope of Rb atom. Thus we can say that spectrum shown in Fig. 3.11 is determined by EIT. This conversion of EIA into EIT also been observed by Z. Y-Ting *et al*. [42] in closed system of Cs atoms.

# Chapter 4
# Spectral features of electromagnetically induced absorption in $^{85}$Rb atoms

## 4.1 Introduction

Previously there have been lot of research works related to broad EIA-dip signals based on different parameters like powers of beams, different polarization configuration, beam size, and geometry of the experimental setup *etc*., but thermal averaging effects on spectral features like ultranarrow signals of EIA were not investigated theoretically and experimentally with respect to power of pump beam by many researcher groups. In high power pump limit of circular and orthogonal polarization configuration, thermal averaging effects play decisive role in the splitting of EIA spectra.

In this chapter we provide comprehensive detail of absorption spectra by using newly developed theoretical technique. This technique is used for solving the generalized time dependent density matrix equation to explain the features of absorption spectra without considering phenomenal parameters. This new method unravels EIA spectra with ultra-narrow and split signals based on intensity of pump laser beam in both thermal and stationary atoms. In this chapter we mainly focused on obtained transmission spectra for the case of $F_g = 3 \rightarrow F_e = 4$ cycling transition D2 line of $^{85}$Rb atoms. Pump beam power dependent ultranarrow and split spectral features of EIA in broad subnatural EIA have been investigated. Sensational variations in ultranarrow signals are observed with an increase in pump

power due to thermal average effects. In case of same-circular and circular and orthogonal polarization of pump and probe beams, the EIA signals have ultranarrow EIA features in low power of pump beam. However at high power of pump beam the behavior of EIA signals are different at different polarization states of pump and probe beams. A complete detail of EIA features with respect to pump power in case of same and orthogonal polarization configuration is present in upcoming sections of this chapter. A part from these EIA features we make sure the coherent effect in EIA by investigating the difference between transmission signal with and without coherence terms in density matrix equation such as transfer of coherence or Zeeman coherence. We concluded that the coherence terms of density matrix equation determined the broad dips in normally coherent EIA features instead of incoherent power saturation effects.

Our experimentally observed results in case of two independent lasers for each of pump and probe match well with the calculated features for same and orthogonal polarization configuration except ultra-narrow EIA peak. This is because of lasers linewidth of two independent pump and probe lasers which is approximately equal to 2 MHz.

## 4.2. Calculated absorption spectra from various coupling beam Rabi frequencies

### 4.2.1Theoretical calculated spectra

Probe absorption signals with coherence effects between magnetic sublevels were calculate by using above mentioned technique. Pump-beam Rabi frequencies dependent absorption spectra have been calculated. The coupling beam frequency detuning is fixed at the resonance line while the probe beam frequency is detuned. The results for the stationary atoms ($v = 0$) and Doppler thermal averaged results in case of same polarization configuration are shown in Fig. 4.1(a) and (b) and for orthogonal polarization configuration of pump and probe beams are shown in Fig. 4.1(c) and (d), respectively. In Fig. 4.1, the Rabi frequency of the probe beam is $2\pi$ × 1MHz (hereafter, $2\pi$ is omitted). At low pump Rabi frequencies the ultranarrow EIA spectra are observed in both, same and orthogonal polarization configuration when the stationary atoms are considered which are shown in Fig. 4.1(a) and (c). As the pump Rabi frequency increases, famous Mollow-type three-peaks are observed and shown in Fig. 4.1(a), while four absorption peaks are found in Fig. 4

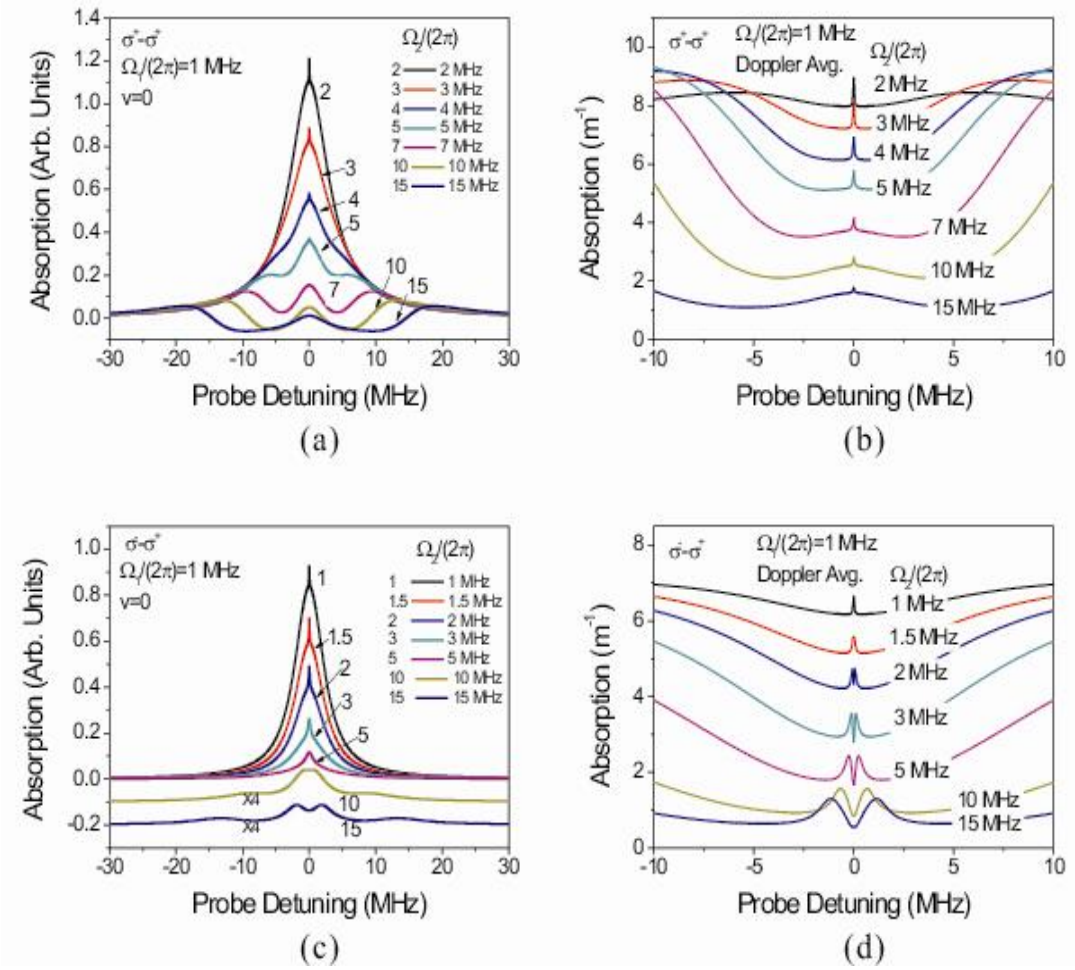


Fig. 4.1 Theoretical probe absorption spectra obtained in the cases of same ($\sigma^+ - \sigma^+$) polarization configuration (a) between −30 and= 30MHz with v = 0, (b) between −10 and 10 MHz with thermal motions of atoms, (c) orthogonal ($\sigma^- - \sigma^+$) polarization configuration between −30 and 30 MHz with v = 0, and (d) between −10 and 10 MHz with thermal motions of atoms, respectively.

Fig. 4.1(d) shows the results of case when thermal average effect is taken into account. It can be seen that as the pump Rabi frequency increases the

ultra-narrow EIA peaks become wider and splitted but still the linewidth of these peaks remains sub-natural. In Fig 4.1(c) the ultra-narrow signals which were observed up to 3 MHz of pump Rabi frequency remain only at 1 MHz of probe Rabi frequency. In case of same polarization combination of pump and probe laser beams, the ultra-narrow peak can be observed at low power of pump beam and even at high power of pump laser this ultra-narrow peak are generated but the magnitude of this ultra- narrow signal become weak as shown in Fig.4.1(b).

To examine various aspects of thermal averaged absorption coefficient for same and orthogonal polarization configuration cases, particular absorption coefficient at v = 0 and ± 5ms$^{-1}$ are calculated as shown in Fig.4.2. As observed in the partial energy level diagrams using a dressed state formalism shown in Fig. 4.2, the resonances of the probe detuning ($d_p$) for the same and orthogonal polarization cases at $d_c = 0$ are given by

$$d_p = 0, \pm \sqrt{(kv)^2 + \Omega_2^2} \tag{4.1}$$

for same polarization,

$$d_p = \pm 1/2[\sqrt{(kv)^2 + \Omega_2^2} + \sqrt{(kv)^2 + 15\Omega_2^2/28}\ ], \quad \pm 1/2[\sqrt{(kv)^2 + \Omega_2^2} - \sqrt{(kv)^2 + 15\Omega_2^2/28}] \tag{4.2}$$

for orthogonal polarization case respectively.

It can be seen in Fig. 3 that separation of dressed state is different. In case of same polarization configuration ultra-narrow peaks can be observed at all pump laser power in thermal averaged absorption spectra. This fact can be

explained and understand in straight forward way: despite the consequences of motion of atoms, there exist a dispersive-shaped resonance at $d_p = 0$ as mentioned in equation (4.1). The slope of this resonance for positive and negative value of atomic velocity is totally opposite to each other which can be seen in Fig. 3(a). The narrow absorptive signal which is shown in Fig 4.2(b) is the consequence of combined velocities effect contributed by individual atom. On the other hand in case of orthogonal polarization configuration, refer to equation (4.2) the atomic velocities dependent four resonances exist. Fig. 4.2(b) show the result of these particular case for v = 0 and $V = \pm 5 ms^{-1}$. After taking thermal averaging effect the two outer resonances result flat signals. Similarly two interior resonances results in two splitted EIA signal centered at $\sim \pm (1 - (15/28)^{1/2})\Omega_2$. So ultra-narrow signal can only be observed at very low power of pump beam and splitted EIA spectral profile at moderate or high pump power.

In Fig. 4.3 we show the results for pump scanning at resonant condition of probe ($d_p = 0$). All the parameters and schemes are just similar as those in Fig. 4.1. The narrow features for zero velocity atoms are similar to those result which are presented in Fig 4.1 due to coherent effect which is commonly depends upon the difference in detuning of pump and probe laser beams. But on the other hand the Mollow-type three resonance peaks due to same polarization

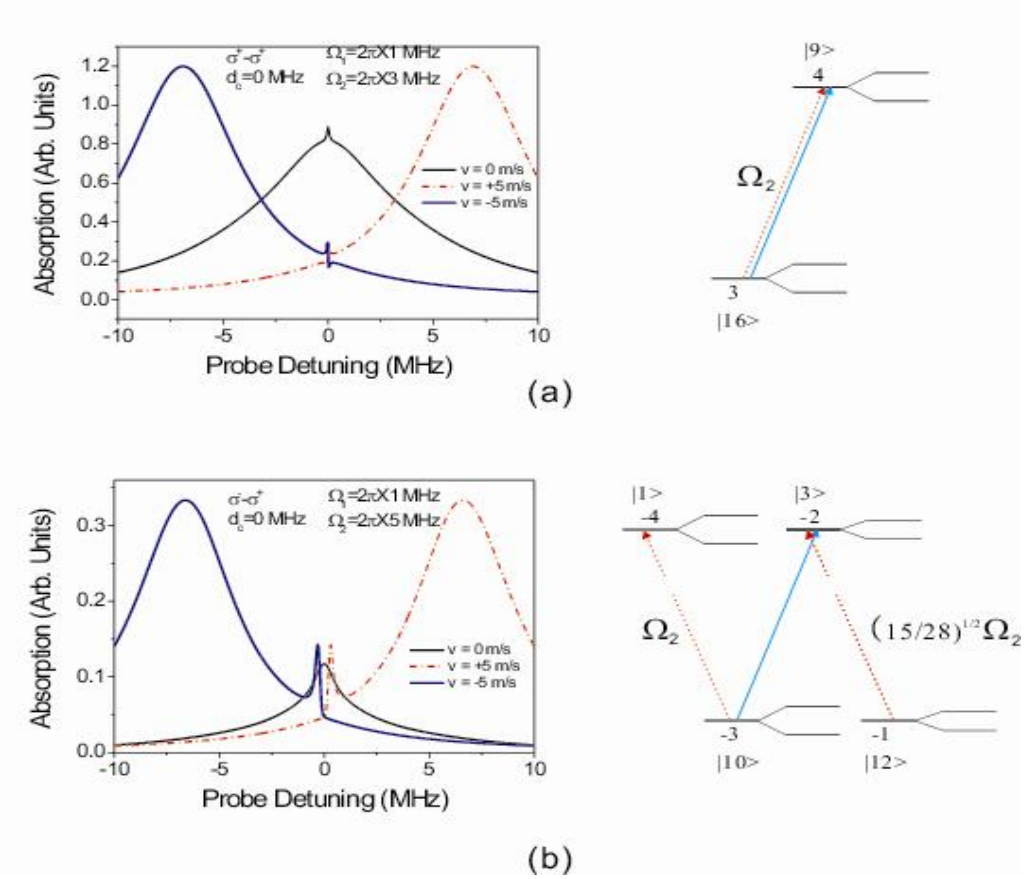


Fig. 4.2 Calculated absorption coefficients for (a) the same and (b) orthogonal polarization cases at v = 0 and ±5 m s−1. Simple dressed state energy level diagrams are also shown to explain the resonances.

and four absorption peaks in case of orthogonal polarization combination are not easily visible. This happened because the exact location of resonance depends upon the Rabi frequency and detuning of pump beam. As pump beam is scanning so there will be variation in its detuning and that is why the resonance become unclear. When thermal averaging effect and small

scanning range are considered then non coherent effects are averaged out so we can observe almost similar absorption spectra shown in Fig. 4.1. At far detuning region, it is mostly observed that the results for two scanning schemes are different.

## 4.3 The origin of the broad sub-natural EIAs

To investigate the origin of broad sub natural EIAs, we solved density matrix equation in such conditions that coherence effect such as Zeeman coherence and transfer of population were not taken into account. Theoretically calculated probe absorption spectra with and without coherence effects between magnetic sub levels are shown in Fig 5. The absorption spectra with coherence effect is represented with solid line and without coherence effect is shown by dash line are observed in case of same ($\sigma^+ - \sigma^{+)}$ and (b) orthogonal ($\sigma^- - \sigma^+$) polarization configurations. For numerical calculation we take the circular laser beam with radius 2mm and Rabi frequencies of 15.7 MHz for pump and 0.94 MHz for probe beam. The method of calculation without considering the coherence effect is called simply rate-equation. As shown in Fig. 4.5, in the results of the rate-equation calculations disregarding coherence effects such as TOC and TDTOP, EIA spectra disappear. So the occurrence of EIA in both case due to coherence effects instead of incoherence effects.

In Fig. 4.4(a), rate-equation calculations were performed by neglecting time-dependent terms in equation (2.4) and terms of $e^{-2i\delta pt}$ and $e^{i\delta pt}$ in

equation (2.5), which result from the nonlinear wave mixing between the pump and probe field. There exists significant difference between the cases when calculating the absorption spectra with and without coherence effects. This mean that the coherence term leads to results in both ultra-narrow absorption signal and broad subnatural EIA signals. In off resonance condition the population oscillation term do not disappear so big difference is exists between two results. even though absolute inequity of the signals due to coherence effects was reported in the case of pure two-level atoms [43, 44], it was not likely to discriminate the signals for the complex levels of $F_g = 3 \rightarrow F_e = 4$ of the $^{85}$Rb-D2 line. In Fig. 4.4(b) the rate equation calculations are carried out by neglecting the Zeeman coherences between the magnetic sublevels in the excited and the ground states. But, the difference between cases with and without coherence effects exists only near zero detuning because the Zeeman coherences established between the magnetic sublevels in the excited state die out in the off resonance situation. Obviously it can be seen that the EIA was take place due to transfer of Zeeman coherence of the excited states.

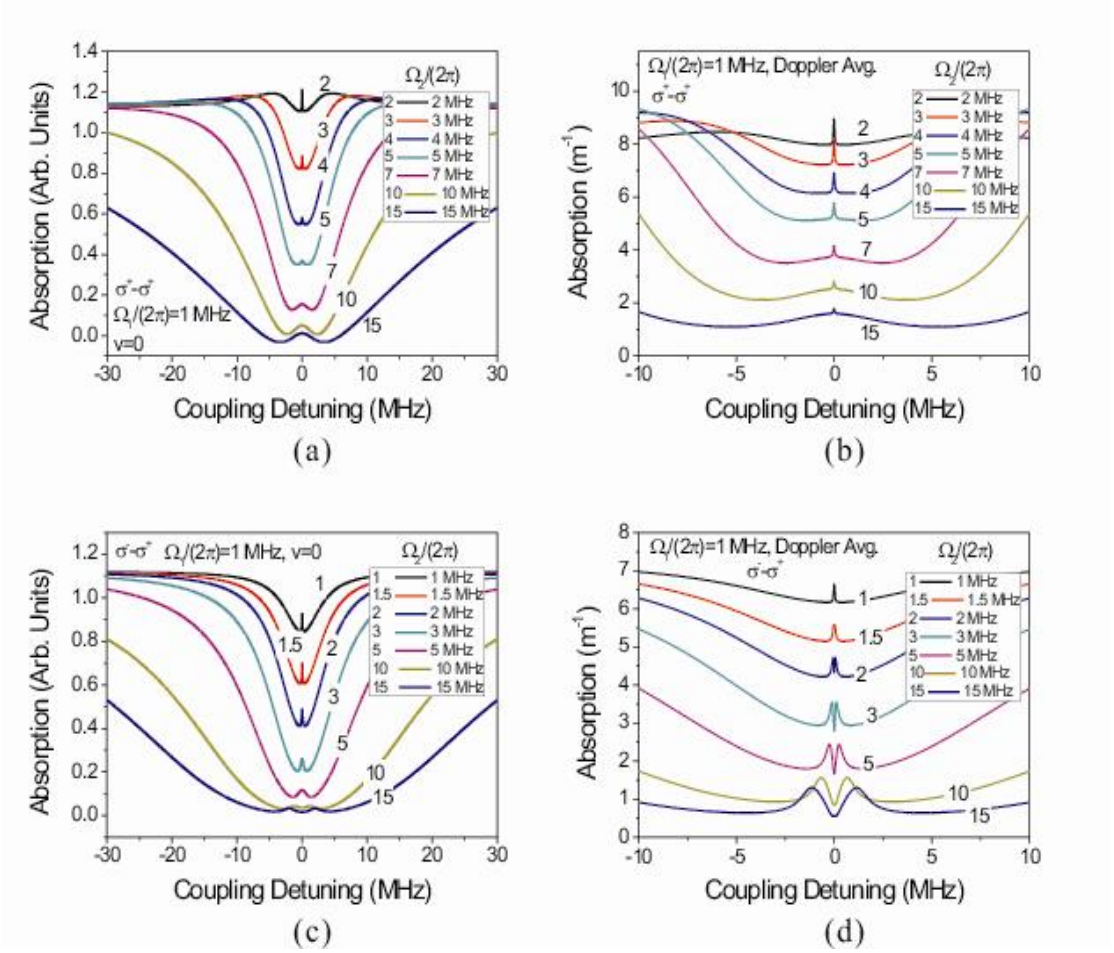


Fig. 4.3 Theoretical probe absorption spectra for the coupling-detuning scanning, obtained in the cases of same ($\sigma^{+} - \sigma^{+}$) polarization configuration (a) for stationary atoms, (b) for thermal atoms, and (c) orthogonal ($\sigma^{-} - \sigma^{+}$) polarization configuration for stationary atoms,(d) for thermal atoms.

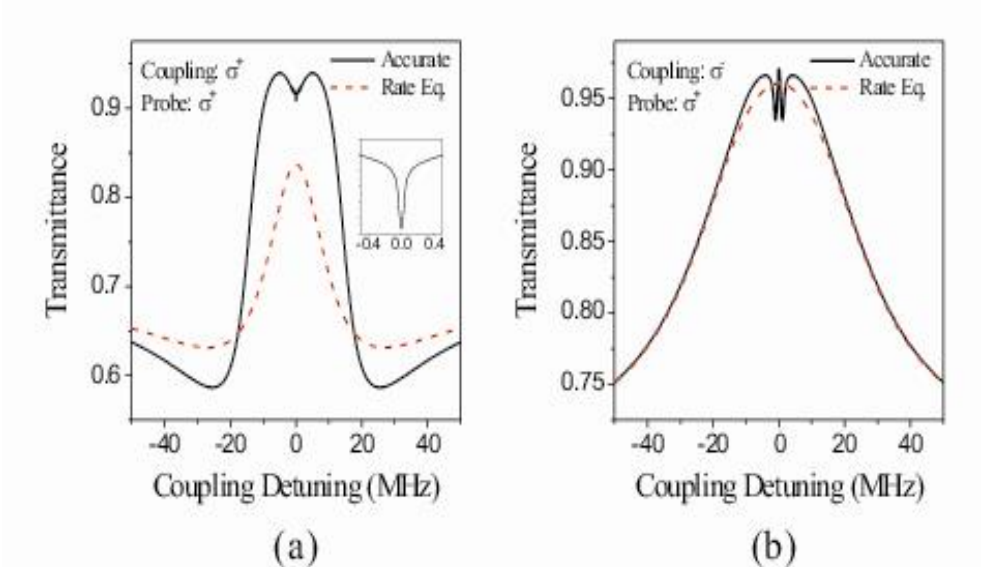


Fig. 4.4 Theoretical probe transmission signals with coherence effects between magnetic sublevels, represented with solid line, and without coherence effects between magnetic sublevels, represented with dashed line, obtained in the cases of (a) same- ($\sigma^+ - \sigma^+$) and (b) orthogonal-($\sigma^- - \sigma^+$) polarization configurations. In the inset of Fig. 4.4 (a) ultra-narrow spectrum is shown.

## 4.5 Explanation of Experimental results.

The experimental setup is described schematically in Fig. 3.1 and also a comprehensive detail of this setup is present in section 3.2. For this particular case of experimental results we used the same experimental setup. The lasers beams with diameter of 4mm and Rabi frequencies of 15.7 MHz for pump and 0.94 MHz for probe are used to observe EIAs absorption spectra. By using saturation absorption spectroscopy (SAS), the probe beam is locked to the hyperfine $F_g = 3 \rightarrow F_e = 4$ transition line while the pump laser is scanned

in wavelength around the same ( $F_g = 3 \rightarrow F_e = 4$) transition.

Fig. 4.5 shows theoretical (upper curve) and experimental (lower curve) probe transmission spectra for the transition $F_g = 3 \rightarrow F_e = 4$ of the $^{85}$Rb-D2 line obtained in the cases of (a) same ($\sigma+ - \sigma+$) and (b) orthogonal ($\sigma- - \sigma+$) polarization configurations of pump and probe beams. For theoretical calculation and experimental observation the spectral features which are shown in Fig. 4.5 have observed when pump beam scanned between frequency range −50 to +50 MHz with respect to the fixed probe-laser frequency of the $F_g = 3 \rightarrow F_e = 4$ transition,

In case of same polarization configuration the pump and probe beams ($\sigma^+ - \sigma^+$) both the lasers excite the same magnetic sublevel between ground and excited states. Thus it is obvious that in this situation pump-probe laser beam cannot form N-type atomic system between magnetic sub-levels so that EIA resonance signal cannot be observed. But there are theoretical predictions for observing EIA signal even in case of same polarization of pump and probe beams due to transfer of population. On the basis of theoretical prediction and calculation we expect not only sub natural EIA signal but also extra ultranarrow EIA signal implanted in broad sub natural EIA. Three different features can be observed in theatrically calculated spectra shown in Fig. 4.5(a). These features like an ultra-narrow EIA, a broad Subnatural EIA, and a very broad probe transmission. All of these signals are enclosed in the Doppler absorption profile. The middle wide probe-transmission spectrum results from pump power-dependent saturation effects and its spectrum increases as the power of pump laser increased. The inset in Fig. 4.5(a) shows stretched spectra of the calculated EIA signal, which shows a spectral

linewidth of ~0.1 MHz. These ultra-narrow and broad sub-natural EIA spectra vanish whenever coherent effect such as TDTOP is eliminated. Asymmetries of the main broad peak in Fig. 4.5 result from overlapping of a closely adjacent spectrum due to power broadening without EIA, which are not shown in Fig. 4.5.

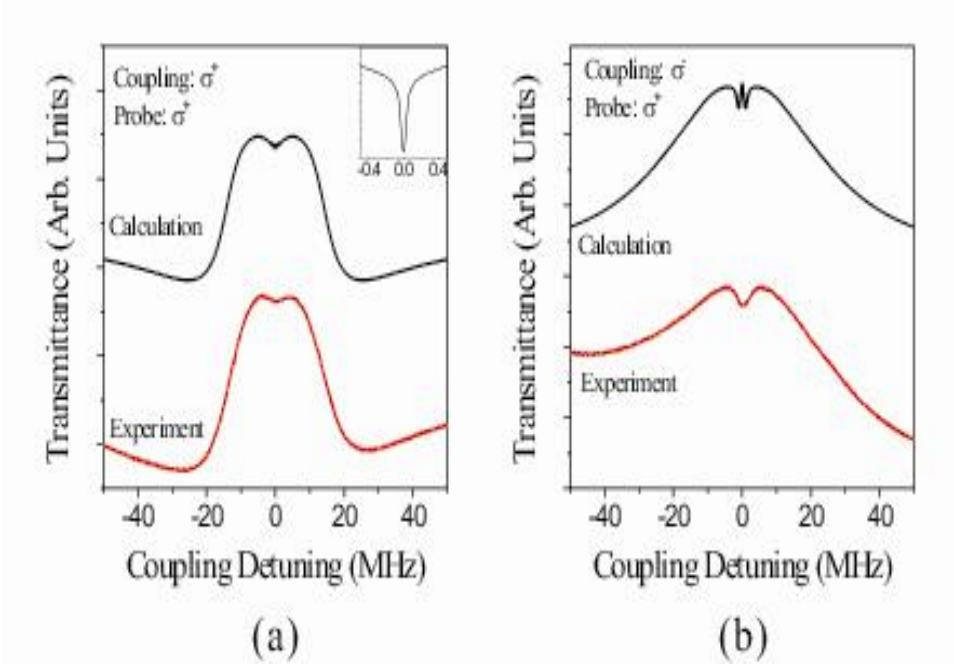


Fig. 4.5 Theoretical (upper trace) and experimental (lower trace) probe transmission spectra obtained in the cases of (a) same ($\sigma+ - \sigma+$) and (b) orthogonal ($\sigma- - \sigma+$) polarization configurations, respectively. The inset in (a) shows expanded portion of ultra-narrow EIA embedded in broad sub-natural EIA obtained from the theoretical calculation.

We mainly concentrate on the middle peak with EIA in the calculation

without considering effects from neighboring peaks. In the theoretical calculation, the effect of neighboring peak on the middle peak is not taken into account so that a symmetric line is observed. The major dissimilarity between theoretical and experimental results is situated at the central part of the spectra, where results from the coherence effects of TDTOP are due to spontaneous decay from upper excited magnetic sublevels for the same polarization configuration.

A.D.W. Gordon *et al*. [43] and V.S. Letokhove *et al*. [44] reported that in the case of a pure two-level system when the decay rate of the upper level is less than that of the lower level due to collisional effects then the additional ultra-narrow line can be observed. They did not consider coherence effects due to interlinking between magnetic Zeeman sublevels. However, EIA is created because of time-dependent oscillating population decays from levels interlinked between magnetic sublevels even in our case, without such collisions as hyperfine-changing collisions in the ground state where the decay rate of the ground state is much slower than those of the excited states. Ultra-narrow EIA signal was not observed in the experiment. The reason that there is no ultra-narrow line in the central part of the spectra is that two different lasers with linewidth of ~1 MHz produce an approximate 2 MHz linewidth difference. Thus, spectral shapes much narrower than the laser linewidth cannot be observed because of the large shared linewidths of the two different lasers. In orthogonal polarization case the observed EIA signal is slightly wider but not much deeper. Experimentally observed linewidth of EIA is 3.8 MHz, which is similar to the theoretically calculated 3.3 MHz. The linewidth of the EIA signal is smaller than the natural linewidth of 6

MHz. At low pump power the EIA signal was not observed. With an increase in pump power the EIA signal steadily increase. Fig. 4.5 (a) and (b) show the agreement between theoretical and experimental transmission signal except for central region. But we performed another experiment by using one laser combined with acousto-optic modulators (AOM) which provided much narrow linewidths of observed EIA spectra so that such ultra-narrow EIA signal has revealed and presented in chapter 5.

The theoretical calculated spectrum in case of orthogonal polarization of pump and probe laser beams shown in Fig. 4.5 (b) consist of two narrow, split EIA signal in upper curve, which splits into two EIAs due to the high power of the pump laser beam. The split EIAs in the central area have a spectral linewidth of ~1 MHz. The experimental spectrum in Fig. 4.5(b) composed of an EIA signal inside the wide probe transmission in the lower curve because of coupling-power saturation. The observed linewidth of EIA is 3.7 MHz, which is similar to the calculated 3.2 MHz without taking into consideration a narrow central peak with a linewidth of 1 MHz. The linewidth of the EIA dip signal is smaller than the natural linewidth of 6 MHz. the experimentally observed spectrum which is compose of an EIA signal. The absence of narrow and split EIA spectra inside the probe transmission is due to pump power saturation effect. As mentioned above that pump and probe laser beam together have broad linewidth so these ultra-narrow and split EIA line could not observed. The increase in pump laser power results in splitting of EIA signals. In case of same polarization combination of pump and probe laser beams, the decrease in pump power does not results in EIA signal. Except central region of spectra strong

agreement between experimental and theoretical transmission spectra is shown in Fig. 4.5 (a) and (b).

# Chapter 5

# Observation of ultra-narrow spectral features of electromanetically induced absopton in two-level system with Zeema multiplet degeneracies of $^{85}$Rb atom

## 5.1 Introduction

Some researcher groups bevlied that there should be existance and splitting of ultranarrow EIA signals based on powers and different polarization combination of pump and probe laser fields. Even at significantly low power of pump beam these ultranarrow signals should have to observe due to time dependent transferof population(TDTOP) in DTLS in case of same polarization combination of pump and probe fields. In closed atomic system the splitting of these ultranarrow signal in case of orthogonal polarization configurtion of pump and probe lasers can occure when the Rabi frequency of pump beam is greater than the decay rate of upper excited state and lower than probe intensity [29].

Uptill now there is no report on experimental obsrevation of such ultranarrow spectral features of EIA signal profile in case of same and orthogonal polarizaition combinations. Althouh an attempt has been made to observe these predicted ultranarrow signals in case of same polarization configurartion by using tow separate lasers sources for pump and probe laser

beams [38] but they did not succed to generate these ultranarrow features. The linewidths of these ultranarrow signal can have in the range of some tens of kilo Hretz (90 to 100 KHz). Useually the lasers systems used for pump-probe experiments have linewidth roughly equal to 1 MHz so in case of two independent laser system experiment the the combined lienwidth of both beam would roughly be equal to 2 MHz which is quite larger than compare to linewidth of predicted ultranarrow signals and we think that this is the main reason that in two laser system of pump- probe experiment no body has generated usch ultranarrow EIA signals.

In this chapter we describe our major experimental breakthrough in which we observe ultra-narrow EIA signals, which were theoretically predicted due to TOP and TOC in cycling transition of DTLS of $^{85}$Rb atoms. The experimentally observed linewidths of EIA signal are less than 100 kHz and much narrower than one predicted in [29]. For this purpose we used two different experimental schemes by using single laser combined with two acousto-optic modulators (AOMs) to investigate theoretical predictions. The experimental ultra-narrow EIA features matched well with simulated spectra obtained by using generalized time-dependent optical Bloch equations.

## 5.2 Experimental Setup

The experimental setup for same circular polarization configuration is shown in Fig. 5.1. We used four different experimental schemes for different polarization combinations of pump and probe laser fields.

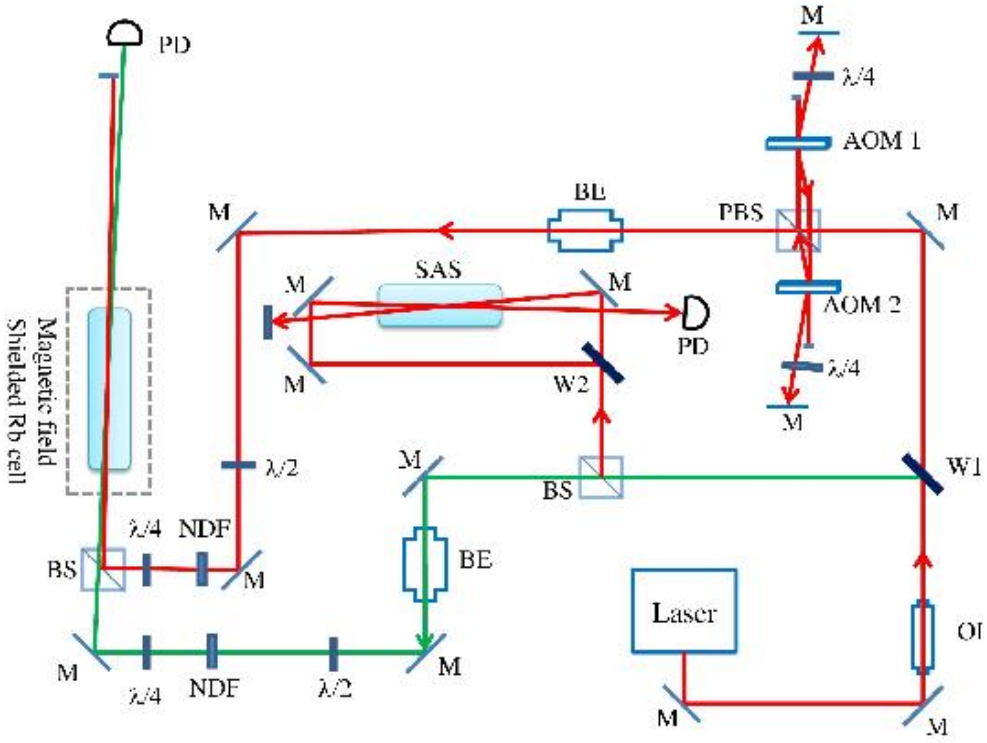


Fig. 5.1 Schematic of the experiment with one laser for both control and probe laser beams. Figure key**:** M-mirror, OI-optical isolator, W-window, AOM-acousto-optic modulator, BE-beam expander, λ/2- half wave plate, λ/4-quarter wave plate, NDF- neutral density filter, PBS-polarizing beamsplitter, PD-photodiode and BS-beam splitter.

A 780 nm homemade external cavity Diode laser (ECDL) is used for both pump and probe beams. The frequency of probe beam is fix and locked on $F_g = 3 \rightarrow F_e = 4$ of $^{85}$Rb D2 transition line by using home-made lock-in amplifier. As shown in Fig, the vertically polarized laser beam is first divided into pump and probe beams by using first window (W1). After window the

reflected beam is further divided into two equal portions by beam splitter (BS). At this point the one part of beam (transmitted) is used as a probe beam for EIA experiment while the other part (reflected) of this beam is used for SAS experiment. The scanning of pump laser frequency is achieved by using two acousto-optic modulators (AOM). The vertically polarized transmitted beam from window (W1) of frequency $\omega_0$ was sent into first AOM1. The AOM will be adjusted to be at Bragg angle such that only first and zero orders beam will be emitted. Here we used the method of double pass of pump beam through AOM1. As zero order beam is not important and there is no more any use of it throughout the experiment that is why we blocked it. To change the polarization state of the first order up-shifted pump beam, this beam passed through quarter wave plate and focused on mirror. Here at this point the pump beam was reflected to trace back the original path passing through all optics and then into AOM1. As the beam has passed through AOM1 twice which results the beam frequency up-shifted to $\omega_0 + 2\omega_1$ , where $\omega_1$ is the central frequency of AOM1. Here the polarization of pump beam has changed from vertical to horizontal polarization because this beam passed twice through quarter wave plate. Now at this stage pump beam can pass through PBS. This doubly up-shifted ($\omega_0 + 2\omega_1$) pump beam was once again sent into second AOM2 for double pass down shift in frequency which results as $\omega_0 + 2\omega_1 - 2\omega_2$ where $\omega_2$ is the central frequency of AOM 2. Again this pump beam passed through $2^{nd}$ quarter wave plate twice so the polarization of this doubly down shifted beam will be vertically polarized just before PBS. Now this beam will be deflected by PBS at 90 degree. Two separate beam expanders were used to expand the pump and probe lasers

beams equal to 4mm in diameter. The polarization of pump and probe lasers beams were made perfectly vertical and horizontal respectively just before first common beam splitter (PBS) by using two half wave plates.

This experimental setup can be used for two different polarization configurations of probe and pump lasers beams. One of them is linear and parallel case while the other is same-circular polarization configuration. As discussed above that pump beam is vertically polarized. Now by using half wave plate, the probe beam was also made as vertically polarized which can be checked by using polarimeter. Two separate quarter wave plates with optics axis angle $\varepsilon = 45$ with respect to y-axis are inserted in front of both pump and probe laser beams just before the BS which prepared the right circular polarized pump and probe lasers beams. Both beams are mixed at BS and well overlapped in the vapor cell. At long distance these two beams are separated. The pump beam is blocked while the probe beam is focused on photodiode.

In case of linear and parallel polarization configurations of pump and probe lasers beams, one need to remove only two quarter wave plate from above setup of same-circular polarization configuration. In this case both the beams are vertically polarized which interacts with atoms in the cell. Similarly this setup can also be used in case of circular and orthogonal polarization configuration as well as linear and perpendicular polarization configuration of pump and probe laser beams by changing the optics axis angle of half wave plate and quarter wave plate. But one can get more batter and narrow EIA signal by making some modification in above experimental setup without disturbing main setup. Replacing BS by PBS and inserting two

quarter wave plates just before and after Rb vapor cell. Finally one PBS should be inserted before the photodiode. In this way when vertically polarized control and horizontally polarized probe beams are mixed at first PBS then these two beams look like to be one beam because of very well overlapping. First of all these two beams passed through first quarter wave plate. When the polarization angle of quarter wave plate is set at ε = -45 degree with respect to y-axis, then This arrangement prepared pump beam as left circularly polarized and at the same time initially horizontally polarized probe beam will be right circularly polarized. These two circular and orthogonal pump and probe lasers beams interact with Rb atoms in the cell. Now placing another quarter wave plate after cell at ε =- 45 degree with respect to y-axis will make again control beam as vertical polarized and probe bean as horizontal polarized. These two beams can be separated by placing another PBS after Rb cell. This PBS reflects the vertically polarized pump beam and allow horizontally polarized probe beam to transmit. The transmitted probe beam is detected by photo diode.

Similarly in case of linear and perpendicular polarization configuration we need to remove both quarter wave plates from the setup. In this situation after $1^{st}$ PBS the control beam is vertically polarized while the probe beam is horizontally polarized. When these two well overlapped beams reached at $2^{nd}$ PBS after passing through Rb vapor cell, the vertical pump beam reflected at 90 degree and horizontally polarized probe beam is transmitted. The reflected beam is blocked while the transmitted beam is detected by photodiode.

A ramping voltage of $125mV_{pp}$ (peak to peak) which allow the pump beam

to detune in the range of 5MHz. The intensities of both beams were controlled by two separate neutral density filters (NDF). Maximum power of control beam which is used in this experiment was 1mW while the power of probe beam used here between 10 and 20 μW.

## 5.3 Experimental results

In this part of thesis we explain the theoretical calculated and experimentally observed ultra-narrow EIA signals which are obtained by using experimental setup shown in figure 5.1.

### 5.3.1 Circular polarization case

In case of same circular polarization combination of pump and probe laser fields, the theoretically calculated and experimentally observed probe absorption spectra are shown in Fig 5.2 (a) and (b) respectively. The absorption spectra from the cycling transition line in DTLS of thermal $^{85}$Rb atoms were obtained between -2 MHz and 2 M Hz. To investigate the spectral variations in probe absorption spectra, we changed the power of pump laser beam while the power of probe beam was fixed at constant value

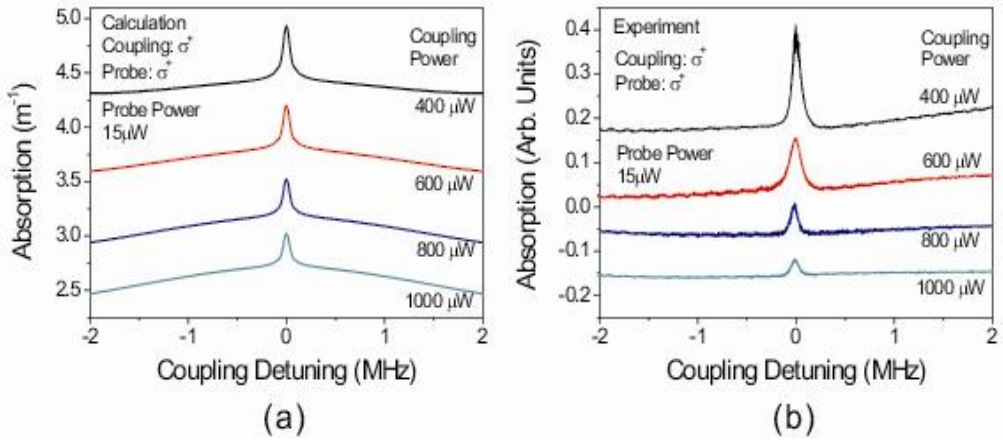


Fig. 5.2 (a) Theoretical and (b) experimental EIA spectra in the case of same circular polarizations of the probe and coupling beams with respect to the changes of pump powers.

Compare to natural linewidth of upper state which is 6.1M Hz the observe linewidth is much narrow. Doppler broadening, laser line linewidth, laser power, decay rate *etc*. are some factors which can affect the linewidth of EIA signal. The experimentally measured linewidth of EIA signal at pump power of 400 μW is approximately equal to 90 kHz while the theoretically calculated linewidth is equal to 87 kHz which show the higher degree of matches between observed and calculated linewidth. Much narrower linewidth of EIA signal can be produced by using laser with linewidth narrow than our case. This EIA spectrum is not split differently from orthogonal circular and linear cases, which the EIA signals are split and broadened when the coupling powers are increased moderately and because of thermal averaging effects there is no splitting in spectra with strong power of pump beam. In case of same polarization of pump and probe beams, there

have been some theoretically predictions about such EIA spectra but no one reported this type of observation in case of same polarization. Only one experimental observation [38] was reported with same polarization configuration but they could not able to produce such ultra-narrow EIA signal and most probably it happened due to high power of pump laser and combined linewidth of two independent lasers sources.

As shown in Fig. 5.2 when the powers of the pump beam increase, the strengths of the EIA signal are decreasing. As explained in detail in chapter 4 the ultra-narrow EIA signal for a stationary atom exists at lower coupling beam power and diminishes with the increased pump beam power. This ultra-narrow signal remains for thermal atoms and also another factor can cause to produce narrow EIA signal. In this case at zero detuning of pump beam the resonance exist irrespective of atomic velocity. Since the slope of the resonance at positive and negative value of the velocity is precisely opposite, a narrow absorption signal can be observed. This effect can only support to produce narrow signal when the power of pump beam is high. That is why the intensity of whole EIA signals decreases as the power of pump beam increases.

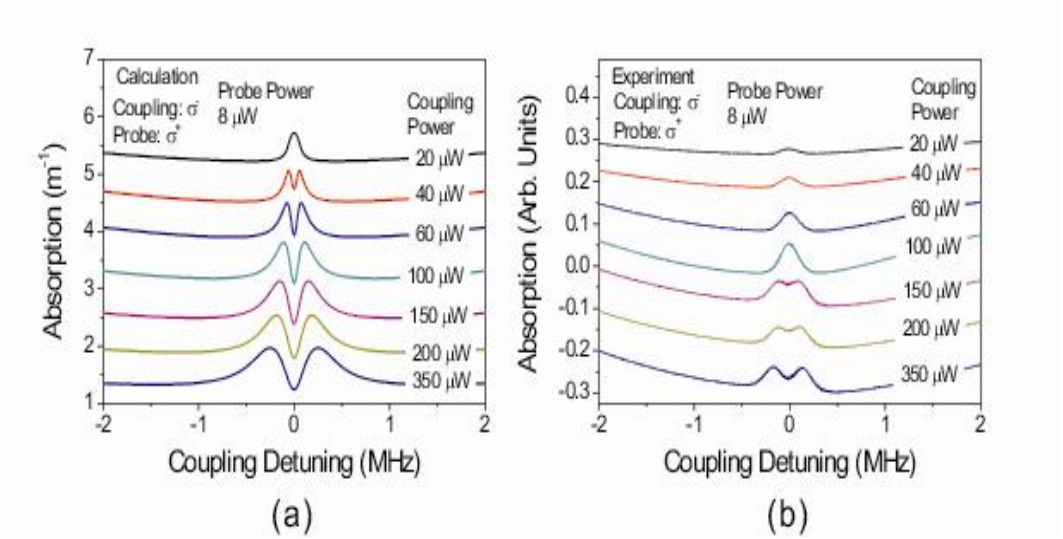


Fig. 5.3 (a) Theoretical and (b) experimental EIA spectra in the case of orthogonal circular polarizations of the probe and coupling beams with respect to the changes of pump powers.

The theoretical calculated and experimentally observed probe absorption spectra between -2 MHz and 2 MHz in case of circular and orthogonal polarization configuration are shown in Fig 5.3 (a) and (b) respectively. Based on theoretical prediction the splitting of EIA signal into two at even sufficient low power of pump beam is due to thermal averaging effect. In chapter 4 as we discussed in detail that in cold atomic case the splitting of EIA signal could not be observed. In splitting of EIA signal the power of pump laser play vital role due to TOC effects. Compare to linear and perpendicular polarization case the splitting in circular and orthogonal case of polarization occur at relatively low power of pump beam. The author of reference [48] also described that TOC effect in case of linear and

perpendicular polarization combination of pump and probe laser can take place in higher pump power than decay rat of upper excited state. The strong pump power can generate Mollow-triplet [59] type splitting lines. But so far there is no any report to observe these ultranarrow splitted resonances due to TOC which provide the linewidth below 100 kHz instead of very wide feature due to power of pump laser. In chapter 4 we have explained the thermal averaging effects on splitting of line due to pump powers between same and perpendicular circular polarization cases by using dressed state formalism. We could not observe the splitting at the central region of resonance line in case of same circular polarization of both beams because absorption resonances due to positive and negative atomic velocities cancel each other. On the other hand at central region in case of orthogonal polarization of pump and probe beams, the ultranarrow split EIA signals exist at $\sim\pm[1-(15/28)^{1/2}]\,\Omega_2$. From these theoretical and experimental investigation and discussion we understand that power dependences of the spectral profiles in the orthogonal- and same- polarization configurations in thermal state are pretty dissimilar from those in cold state. Because of wider linewidth of laser being used in experiment the experimentally observed spectra shown in Fig 5.3 (b) in lower power of pump beam are not splitted well as in case of theoretical calculation shown in Fig. 5.3(a).

## 5.4 Linear polarization cases.

Now we explain our next experimental results which were performed in case of linear polarized of pump and probe beams. The optical pumping effect in linear polarization case is weaker as compare to circular polarization case. As linearly polarized pump beam can cause to exist the atomic

populations at magnetic sub-levels so the theoretical calculation in linear polarization cases are more tedious and complex as compare to circular polarization case. The comparison between calculated and experimentally observed probe spectra in case of same-linear polarization combinations are shown in Fig. 5.4 (a) and (b) respectively

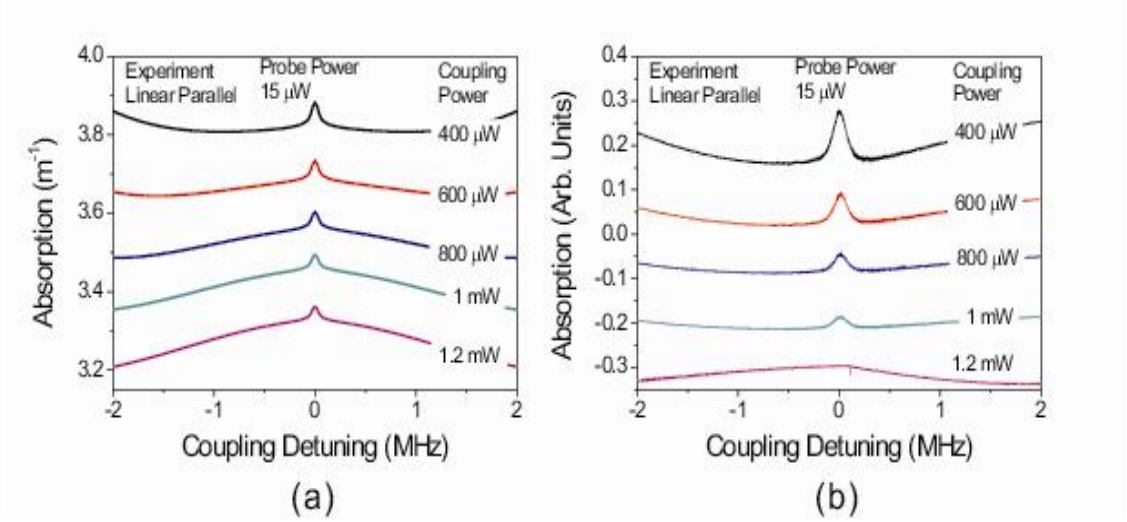


Fig. 5.4 (a) Theoretical and (b) experimental EIA spectra in the case of same linear polarizations of the probe and coupling beams with respect to the changes of pump laser powers.

The observed linewidth of ultra-narrow signals in case of linear polarization is 150 kHz. In case of same polarization, it is interesting to have similar spectra between linear and circular polarization configuration because these two schemes primarily identical except for different transitions strength and population accumulation in circular polarization case. The pump and probe beams tuned to the same transition line and TOP play important role in

generating EIA signals in both cases.

It can be seen from Fig 5.4 (b) that the magnitudes of observed signals are decreasing with the increases of pump powers which show quite similar behavior as in case of same-circular polarization and above 1 mW, the experimental EIA signal disappear. May be in all previous experimental works different researcher groups used high powers of pump and probe lasers in case of same polarization configuration and concluded that in same polarization case N or V-type connection cannot be formed so occurrence of EIA in this case is not possible.

The comparison between theoretically calculated and experimentally observed spectra in case of linear and orthogonal polarization combinations are shown in Fig. 5.5 respectively. With an increase in pump power the subnatural ultranarrow EIA signal become wider and then split into two near 2 mW theoretically as shown in Fig. 5.5 (a) but in case of circular and orthogonal case this splitting start relatively very low power of pump beam. Up to 1 mW we can observe well matched theoretical calculated and experimental observed spectra shown in Fig. 5.5 (a) and (b). Due to some experimental limitations we could not increase the power of pump beam more than 1mW and that is why we could not observe the splitting in experimental spectra which is shown in theoretical calculated one.

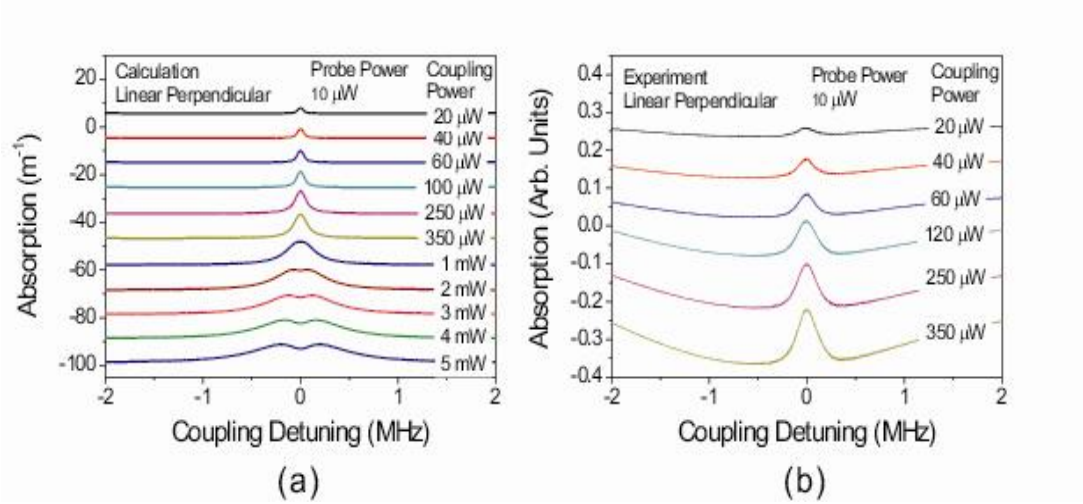


Fig. 5.5 (a) Theoretical and (b) experimental EIA spectra in the case of orthogonal linear polarization configuration with respect to the changes of pump powers.

Compare to circular and orthogonal polarization, the splitting power of pump beam is very high in linear and perpendicular polarization case because the separation of the dressed state for a magnetic sublevel is not quite different from that for closest magnetic sublevel. The separations between the resonances for a stationary atom in the orthogonal linear scheme are 0.024 $\Omega_2$, 0.077 $\Omega_2$, 0.15 $\Omega_2$, and 0.5 $\Omega_2$, while the separation in the orthogonal circular scheme is 0.27 $\Omega_2$. Therefore, we need approximately 10 times larger Rabi frequency in linear scheme than in circular scheme in order to see a similar spacing between the two absorption peaks.

# Chapter 6

## Conclusions

Based on different polarizations combinations, powers and direction of pump and probe laser fields we have shown the variations in probe transmission spectra from hyperfine levels between ground $5S_{1/2}$ and excited $5P_{1/2}$ D2 line of Rb atoms at room temperature using degenerate two-level atomic system. Various polarization dependent profiles in absorption and transmission signal with EIT-like and EIA signal have been observed. We calculate EIA spectra by solving time-dependent full density matrix equations for the transition $F_g = 3 \rightarrow F_e = 4$ of the $^{85}$Rb-D2 line. Compared to the existing calculating methods more accurate EIA spectra can be produced since our method does not employ any phenomenological constants and is based on temporal solutions of the density matrix elements. From this new theoretical method, EIA spectra with ultra-narrow linewidths embedded in broad sub-natural EIA, in the case of the same and orthogonal circular-polarization configurations of coupling and probe lasers have been obtained theoretically.

Thermal averaging effects on spectral features such as additional ultra-narrow and split spectral profiles of EIA embedded in broad sub-natural EIA have been investigated with respect to powers of coupling beam. The EIA signals have ultra-narrow EIA signals in low powers of coupling and probe laser beams in both same- and orthogonal-polarization configurations irrespective of thermal averaging of the EIA signals. However, the ultra-narrow EIA signals from high powers of coupling laser beams in the same-

polarization configuration have disappeared and still remained in the ultra-narrow state in zero velocity and thermal averaging cases, respectively. The ultra-narrow EIA signals in the orthogonal-polarization configuration from high powers of coupling laser beam have disappeared and split into two in zero velocity and thermal averaging cases, respectively. Origins of the existence of ultra-narrow EIA spectra and splitting of the ultra-narrow EIA spectra under high power and thermal averaging have been revealed. The observed EIA spectral profiles of probe transmission for the case of same- and orthogonal-polarization configurations of coupling and probe laser beams match well with the calculated spectral profiles of probe transmission. We also confirm coherent effects in EIAs by checking the differences between probe-transmission profiles with and without coherence terms of density matrix elements in the density matrix equations, which elucidates in detail the EIA spectral-line profiles according to laser detuning.

We observe strange behaviors of observed EIA signals depending on circular and linear polarizations and power variations of the coupling and probe lasers. The EIA signals with sub-natural linewidth of ~ 90 kHz even in the cases of same circular and linear polarization configuration have been obtained for the first time to the best of our knowledge. Ultra-narrow splittings of EIA spectra with the increase of the laser powers in the case of orthogonal polarization were obtained. EIA signal was decreased in the case of same polarization case with the increase of coupling powers due to TOP. In weak coupling power limit of orthogonal polarization configurations, thermal averaging effects plays major role in the splitting of the EIA spectra while in strong coupling power, Mollow triplet-like mechanism due to strong

power bring into broad split feature. The experimental ultra-narrow EIA features using one laser combined with an AOM match well with simulated spectra obtained by using generalized time-dependent optical Bloch equations.

# References

[1] A. M. Akulshin, S. Barreiro and A. Lezama, "Electromagnetically induced absorption and transparency due to resonant two-field excitation of quasi degenerate levels in Rb vapor," Phys. Rev. A **57**, 2996-3002 (1998).

[2] A. Lezama, S. Barreiro and A. M. Akulshin, "Electromagnetically induced absorption," Phys. Rev. A **59**, 4732 -4735 (1999).

[3] H. Failache, P. Valente, G. Ban, V. Lorent and A. Lezama, " inhibition of electromagnetically induced absorption due to excited-state decoherence in vapor cell," Phys. Rev. A **67**, 043810-043817 (2003).

[4] I. B. Aroya and G. Eisenstein, "Observation of large contrast electromagnetically induced absorption resonance due to population transfer in a three level Λ-system interacting with three separate electromagnetic fields," Opt. Express **19**, 9956-9961(2011).

[5] S. R. Chanu, K. Pandey and V. Natarajan, "Conversion between electromagnetically induced transparency and absorption in a three-level lambda system," Euro. Phys. Lett. **98**, 44009-44015 (2012).

[6] X. Yang, J. Sheng and M. Xiao, "Electromagnetically induced absorption via incoherent collisions," Phys. Rev. A **84**, 043837-043842 (2011).

[7] H. J. Kim and H. S. Moon, "Electromagnetically induced absorption with sub-kHz spectral width in a paraffin-coated Rb vapor cell," Opt. Express **19**, 168-173 (2011).

[8] F. Fleischhauer, A. Imamoglu and J. P. Marangos, "Electromagnetically induced transparency: Optics in coherent media," Rev. Mod. Phys. **77**,

633-673 (2005)

[9] Y. Wu and X. Yang, "Highly efficient four-wave mixing in double-Λ system in ultraslow propagation regime," Phys. Rev. A **70**, 053818-053823 (2004).

[10] Y. Wu and X. Yang, "Electromagnetically induced transparency in V-, Λ-, and cascade-type schemes beyond steady-state analysis," Phys. Rev. A **71**, 053806 – 053813 (2005)

[11] M. D. Lukin, "Trapping and manipulating photon states in atomic ensembles," Rev. Mod. Phys. **75**, 457-472(2003).

[12] K. HaAmmerer, A. S. Sørensen and E. S. Polzik, "Quantum interface between light and atomic ensembles," Rev. Mod. Phys. **82**, 1041 - 1093(2010)

[13] A. M. Akulshin, A. Cimmino, A. I. Sidorov, P. Hannaford and G. I. Opat, "Light propagation in an atomic medium with steep and sign-reversible dispersion," Phys. Rev. A **67**, 011801(R) -011805(R) (2003).

[14] A. Lezama, A. M. Akulshin, A. I. Sidorov and P. Hannaford, "Storage and retrieval of light pulses in atomic media with "slow" and "fast" light," Phys. Rev. A **73**, 033806- 033810(2006).

[15] S. R. Chanu, A. K. Singh, B. Brun, K. Pandey and V. Natarajan, "Subnatural linewidth in strongly-driven degenerate two-level system," Opt. Commun. **284**, 4957-4960 ( 2011).

[16] J. Dimitrijević, A. Krmpot, M. Mijailović, D. Arsenović, B. Panić, Z. Grujić and B. M. Jelenković, "Role of transverse magnetic fields in electromagnetically induced absorption for elliptically polarized light," Phys. Rev. A **77**, 013814-013826 (2008).

[17] F. Renzoni, C. Zimmermann, P. Verkerk and E. Arimondo, "Enhanced absorption Hanle effect on the $F_g = F \rightarrow F_e = F + 1$ closed transitions," J. Opt. B: Quantum Semiclass. Opt. **3** S7-14 **(**2001).

[18] S. M. Iftiquar**,** G. R. Karve , and V. Natarajan, "Subnatural linewidth for probe absorption in an electromagnetically induced transparency mediumdue to Doppler averaging," Phys. Rev. A **77,** 063807- 063812 (2008).

[19] M.M. Hossain, S. Mitra, B. Ray, and P.N. Ghosh, "Double EIT and enhanced EIT signal in a combination of Λ- and V-type system of Rb-$D_2$ transition," J. Phys B: At. Mol. Opt. Phys. **103**, 117-122 (2010).

[20] S. R. Chanu, K. Pandey, and V. Natarajan, "Conversion between electromagnetically induced transparency and absorption in a three-level lambda system," EPL **98**, 44009-44015 (2012).

[21] H. J. Lee and H. S. Moon, "Intensity correlation and anti-correlation in electromagnetically induced absorption," Opt. Express **21**, 2414-2422 (2013).

[22] X. Yang, J. Sheng, and M. Xiao, "Electromagnetically induced absorption via incoherent collisions," Phys. Rev. A **84**, 043837-043841 (2011).

[23] H. U. Rehman, M. Adnan, H.-R. Noh, and J. T. Kim, "Spectral features of electromagnetically induced absorption in $^{85}$Rb atom," J. Phys. B. **48**, 115502-115511 (2015).

[24] R. Drampyan, S. Pustelny, and W. Gawlik, "Electromagnetically induced transparency versus nonlinear Faraday effect: Coherent control of light-beam polarization," Phys. Rev. A **80,** 033815-033824 (2009).

[25] Z. J. Ming, Z. Y. Ting, H. Tao, X. L.Tuan and J. S. Tang, "Observation of EIA in closed and open cesium atomic system," Chin. Phys.soc. **14,** 725-728 (2005)

[26] P. M. Anisimov, J. P. Dowling, and B. C. Sanders, "Objectively Discerning Autler-Townes Splitting from Electromagnetically induced transparency," Phys. Rev. Lett. **107**, 163604-63608 (2012).

[27] C. Andreeva, S. Cartaleva, Y. Dancheva, V. Biancalana, A. Burchianti, C. Marinelli, E. Mariotti and L. Moi, "Coherent spectroscopy of degenerate two-level systems in Cs," Phys. Rev. A **66**, 012502-012514 (2002).

[28] A. Lezama, S. Barreiro, A. Lipsich and A. M. Akulshin, "Coherent two-field spectroscopy of degenerate two-level systems," Phys. Rev. A **61**, 013801-013812 (1999).

[29] T. Zigdon, A. D. W-Gordon, and H. Friedmann, "Pump-probe spectroscopy in degenerate two-level atoms with arbitrarily strong fields," Phys. Rev. A **77**, 033836- 033846 (2008).

[30] S. K. Kim, H. S. Moon, K. Kim and J. B. Kim, "Observation of electromagnetically induced absorption in open systems regardless of angular momentum," Phys. Rev. A **68**, 06813-06818 (2003).

[31] H. S. Chou and J. Evers, "Dressed-atom multiphoton analysis of anomalous electromagnetically induced absorption,"Phys. Rev. Lett.

**104**, 213602- 213604 (2010).

[32] A. Lezama, G. C. Cardoso and J. R. Tabosa, "Polarization dependence of four-wave mixing in a degenerate two-level system," Phys. Rev. A **63**, 013805-013812 (2000).

[33] A. Akulshin, M. Singh, A. sidrovo and P. Hannaford, "steep atomic dispersion induce induced by velocity-selective optical pumping," Opt. Exp. **29**, 15463-15468 (2008).

[34] C. Goren, A. D. W. Gordon, M. Rosenbluh and H. Friedmann, "Atomic four-level N system," Phys. Rev. A **69**, 053818-053828 (2004).

[35] A. Lezama, S. Barreiro, and A. M. Akulshin, "Electromagnetically induced absorption," Phys. Rev. A 59, 4732-4735 (1999).

[36] D. V. Brazhnikov. A. M. Tumaikin, and V. I. Yudin "Electromagnetically induced absorption and tranperency in magneto optical resonances in ellipitically polarized field," Opt. Sco. Am. B **22**, 010057-010064(2005).

[37] M. Kwon, K. Kim, H. D. Park, and J. B. Kim, "Dependence of EIA spectra on mutual coherence between pump and probe fields in Cs atomic vapors," J. Kor. Phys. Soc. **40**, 452-455 (2002).

[38] A. Lipsich, S. Barreiro, A. M. Akulshin, and A. Lezama, "Absorption spectra of driven degenerate two-level atomic systems," Phys. Rev. A **61**, 053803-053813 (2000).

[39] Y. C. Chen, I. A. Yu, "*The coherence induced phenomena in cold atom,"* (Tsinghua University,) 2002

[40] K. J. Boller, A. Imamoglu and S. E. Harris, " Observation of

electromagnetically induced transparency, “ Phys. Rev. Lett. **66**, 2593-2596 (1991).

[41] K. Dahl, L. S. Molella, R.H. Rinkleff, and K. Danzmann, “Switching from “absorption within transparency” to “transparency within transparency” in an electromagnetically induced absorption dominated transition,” Opt. Lett. **33** (9), 983-985 (2008).

[42] Z. Y. Ting, Z. J. Ming, X. L. Tuan, Y. W. Bao and J. S.Tang, “Electromagnetically induced absorption and transparency spectra of degenerate tow-level system with a strong coupling field in Cs vapor,” Chin. Phys. Lett. **21**, 76-78 (2004).

[43] A. D. W-Gordon and H. Friedmann ,“Ultranarrow extraresonant antiholes in pump–probe spectroscopy induced by inelastic collisions,” Opt. Lett. **14**, 390 -392 (1989).

[44] V. S. Letokhov and V. P. Chebotayev,” Nonlinear Laser Spectroscopy”, (Springer Series in Optical Sciences) **4**, 80-83 (1977).

[45] A. V. Taichenachev, A. M. Tumaikin, and V. I. Yudin, “Electromagnetically induced absorption in a four-state system,” Phys. Rev. A **61**, 011802-011806 (1999).

[46] C. Goren, A. D. W-Gordon, M. Rosenbluh, and H. Friedmann, “Electromagnetically induced absorption due to transfer of population in degenerate two-level system,” Phys. Rev. A **70**, 043814-043822 (2004).

[47] C. Goren, A. D. W. Gordon, M. Rosenbluh and H. Friedmann, "Electromagnetically induced absorption due to transfer of coherence and to transfer of population," Phys. Rev. A **67**, 033807-033815 (2003).

[48] T. Zigdon, A. D. Wilson-Gordon, and H. Friedmann, "Absorption spectra for strong pump and probe in atomic beam of cesium atoms," Phys. Rev. A **80**, 033825-033834 (2009).

[49] H. S. Moon, L. Lee, and J. B. Kim, "Double resonance optical pumping effects in electromagnetically induced transparency," Opt. Express **16**, 12163-12167 (2008).

[50] C. G. Aminoff, M. Pinard, "Velocity selective optical pumping" J. Physique **43**, 263-277 (1982).

[51] S. J. Park, H.S. Lee, H. Cho, and J. D. Park,"velocity selective optical pumping spectroscopy of 87Rb D2 line by using two co-propagating laser beams," J. Kor. Phys. Soc. **33,** 281-287 (1998).

[52] S.Chakrabarti, A. Pradhan, B. Ray and P. N. Ghosh. "Velocity selective optical pumping effects and electromagnetically induced transparency for D2 transitions in rubidium," J. Phys. B: At. Mol. Opt. Phys. **38** 4321-4327 (2005).

[53] S. Chakrabarti, B. Ray and P. N. Ghosh. "Velocity selective optical pumping effects with counter and co-propagating laser radiation for D2 line of rubidium," Eur. Phys. J. D. **42**, 359-368 (2007).

[54] A. J. Krmpot, M.D. Rabasvic, and B.M. Jelenkovic, "Optical pumping

spectroscopy of Rb vapor with co-propagating laser beams: line identification by a simple theoretical model," J. Phys. B: At Mol. Opt. Phys. **43,** 135402-135409 (2010).

[55] S. Mitra, M.M Hossain, B. Ray, P. N Ghosh, S Cartaleva, D. Slavov, "Coherent laser spectroscopy of rubidium atoms," Laser phys. Application SPIE.**7747**, 77470-77479 (2011).

[56] D. Bhattacharyya, A. Bandyopadhyay, S. Chakrabarti, B. Ray, P. N. Ghosh, "Velocity dependent pump-probe spectroscopy for a five-level system: An application to Rb D2 transitions," Chem. Phys. Lett **440**, 24-30 (2007).

[57] S. Chakrabarti, A. Pradhan, A. Bandyopadhyay, A. Ray, B. Ray, N. Kar, P.N. Ghosh, "Velocity-selective resonance dips in the probe absorption spectra of Rb D2 transitions induced by a pump laser," Chem. Phys. Lett. **399**, 120-124 (2004**).**

[58] A. Krasteva, B. Ray, D. Slavov, P. Todorov, P. N. Ghosh, S. Mitra, and S, Cartaleva, "Observation and theoretical simulation of electromagnetically induced transparency and enhanced velocity selective optical pumping in cesium vapor in a micrometric thickness optical cell," J. Phys. B: At Mol. Opt. Phys. **47,** 175004 -175016 (2014).

[59] B. R. Mollow, "Stimulated Emission and Absorption near Resonance for Driven Systems," Phys. Rev. A **5**, 2217-2222 (1972).

[60] H. R. Noh and W. Jhe,"Semi classical theory of sub-Doppler forces in an asymmetric magneto-optical trap with unequal laser detuning," Phys.

Rev. A **75**, 053411-053420 (2007).

[61] J. Sagle, R. K. Namiotka and J. Huennekens, "Measurement and modelling of intensity dependent absorption and transit relaxation on the cesium D1 line," J. Phys. B: At. Mol. Opt. Phys. **29**, 2629-2643 (1996).

[62] F. Renzoni, W. Maichen, E. Windholz and E. Arimondo, "Coherent population trapping with losses observed on the Hanle effect of the D1 sodium line," Phys. Rev. A **55,** 3710-3718 (1997).

# Acknowledgements

Completing this work has been one of the biggest challenges of my life and I must say that I cannot have got through this without helps of every single person which I mention below. I would like to take this opportunity to pay thanks to all these people who have helped me and given me encourage in making this thesis possible.

First of all I would like to express my gratitude and deep appreciation to my advisor, professor Jin-Tae Kim for his matchless support, valuable discussion, and guidance during all stages of my Ph.D studies.

I would like to thank my parents for their constant support especially to my mother who passed away during my PhD study. I am very thankful to my brothers, Shajahan and Aziz ur Rehman for their support and encouragement. Besides all these I am very thankful to my beloved wife for her efforts with my little loving daughter Rida Fatima in my absence and I really appreciate her efforts. It has been a great opportunity for me to do my research in the laser application lab, Chosun University in Korea. During this study I have really enjoyed the group meetings and discussions with my advisor professor Jin-Tae Kim, Muhammad Adnan, and Muhammad Mohsin Qureshi to boost up my knowledge about atomic physics and laser spectroscopy.

I have received the enormous support from professor Heung-Ryoul Noh in Chonnam National University in Korea and I also express my gratitude to him. It was great pleasures for me to do work with previous and present students in a dark laboratory under the supervision of my advisor.

Finally I would like to thank my professors in Pakistan Dr. Muhammad

Khalid and Dr. Noor Abas Din for their engorgements and supports.

**August 2015**

**Ph.D. Dissertation**

# Study on spectral features of electromagnetically induced absorption in degenerate two-level system of $^{85}$Rb atoms

Graduate School of Chosun University

**Department of Photonic Engineering**

**Hafeez-Ur- Rehman**

# Study on spectral features of electromagnetically induced absorption in degenerate two-level system of $^{85}$Rb atoms

축퇴된 이준위 시스템 루비듐 원자의
전자기적으로 유도된 흡수 분광선 특성 연구

**August 25, 2015**

Graduate School of Chosun University

**Department of Photonic Engineering**

**Hafeez-Ur- Rehman**

# Study on spectral features of electromagnetically induced absorption in degenerate two-level system of $^{85}$Rb atoms

**Advisor: Prof. Jin-Tae Kim**

*This dissertation is submitted to the Graduate School of Chosun University in partial fulfillment of the requirements for the degree of Doctor of Philosophy in Science*

**April 2015**

Graduate School of Chosun University

**Department of Photonic Engineering**

**Hafeez-Ur- Rehman**

This is to certify that the PhD thesis of **Hafeez-Ur-Rehman** has successfully met the dissertation requirements of Chosun University**.**

Chairman (Chosun Univ.) : Prof. Jong-Rak Park .....

Member (Chosun Univ.) : Prof. Jin-Tae Kim .....

Member (Chosun Univ.) : Prof. Hyun Su Kim .....

Member (Chosun Univ): Prof. Tae-Jung Ahn .....

Member (Chonnam Univ):Prof. Heung-Ryoul Noh.....

**June 2015**

Graduate School of Chosun University

# Contents

# List of figures

# 초록

# 축퇴된 이준위 시스템 루비듐 원자의 전자기적으로 유도된 흡수 분광선 특성 연구

Hafeez-Ur- Rehman

Advisor: Prof. Jin-Tae Kim

Graduate School of Chosun University

Department of Photonic Engineering

결합광과 조사광의 편광, 파워, 방향에 따른 축퇴된 상온 셀내에 있는 루비듐 원자의 기저준위와 여기준위 D2 사이의 초미세 구조에서 약한조사빔의 투과 신호의 분광선에 대한 실험적, 이론적 고찰을 본 논문에서 연구한다. 조사광은 $F_g$ =3→$F_e$ =4 에 주파수 잠금되고, 결합광은 기저준위 $F_g$ = 2와 3에서 여기준위 $F_e$= 1, 2, 3, 4 사이를 주사 한다. 축퇴된 이원자 준위에서 조사광과 결합광의 편광은 여기준위로부터의 밀도 이전,EIA 혹은 EIT 신호 의 분광선 모양 등에 중요한 역할을 한다. 약한 조사광과 강한 결합광의 경우에 닫혀진 계에서 좁은 선폭과 넓은 선폭을 가지는 이중 구조 분광선이 광펌핑에 의해 얻어진다. 이러한 광펌핑 효과 등이 광 밀도 방정식에 의해 얻어진 분광선과 실험적으로 얻어진 분광선과 비교되었다.

또한, 상온에서 매우 좁은 분광선 선폭을 가지는 EIA 신호가 얻어졌

다. 이러한 매우 좁은 선폭을 가지는 분광선이 같은 편광 ($\sigma^+$-$\sigma^+$, $\pi \parallel \pi$) 과수직 편광 ($\sigma^+$-$\sigma^-$,$\pi \perp \pi$) 구도에서 연구되었다. 같은 편광의 경우 ~90 kHz 정도의 EIA 신호가 처음으로 실험적, 이론적으로 확인되었다. 이러한좁은 선폭을 가지는 EIA 신호를 연구하기 위해 파워와 편광이 일반화된 광 밀도 방정식의 해의 결과와 실험적으로 얻은 결과와 비교한 결과, 매우 잘 일치함을 확인하였다.

# ABSTRACT

## Study on spectral features of electromagnetically induced absorption in degenerate two-level system of $^{85}$Rb atoms

Hafeez-Ur- Rehman

Advisor: Prof. Jin-Tae Kim

Graduate School of Chosun University

Department of Photonic Engineering

We present experimental and theoretical studies on spectral profile variations of weak probe beam transmission signal from hyperfine level between the ground 5 $S_{1/2}$ and excited 5 $P_{3/2}$ D2 lines of $^{85}$Rb atom at room temperature with degenerate magnetic sublevels in the case of polarization configurations, powers, and directions of control and probe beams. The probe laser frequency is fixed and locked at the $F_g = 3 \rightarrow F_e = 4$ degenerate two level system of $^{85}$Rb atom while the control beam is scanned through F" = 2 and 3 → F" = 1, 2, 3, and 4. In degenerate two-level system polarizations of probe and control laser fields play important roles to transfer of population from excited states. Consequently variation in absorption and transmission signal profiles including EIA and EIT-like signal have been observed when the polarization state of control and probe lasers fields were changed. In case of weak probe and strong coupling laser field we observed double structure transmittance spectrum, a narrow due to

coherence and broad due to optical pumping in cycling transition. The experimental results are compared with the results calculated by solving time-dependent density-matrix equations including the optical and Zeeman coherences connected via multi-photon interactions process between magnetic levels and match well with the calculated signal profiles.

We also present theoretical and experimental study of EIA for different hyperfine transitions of $^{85}$Rb-D2 line. The calculated result in case of cycling transition of $^{85}$Rb show that EIA signal have ultra-narrow feature in low power of coupling beam in both stationary and thermal atoms. In case of thermal atom the ultra-narrow EIA signal due to high coupling power beam still remained in ultra-narrow state in the same polarization configuration. Ultra-narrow EIA spectral features of thermal $^{85}$Rb atom with respect to coupling Rabi frequencies in a degenerate Zeeman multiplet system have been unraveled in the cases of same ($\sigma^+$-$\sigma^+$, $\pi \parallel \pi$) and orthogonal ($\sigma^+$-$\sigma^-$, $\pi \perp \pi$) polarization configurations. The EIA signals with subnatural linewidth of ~ 90 kHz even in the cases of same circular and linear polarizations of coupling and probe laser have been obtained for the first time theoretically and experimentally. In weak coupling power limit of orthogonal polarization configurations, time-dependent transfer of coherence plays major role in the splitting of the EIA spectra while in strong coupling power, Mollow triplet-like mechanism due to strong power bring into broad split feature. The experimental ultra-narrow EIA features using one laser combined with an AOM match well with simulated spectra obtained by using generalized time-dependent optical Bloch equations

# Chapter 1

## Introduction

Many applications such as slowing light, quantum information processing, high-resolution spectroscopic measurements, sensitive magnetometery, atomic clocks, lasing without inversion, and light information storage [1- 23] have been developed using changes of the refractive index and nonlinear susceptibility of atoms. Electromagnetically induced absorption (EIA) [1-7] and transparency (EIT) [8-10] have been nice methods to investigate effects on the atoms due to quantum interference and coherences between atomic quantum states, which leads to the abrupt changes of the refractive index and nonlinear susceptibility, *etc*. The EIA involves two laser fields such as strong coupling and weak probe beams interacting with properly selected three quantum states [15, 20-21] and enhances probe absorption due to quantum coherence effects through three different quantum states connected with the coupling and probe lasers. EIT also occurs in three-level atomic systems which interacts with two lasers fields similarly as the EIA under proper required conditions. However, destructive quantum coherences between the quantum states in the EIT differently from the EIA cases make probe laser beams transparent to the atoms. Simple three level atomic systems [4-6, 24-26] and degenerate multilevel configuration system have been used to investigate such quantum coherence effects. Compared to non-degenerate simple three levels, degenerate two level configurations is much more complex than three level systems in reality.

The spectral profiles of the EIA and EIT are also dependent on directions, polarizations, intensities, beam sizes of the coupling and probe laser beams. The spectral profiles of the EIA and EIT show peculiar behaviors depending on directions, polarizations, intensities, beam sizes of the coupling and probe laser beams. In this work the EIA phenomena in degenerate two level system (DTLS) of rubidium atom have been investigated instead of simple three level quantum systems. Previous EIA works done in the degenerate quantum system and goals of this work have been introduced in this chapter. In this chapter previous works due to velocity selective optical pumping (VSOP) effects have also been introduced.

## 1.1 Previous EIA works in DTLS

In pump-probe experimental setup two independent laser sources or one laser combined with AOMs can be used to observe pump-probe absorption spectra of atomic samples. The advantage of one laser instead of two laser beams overcomes limit of laser beam linewidth in observed spectral width so that much narrower spectral linewidth can be obtained. Although there are many subnatural experimental observations of EIA in DTLS, the observed linewidths are still close to laser linewidths. Early previous EIA works of DTLS have focused on subnatural lineshape using two different pump and probe lasers because it brought out subnatural linewidth.

Prepared samples can be in thermal or cold state depending on how the samples have been prepared. Recent progresses in atomic cooling and

trapping have provided cold atomic samples. Also atomic beam experiments can prepare cold samples. Thermal atomic samples with large velocity distributions can also be used to do EIA experiments. Moving atoms in a cell provide velocity dependent distributions interacting with laser beams so that steady state solution cannot be applied to the system and interaction region of the atoms with the laser beam should be considered. However, most of previous works have not considered those effects. Thus thermal averaging effects occurred in hot sample have been overlooked considering only atomic samples with cold internal temperatures.

There have been number of experimental and theoretical reports [1-3, 27-42] to observe sub-natural EIA signals in DTLS depending on powers and polarizations of pump and probe laser beams. Lezama *et al*. [1] observed for the first time EIA in DTLS and reported experimental observation of narrow spectral features in the presence of two laser fields which interacts with common ground state of Rb atom. Lezama *et al*. [2] explained also that EIA occur due to transfer of coherence between interacting degenerate system in which (i) $F_g \rightarrow F_e = F_g + 1$, where $F_g$ and $F_e$ are the hyperfine quantum number of ground and excited states respectively (ii) the ground state must be degenerate ($F_g > 0$ ) and (iii) the system should be closed. Under this situation the two photon resonance conditions will populate to those Zeeman sub-levels which are coupled to that laser field.

However, Kim *et al*. [30] observed EIA signal in an open system using an orthogonal linear polarization configuration of coupling and probe laser beams with co-propagating beam directions differently from expected results of Lezama *et al*. [2]. Chou *et al*. [31] interpreted that the anomalous EIA

signal in [30] is due to splitting of the EIA signals in an open system with $F_e = F_g - 1$ using a dressed atomic picture and qualitative perturbation methods employing different power-dependence of the coupling laser. They have provided comprehensive detail to explain probe absorption spectra in DTLS on the basis of dressed-atom multiphoton spectroscopy (DAMS).

There are few experimental works using one laser to investigate EIA in DTLS. Y. C. Chen [39] used similar experimental scheme using one laser to observe the EIA single in cold $^{87}$Rb atoms. But he [39] could not observe the splitting of EIA at moderate high power of pump beam. Instead of two independent lasers experiment the author of [30] performed also one laser experiment using linear and orthogonal polarized pump and probe beams to observe ultranarrow EIA signal in Cs atom. They investigated that how the intensity of pump laser bean effect the line shape of observed ultra-narrow EIA signals.

One of other interesting features in the coherence experiments, conversion from EIA to EIT or EIT to EIA. K. Dahl *et al*. [41] presented the pump laser absorption profile for four different polarization configurations in DTLS of Cs atom. In case of circular and orthogonal polarization of pump and probe beams, the absorption within transparency and transparency within transparency were detected when the power of probe laser exceeded from power of pump beam. Absorption with in transparency was observed in case of linear and circular polarization combination of pump and probe laser fields. Z. Y. Ting *et al*. [42] observed pump power dependent EIA spectra in DTLS using linear and perpendicular polarized pump and probe laser fields. Conversion of EIA to EIT is also studied. At low power of pump beam EIA

dip signal show sub-natural line width but when the power of pump beam increase to 650 mW then EIA-dip become broader and EIT appear at the central area.

Theoretical works to understand EIA in real DTLS, especially multi-oscillation effects of pump and probe beams make the system more complex because of more sub-Zeeman levels are involved in the contribution of EIA. A. D. W-Gordon *et al*. [43] theoretically investigated the ultra-narrow extra resonant anti-hole and its origin in an open atomic two level system in which relaxation rate of excited state is less than that of ground state. Origins of EIA signal in DTLS in the same and orthogonal polarizations have not been revealed. Obviously pure two-level system cannot provide EIA signal if there is no external population or coherence input to the two levels. If we use two pump and probe lasers, N type connections cannot be provided so that EIA cannot be formed. The EIT and EIA have been explained by using V and N type of connections between two levels. However, one can expect that V or N type system cannot be formed in the case of the same polarization configuration of pump and probe laser beams so that EIA cannot occur in this case.

One of very intuitive way to understand EIA origin was investigated by A. V. Taichenachev *et al*. [45]. They used this four-level system and interpreted that decay from TOC could create EIA signal which was similar to the case of perpendicular polarization combination. In the DTLS differently from this simple 4-levels system, the polarizations of the pump and probe laser beams play vital role in Zeeman coherences of the ground and excited states, transfer of the coherence from the excited states,

contribution to optical coherences between the ground and excited states because the polarizations connect magnetic sublevels of the ground state with those of the excited states. C. Goren *et al*. [46] predicted and explained that the ultranarrow EIA-TOP can be observed in DTLS even in case of same polarization configuration of pump and probe laser beams. For observing EIA-TOC, they used double two-level system which was later compared with four-level N-type system. In each model Doppler broadening increases the width of dip. In double two level system EIA peak become narrower on Doppler broadening but in contrast N-type system, does not devolved a dip at line center. In case of same polarization configuration of pump and probe lasers fields, the time dependent TOP can also be observed at sufficient low powers of pump beam in the absence of inelastic collision. C. Goren *et al*. [47] presented EIA-TOP and EIA-TOC models and show that at low power the both model give EIA peaks at the line center, whereas at high intensity the double two level system has the same spectrum as a simple two level system. T. Zigdon *et al*. [48] used circular- orthogonal and linear-perpendicular polarized pump-probe spectroscopy in cycling transition of $F_g = 2 \rightarrow F_e = 3$ of $^{87}$Rb to explained that the TOC played important role in splitting of narrow signals in such case when pump power is greater than decay rate of upper excited state and lower than probe power. To calculate absorption spectra, the stationary case with phenomenal parameter was taken into account which is quite different form that calculation which presented in [23].

In Hanle configuration the ultranarrow EIA resonance in absorption and transmission signal can be measured by scanning magnetic field, either

orthogonal to the direction of propagation of radiation field or parallel to the direction of propagation of optical field instead of pump or probe scanning. However, these origins of the ultranarrow Hanle signals are different from ours which are from TOC and time-dependent TOP, *etc*.

In our one laser experiment we produced ultranarrow EIA signal differently from the case of Hanle configuration by scanning pump laser beam. In our case no magnetic field has been applied to observe ultranarrow EIA signals.

To observe the ultranarrow EIA signal experimentally we made major changes in conventional two lasers pump-probe experimental setup and used single laser coupled with an Acousto-optic modulator (AOM) to observe TOP and TOC effects for such ultra-narrow EIA resonances where relative linewidth is limited to AOM scanning resolution. In this way we observed these ultranarrow signals successfully not only in orthogonal polarization configuration case but also in same polarization combination of pump and probe laser beams.

Polarization and power dependent ultra-narrow and split EIA signal inside the broad probe transmission spectra are still to be investigated. We performed several experiments using Rb vapor cell at room temperature. In case of circular and orthogonal polarization configuration we observed that these ultranarrow EIA signals are split into two even at low pump powers. The pump laser power plays a major role in the splitting due to TOC effects. This splitting occurs even at the relatively lower power of the pump laser differently from the orthogonal case of linear polarization as performed by [39]. In EIA experiments usually two independent laser beams have been

used for pump and probe beams. Each of these two lasers can have linewidth approximately equal to 1 MHz and together these two lasers produce linewidth of 2 MHz. That is why in our two lasers experimental results which are presented in chapter 4, we could notable to produced ultra-narrow EIA signal because of the large combined linewidths of the two different lasers. The observed EIA signal is slightly wider and shallower than we expected in the case of orthogonal polarization.

## 1.2 Velocity selective optical pumping

In the pump-probe experiment, multilevel atomic system prepared with strong pump laser beams can be probed by a weak probe beam. Pump beam frequency is fixed and locked to specific atomic transition and probe beam is scanned over wide frequency range. The probe transmission signal changes when probe laser also comes into resonance with same or other hyperfine transitions for atoms with zero velocity. Atomic coherences and optical pumping effects on atomic samples with hyperfine components due to laser interaction have been investigated. Hyperfine splittings in the alkali atoms are less than the Doppler width so that optical pumping effects between the hyperfine transitions due to Doppler profiles occurs including atomic coherence effects depending on the conditions of polarizations, intensities, *etc*. of pump and probe laser beams. When strong pump beam counter-propagating or co-propagating with weak probe beam in a vapor cell, a set of velocity selective resonance peaks can be observed at different velocities.

Doppler-free experiments with counter-propagating pump-probe geometry can provide nice Doppler free spectra. However, in the co-propagating case Doppler shifted resonance lines can be observed. Because EIA and EIT signals depend on the directions, polarizations and powers of pump and probe lasers. Thus broad Doppler and sharp coherence spectra can be obtained [49-51] together. The sharp interference spectra come from EIT or EIA depending on signal shapes while the broad spectrum resulting from optical pumping by pump laser field called VSOP. The sharp interfered spectra can be affected by the optical pumping. However, the effects are limited because of small coherence effect in the case of large detuning of the probe laser.

The VSOP can be used as a sensitive technique for precise measurements using a relationship between atomic velocity and internal parameters of the atoms in the ground or metastable state [50]. S. J. Park *et al*. [51] used co-propagating pump and probe laser beams to demonstrate VSOP spectroscopy on Rb atom and explained the position and magnitude of absorption spectra with respect to frequencies of both beams. S. Chakrabarti *et al*. [52-53] explained the experimentally observed EIT dip signal along with five extra peaks in probe transmission spectra transition line of $^{87}$Rb atoms. Also they studied the effect of co-propagation and counter propagation of pump beam on the absorption spectra of Rb atoms. In both case a set of extra resonance dips are observed A. J. Krmpot et al. [54] explained the pump transmission spectra by using rate equation. These results were obtained in wide scanning range of probe laser while pump laser is locked to particular transition. In co-propagating beams experiment they [54] observed several lines as a result of

contribution from laser absorption on atoms in different velocity groups. S. Mitra *et al*. [55] did both, theoretical and experimental investigation on EIT-dip signal with respect to pump Rabi frequency along with existence of VSOP peaks in probe transmission profiles by using V, Λ and V+Λ type atomic system.

D. Bhattacharyya *et al*. [56] developed theoretical model to describe the occurrence of seven transmission peaks due to VSOP in case of co-propagating and six peaks in case of counter-propagating pump and probe beam but experimentally they could not observed all peaks due to Doppler broadened background. S. Chakrabarti *et al*. [57] demonstrated the VSOP resonances in probe absorption spectra of both isotopes of rubidium D2 transitions in their experimental investigation. They used strong pump and weak probe beam which co-propagates through Rb vapor cell and explained the size of dips based on population depletion for different velocity groups. A. Krasteva *et al*. [58] used linear and orthogonal polarized pump and probe laser beam to investigate the pump-probe spectra of Cs atom in thin cell without buffer gas. Their theoretical model is based on optical Bloch equation. On the basis of this theoretical model they explain experimentally observed sharp EIT peaks and enhanced VSOP resonances for probe absorption and transmission spectra.

Most of the results from these VSOP experiments have been explained using a simple rate equation model. Stationary cases have been considered instead of generalized time-dependent OBEs. Arbitrary intensity and polarization effects of probe absorption spectra including EIA and EIT due to adjacent hyperfine levels and velocity groups of atom in cell have not

been investigated well both theoretically and experimentally.

Here we present pump-probe transmission spectra in the case when co-propagating pump beam scanned frequency in wide range and fixed frequency of probe laser transmission is observed. The spectral broad spectral profiles due to VSOP and sharp coherence effects have been investigated in the cases of arbitrary polarizations and intensities of the probe and pump lasers in $^{85}$Rb and $^{87}$Rb vapor cell at room temperature. In this research a theoretical method without phenomenal parameters is developed by H. R. Noh [23] for obtaining pump-probe absorption spectra from generalized solutions such as populations, optical coherences, transfer of the coherences from the excited states to the ground state and Zeeman coherences of the ground and excited states. The density matrix considering arbitrary polarization, power combinations of the pump and probe laser beam, time dependences of velocity groups of the atoms in a cell instead of steady state, and high-order Zeeman and optical coherence terms due to multi-order mixings of the pump and probe, by themselves, *etc*. have been applied to DTLS between 5 $S_{1/2}$ to 5 $P_{3/2}$ multi-level transitions of both isotopes of the Rb atom. The experimentally observed signal profiles are compared with probe transmission signals calculated from the generalized time-dependent density matrix equations and match well with the calculated signal profiles. Peculiar behaviors of coherence signals depending on powers and polarizations have been investigated in detail.

## 1.3 Motivation

In pump-probe experiments when both beams, which derive from two separate laser sources co-propagates through vapor cell with probe frequency fixed and locked to specific transition line and the pump laser tuned across the same transition line. Then in probe absorption spectra extra transmission peaks can be observed due velocity selective optical pumping effects with arbitrary polarizations and intensities of pump and probe lasers in closed and open system.

To investigate spectral features of ultra-narrow EIA signals experimentally we used two independent lasers systems for pump and probe laser beams but ultra-narrow EIA signal was not observed in the experiment. Because two different lasers with linewidth of 1 MHz produce together 2 MHz linewidth so the observed EIA signals are wider than calculated value of EIA signal. So we made major advance to observe these ultra-narrow signals using one laser combined with two AOMs.

The motivation behind our research work is also to understand the thermal averaging effects on spectral features of EIA and to investigate origin of formation of ultra-narrow and split EIA signal unknown previously in case of same and orthogonal polarization configuration with one laser discussed above.

.

## 1.4 Summary of this work

This work describes the experimental and theoretical investigation of rubidium vapor-cell EIA and EIT in a DTLS. Polarization and power dependent experimental and theoretical EIT and EIA spectra of both isotopes of rubidium are presented.

In chapter 2 we explain theoretically EIA and EIT spectra. Different atomic system and conditions which are necessary for occurrence EIA are also discussed.

The EIT mainly observed in three-level Λ-type system. DTLSs also provide possible way to analyze coherent effects in light-matter interaction. These systems are not only suitable for observation of coherent effects predicted and observed in three-level configurations, but also use for another opposite effect such as EIA. As each level of degenerate consists of multiple magnetic sublevel so EIA and EIT can also be observed in two level $F_g \rightarrow F_e$ transition. in degenerate two leve system EIA mainly occure due TOP and TOC. The occurrence of EIA due to TOC needs a particular type of system which consists of at least four degenerate states. Two of these states should be ground state and two excited state.

Theoretical calculation for spectral features of EIA in case of two independent laser sources with respect to power of pump beam is presented. Calculation for ultra-narrow and split EIA signal in case of same and orthogonal polarization configuration of pump and probe beam using single laser are also explained in this chapter.

In chapter 3 we describe theoretical and experimental detail of probe absorption spectra due to VSOP depending on polarization, power and direction of pump-probe lasers beam. We explain that due to VSOP effect the occurrence of transmittance peaks in spectra. We demonstrate EIA experiment for both closed and open system of $^{85}$Rb and $^{87}$Rb atom in D1 and D2 transition line. We describe different polarization configuration of pump and probe beam EIA spectra. Pump laser power dependent EIA spectra are also presented. We present our experimentally observed EIA spectra in DTLS of Rb atoms. The experiments were performed in both closed and open atomic system in D1 and D2 transition lines. As polarization combination of pump and probe laser beams play vital role in degerate magnetics sub levles for redistibution of atomic population abmong these levels and variation in polarization of pump and probe beams bring a noticeable change in spectral profile and intensity of EIA dip signal. So we explaine complet ploarzation dependent EIA spectra of $^{85}$Rb in this chapter.

In chapter 4 we describe theoretical and experimental pump-probe EIA spectra in general case of arbitrary polarization and powers of pump and probe beams of $^{85}$Rb atom. Spectral features of EIA in case of different polarization configurations also discussed. Thermal averaging effects on spectral features such as extra ultra-narrow and split spectral profiles of EIA implanted in broad sub-natural EIA have also been studied with respect to powers of pump beam.

In chapter 5 we describe in detail introduction about the features and ultra-narrow-EIA signal in case of all possible polarization configurations of pump and probe laser fields. By using single laser for both pump and probe

laser experiment the observe results in DTLS of $^{85}$Rb atom are also shown. Theoretical and experimental details are also presented.

Two different experimental schemes using one laser combined with an AOM have been used to investigate theoretical predictions for TOESC and TOP in cycling transitions of TSZMD of thermal $^{85}$Rb atoms. The general transient treatments are used to solve optical Bloch equations (OBEs) with full considerations of magnetic sublevels without phenomenal parameters in the arbitrary polarizations and arbitrary powers.

In chapter 6 we present the conclusin of the entire research work done in this thesis.

# Chapter 2
# Theoretical calculation of electromagnetically induced absorption (EIA)

## 2.1 Introduction

A simple two-level model for the atom can explain many light-atom interaction phenomena, while the three-level systems are compulsory to get coherent processes involving two optical transitions. In three-level system a medium which is initially absorbing for a weak probe tuned to one of the transitions becomes transparent when the other transition is irradiate with an intense coupling field.This transparency is a phenomenon of reducing the absorption of weak probe beam passing through a medium in the presence of second relative strong coupling beam. The occurrence of EIT in three-level atomic systems is common in which two lasers fields interacts with properly selected transition lines of atom and the quantum interference causes the ground state population to disappear the medium become transparent to probe laser field.

Two separate lasers fields named pump (strong) and probe (weak) couples to each arm with common excited level of Λ-type system. So absorption of probe laser field in the medium is reduces and very narrow spectral profile can be observed [19]. CPT and EIT are the examples of such dark states. CPT is well known both in three levels Λ-type system and DTLSs [15].

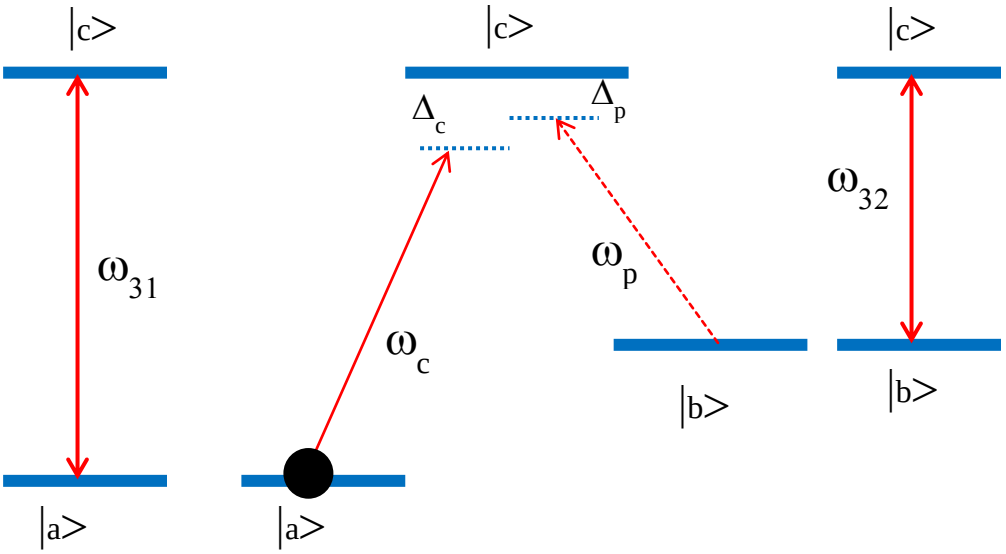


Fig. 2.1 Three levels Λ-type system with dipole allowed transition |a> → |c> and |b> → |c>.

The basic arrangement of Λ-types three levels atomic system is shown in Fig. 2.1 and we label the level as |a>, |b> and |c>. The system consists of two grounds (|a>, |b>) and one common excited states (|c>). $\omega_{31}$ and $\omega_{32}$are the transition frequencies of control and probe laser fields respectively. EIT requires two dipole allowed transitions (|a> → |c> and |b> → |c>) and one forbidden transition (|a>→|b>). In Λ-types three levels atomic system the state |b> being a metastable state has particular importance to produce long lived coherence between state |a> and state |b> which is very important condition for observing EIT in this system. According to quantum mechanics, when there are multiples excitation pathway exists, interference between their probability amplitude will occur. From Fig. 2.1 one possible way to get EIT is the interference between transition path way. Initially the atoms are

accumulated in the lowest ground state (|a>). When we turn on laser field of frequency of $\omega_{31}$then atoms in ground state can absorb energy and makes transition to state |c>. Meanwhile, when an electromagnetic field resonant with |b> → |c> transition is also turned on, now there are two transitions path ways through which atom can make transition from ground state to excited state. Either an atom can make transition in the way from |a> → |c> or it can follow the path to reach the excited state through |a> → |c> → |b> → |c>. Under certain conditions these two transitions path can show zero probe absorption at resonance peak due destructive interfere. EIT resonance can be several orders of magnitude narrower than the natural linewidth of the atomic transition. The interesting effect of EIT is includes large dispersion effect at the atomic resonance especially a very steep linear dispersion relation could be found at the point of minimal absorption.

.

## 2.2 EIA in degenerate two level atomic system of Rb atom

Electromagnetically induced absorption (EIA) [7] is an enhanced absorption of weak probe beam in the presence of strong pump beam. EIA is an absorption due to atomic coherences between the states via coherent laser photons [37]. For this enhanced absorption, there should be additional enhancement supports for a state which is probed absorption externally through transfer of population or transfer of coherence, *etc*. To observe EIA in different atomic system we should have a particular atomic system. For example in DTLS EIA can occur under two different procedures to prepare

induced absorption. One is known as EIA due to transfer of coherence (TOC) while the other is called as transfer of population (TOP). The enhanced absorption based on TOP can occur when both pump and probe laser beams have same polarization configuration. Similarly to observe EIA due to TOC the polarization of both beams must be orthogonal. Generally the occurrence of EIA due to TOC requires a special type of system which consists of at least four degenerate states. Two of these states should be ground state and two excited state. This system is usually known as N-type system which is shown in Fig. 2.2. It is important to note that there should be sufficient amount of population in degenerate excited state which leads to establish coherence and spontaneous emission from excited state to ground state leads the transfer of coherence. As it can be seen from Fig. 2.2 that N-type system is closed system and if pump beam derive to this closed transition then reasonable amount of population can be obtained. In Fig. 2.2 the |b> → |d> transition is closed path which is just similar as $F_g = 3 \rightarrow F_e = 4$ in case of $^{85}$Rb atom and $F_g = 2 \rightarrow F_e = 3$ in case of $^{87}$Rb

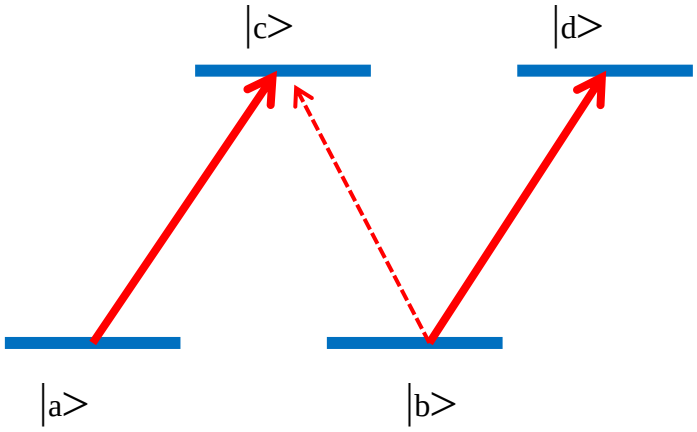


Fig. 2.2 The N-type atomic system in DTLS. Two heavy arrow show the Pump transition and dotted line arrow show probe transition.

Compared to non-degenerate three-level systems, degenerate two-level configurations are much more complicated and it more complex to describe pump-probe system due to many sublevels. Thus, the fundamental origins of EIA in DTLSs have not been investigated well, in contrast to those in three level atomic systems. Both, EIT and EIA occur due to optical pumping and coherence [15]. We present theoretical model for solving the generalized time dependent density matrix equation to explain complete polarization dependence of experimentally observed EIA signals for two rubidium isotopes at room temperature in vapor cell. A simple N-type model which is commonly used to clarify the theoretical explanation of EIA signal under certain polarization configuration of pump and probe laser beam is shown in Fig. 2.3.

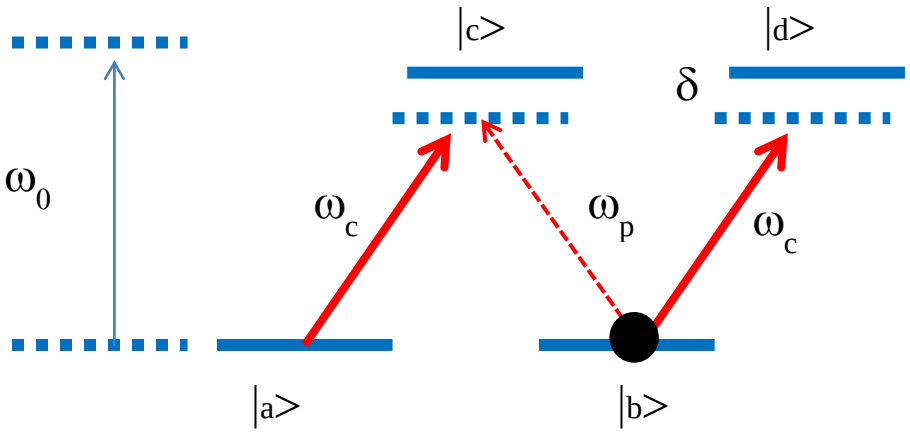


Fig. 2.3 The N-type atomic system in DTLS.

Suppose $\omega_0$ is the resonance frequency between ground and excited sub-level and $\delta$ show the detuning from resonance line. $\omega_c$ is the frequency of coupling beam which derive $|a\rangle \rightarrow |c\rangle$ and $|b\rangle \rightarrow |d\rangle$ transitions while $\omega_p$ is the frequency of weak probe beam which derive the $|b\rangle \rightarrow |c\rangle$ transition. In case of circular and orthogonal polarization configuration of pump and probe laser the population will be pumped into right most or left most ground state Zeeman sublevel. Compare to circular and orthogonal polarization, linear and perpendicular polarization case is more complex and complicated and make many sets of N-type system

## 2.3 Theoretical calculation of pump probe spectra

In case of two independent lasers sources for pump and probe beams, we performed two sets of experiments to observe the spectral features of EIA

signal profile. These experiments were designed to check the effect of different polarization configuration of both beams on spectral features of EIA because the role of polarizations combination in degenerate atomic systems becomes decisive. The polarization combinations can be classified into orthogonal and circular case and same-circular case of both beams. Here we explain the theoretical calculation to describe the line shape of observed EIA signal profile. To explain the procedure used for calculating the pump-probe spectra in straightforward way, we take the general case of an arbitrarily polarized pump beam. Let us consider pump and probe beams having optical frequencies $\omega_c$ and $\omega_p$ respectively co-propagates through vapor cell. Similarly we suppose that $\Omega_1$ and $\Omega_2$ are the Rabi frequencies of pump and probe laser beams respectively. As mentioned earlier that we take the case of cycling transition $F_g = 3 \rightarrow F_e = 4$ of the $^{85}$Rb D2 line. The energy level diagram of this cycling transition line is shown in Fig. 2.4. We have neglected the effect of other transition in calculation because of large hyperfine energy difference.

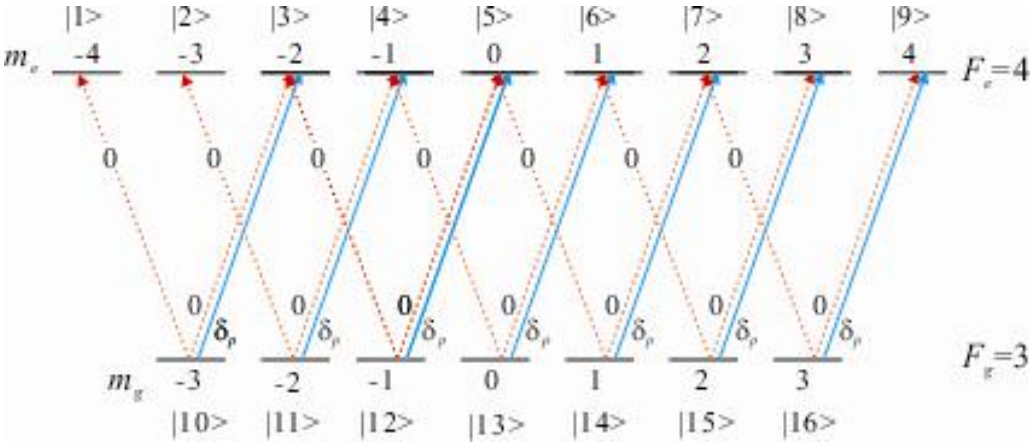


Fig. 2.4 Energy level diagram for the $F_g = 3 \rightarrow F_e = 4$ transition of $^{85}$Rb-D2 line.

In Fig 2.4 the solid line represents the probe beam while the dotted line denotes the pump laser beam. The magnetic sub levels in excited sate are labeled as $|m_e = -4\rangle = |1\rangle, |m_e = -3\rangle = |2\rangle, \ldots | m_e = 4\rangle = |9\rangle$ and magnetic level in ground state ( $F_g = 3$) are label as $|m_g = -3\rangle = |10\rangle, |m_g = -2\rangle = |11\rangle, \ldots. |m_g = 3\rangle = |16\rangle$.

The atoms of the gas are randomly moving in all directions inside the vapor cell. One portion of these atoms is moving in opposite direction of co-propagating pump and probe beams with velocity v. the laser frequencies of these pump and probe beams as observed by an atom are written as. $\omega_1 = \omega_p - kv$ and $\omega_2 = \omega_c - kv$ respectivily, where k ($=2\pi/\lambda$) is the wave vector and $\lambda$ is the wavelength of the coupling or probe beam we define the detuning $\delta_2$ ( $\equiv \omega_2 - \omega_0 = d_c - kv$ ) and $\delta_p$ ( $\equiv \omega_1 - \omega_2 = d_p - d_c$) where $\omega_0$ is the resonance frequency and $d_{p(c)} = \omega_{p(c)} - \omega_0$ is the detuning of the probe (coupling) beam.

When the absorption coefficient is calculated by solving the density matrix equation, all the quantities are expressed in terms of $\delta_2$ and $\delta_p$. The behavior of the internal dynamics of the $^{85}$Rb atom is described by a density matrix equation in the rotating frame with frequency $\omega_{2:}$

$$\dot{\rho} = \frac{i}{\hbar}[H_0 + v, \rho] + \dot{\rho}_{sp} \qquad (2.1)$$

where $\rho$ is the density operator and $H_0$ is the bare atomic Hamiltonian as given by

$$H_0 = \sum_{j=1}^{9} h\,\delta_2 \langle j|j\rangle \qquad (2.2)$$

$\dot{\rho}_{sp}$ denotes the spontaneous emission term. We consider that there is no collisional dephasing in atomic coherence due to pure Rb vapor inside the cell. There will be collisions between atom and wall of the container which can affect the coherence and can induce the dephasing in atomic coherence. But this effect is negligible small so can be neglected in theoretical calculations. Therefore, the decay rate of the optical coherence in $\dot{\rho}_{sp}$ is set to $\Gamma/2$ where $\Gamma$ is the decay rate of the excited state.

The interaction Hamiltonian in equation (1), V, is given by

$$V = \frac{\hbar}{2}\sum_{j=0}^{6}\{C_{10+j}^{3+J}\,\Omega 1 e^{-i\delta pt}|3+j\rangle\langle 10+j| + C_{10+j}^{1+J} a_{-}\Omega 2\,|1+j\rangle\langle 10+j| + C_{10+j}^{3+J} a_{+}\Omega 2\,|3+j\rangle + h.c \qquad (23)$$

where h.c denotes the Hermitian conjugate and $C_u^v$ is the normalized transition strength between the states |v> and |$\mu$> In equation (3), $a_{\pm}$ are the coefficient of the $\sigma\pm$ components of the coupling beam, as given by

$$a_{\pm} = \pm 1/2(1\pm \sin 2e) \pm i/2 \cos 2\varepsilon$$

where c is the angle between the incident electric field of probe beam and optic axis of quarter wave plat. We take two different arrangements for polarization configuration of pump and probe laser fields, the same ($\sigma+ - \sigma+$) polarization case and orthogonal ($\sigma- - \sigma+$) polarization case. In both cases, ε = $\pi/4$ and ε = $-\pi/4$, respectively. To obtained a series of linear differential equation for the density matrix elements, we substitute equations (2.2) and (2.3) in equation (2.1). It can be seen that there is exists obvious time dependence on right side of equation (2.1) so it necessary to expand the density matrix element into terms oscillating at different frequencies [59, 60]. To calculate non vanishing terms of density matrix element, we consider the interaction of two photons for population and Zeeman coherence. Similarly for optical coherence three photons were taken into account. In Fig. 2.4, we see that the oscillation frequencies for the $\sigma+$ transition are {0, $\delta_p$}, whereas that for $\sigma-$ transitions is 0. The oscillation frequencies for the populations can be determined by {0, $-\delta_p$} + {0, $\delta_p$}, and are finally given by 0, $-\delta_p$, and $\delta_p$. Therefore, the populations are expressed clearly as follows:

$$\rho_{jj} = \rho_{jj}^{(1)} + \left(\rho_{jj}^{(2)} + i\rho_{jj}^{(3)}\right) e^{-i\,\delta_p t} + ((\left(\rho_{jj}^{(2)} - i\rho_{jj}^{(3)}\right) e^{i\,\delta_p t} \qquad (2.4)$$

where, j = 1, 2, ⋯, 16. In equation (2.4), $\rho_{jj}^{(1)}$ are real for l = 1, 2, 3.The oscillation frequencies for Zeeman coherences are given by $\{0, \delta_p\}$ for $\rho_{1+j,3+j}$ ( $j$ = 0, 1, ⋯, 6) and $\rho_{10+j,12+j}$ ($j$ = 0, 1, ⋯, 4). The oscillation frequencies for the optical coherences are given by $\{0, -\delta_p, -2\delta_p, \delta_p\}$ for $\rho_{3+j,10+j}$ ( $j$ = 0, 1, ⋯, 6), $\{0, -\delta_p, \delta_p\}$ for $\rho_{1+j,10+j}$ ( $j$ = 0, 1, ⋯, 6),$\{0, -\delta_p, -2\delta_p\}$ for $\rho_{5+j,10+j}$ ( $j$ = 0, 1, ⋯, 4), and $\{0, \delta_p\}$ for $\rho_{1+j,12+j}$ ( $j$ = 0, 1, ⋯, 4). The oscillation frequencies of $\rho_{\mu v}$ are the negative of the oscillation frequencies of $\rho_{v\mu}$ for $\mu > v$. We neglected Zeeman coherences and optical coherences that are connected via interactions greater than three photons. The coherences can be written explicitly. As an example, the optical coherences with $\Delta m = 1$ are given by

$$\rho_{3+j,10+j} = \rho_{3+j,10+j}^{(1)} + \rho_{3+j,10+j}^{(2)} e^{-i\delta pt} + \rho_{3+j,10+j}^{(2)} e^{-2i\delta pt} + \rho_{3+j,10+j}^{(4)} e^{-i\delta pt} \tag{2.5}$$

where $j$ = 0, 1, ⋯, 6. Putting the coherences and populations described in the form of equations (2.4) and (2.5) in equation (2.1), we obtain a set of coupled differential equations for the components of the density matrix elements. These equations are then solved numerically as functions of time, $\delta_2$, and $\delta_p$. The absorption coefficient is given by

$$a_0(\delta_2, \delta_P, t) = \frac{N_{at} 3\lambda^2}{2\pi} \frac{\Gamma}{\Omega_1} \sum_{j=0}^{6} \mathrm{Im}[C_{10+j}^{3+j} \rho_{3+j,10+j}^{(2)}] \tag{2.6}$$

where Γ is the decay rate of the excited state and $N_{at}$ is the atomic number density in the vapor cell. The absorption coefficient is then averaged over the

transverse and longitudinal velocity distributions, and the final results are given by

$$a = 1/t_{av} \int_0^I dt \int_{-\infty}^{\infty} dv \frac{e^{-(\frac{v}{u})^2}}{\sqrt{\pi}\, u} a_0(d_c - j = kv, d_p - d_c, t) \qquad (2.7)$$

where u (=$(2k_BT/M)^{1\,2}$) is the most probable speed (T: temperature of the cell, M: mass of an atom) and $t_{av}$ (=$(\sqrt{\pi}/\ 2)d/u$) is the average transit time traversing a laser beam with a diameter d [61]. The restricted interaction time of the atoms with the laser beam is usually measured by assuming a decay rate of the ground state coherence and solving the steady-state solutions of the density-matrix equations [29, 47]. However, this method is not quite accurate because the included decay rate is a phenomenological constant. Instead of using such a phenomenological constant, we solve time dependent density-matrix equations and averaged the absorption coefficients over the distribution of finite transit times of the atoms crossing the laser beam. Since our method does not need any phenomenological constants differently from other previous calculation methods, the method of calculation is able to predict accurate line shapes of the EIA spectra. It is essential to examine time-dependent solutions of the density-matrix equations instead of stationary solutions to determine accurate EIA line shapes like previously investigated CPT system [62]. Although our system is not CPT system, our time-dependent solutions of the OBEs also give accurate line profiles because of time-dependent consideration in our calculation.

## 2.4 Theoretical backgrounds of ultra-narrow EIA signal

Fig. 2.5 shows the energy level diagram of $^{85}$Rb D2 for cycling transition line. Here in this case we consider the linearly polarized pump and probe beams in perpendicular direction. The procedure adopted for calculating EIA spectra in case of same-linear polarization configuration of both beams is quite similar to that which is used for same-circular polarization condition of both beams.

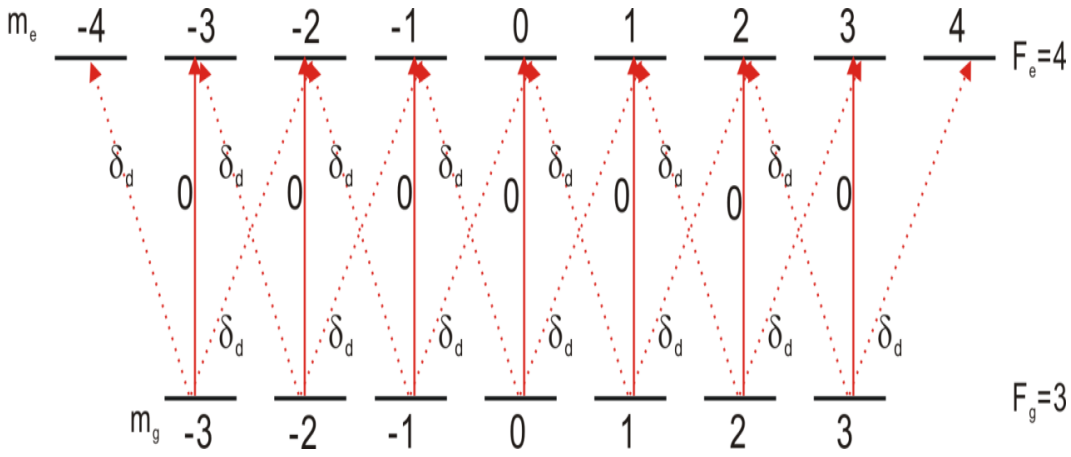


Fig. 2.5 The energy level diagram for the $F_g = 3 \rightarrow F_e = 4$ transition of $^{85}$Rb-D2 line.

In Fig. 2.5 “0” is the frequency of pump beam and “$\delta_d$” is the frequency of probe beam with respect to pump beam frequency $\omega_2$.

The Hamiltonian is given by

$$
\begin{aligned}
H = &-\sum_{m=-4}^{4} \hbar\delta_2 \left|F_e = 4, m\right\rangle\left\langle F_e = 4, m\right| \\
&+ \frac{\hbar}{2}\sum_{q=\pm 1} a_q \sum_{m=-3}^{3} C_{3,m}^{4,m+q}\Omega_1 \left|F_e = 4, m+q\right\rangle\left\langle F_g = 3, m\right| \\
&+ \frac{\hbar}{2}\sum_{m=-3}^{3} C_{3,m}^{4,m}\Omega_2 \left|F_e = 4, m\right\rangle\left\langle F_g = 3, m\right| + \text{h.c.},
\end{aligned}
\tag{2.8}
$$

In Eq. (2.1), $\dot{\rho}_{sp}$ represents the spontaneous emission term, which is given by

$$
\begin{aligned}
\dot{\rho}_{\text{sp}} = &-\Gamma \sum_{m=-4}^{4}\sum_{m'=-4}^{4} \left|F_e = 4, m\right\rangle\left\langle F_e = 4, m'\right| \\
&-\frac{\Gamma}{2}\sum_{m_e=-4}^{4}\sum_{m_g=-3}^{3}\left(\left|F_e = 4, m_e\right\rangle\left\langle F_g = 3, m_g\right| + \left|F_g = 3, m_g\right\rangle\left\langle F_e = 4, m_e\right|\right) \\
&+\Gamma \sum_{m=-3}^{3}\sum_{m'=-3}^{3}\sum_{q=-1}^{1} C_{3,m}^{4,m+q} C_{3,m'}^{4,m'+q} \left|F_e = 4, m+q\right\rangle\left\langle F_e = 4, m'+q\right|,
\end{aligned}
\tag{2.9}
$$

where $\Gamma$ is the decay rate of the excited state.

We consider the decay process from upper excited degenerate level, where TOP between the magnetic sublevels of the ground and excited states generates ultra-narrow absorption. The density matrix elements have large number of Fourier oscillation component in case of circular polarization, so the interaction of two photons will be consider for population and Zeeman coherences while three photons for optical coherence.

Here we describe density matrix elements for simplicity as

$\langle F_e, m'|\rho|F_g, m\rangle = \rho_{e_{m'}, g_m}$ $\langle F_e, m'|\rho|F_e, m\rangle = \rho_{e_{m'}, e_m}$ and Then, the expanded matrix elements of optical coherences are clearly written as $\rho_{e_m, g_m} = \rho^{(1)}_{e_m, g_m} + \rho^{(2)}_{e_m, g_m} e^{-2i\delta_d t}$ $\rho_{e_{m\pm1}, g_m} = \rho^{(1)}_{e_{m\pm1}, g_m} e^{-i\delta_d t} + \rho^{(2)}_{e_{m\pm1}, g_m} e^{i\delta_d t}$ $\rho_{e_{m\pm2}, g_m} = \rho^{(1)}_{e_{m\pm2}, g_m} + \rho^{(2)}_{e_{m\pm2}, g_m} e^{-2i\delta_d t}$ and $\rho_{e_{m\pm3}, g_m} = \rho^{(1)}_{e_{m\pm3}, g_m} e^{-i\delta_d t}$ for all the relevant values of m. Those of Zeeman coherences are given by $\rho_{e_m, e_{m+1}} = \rho^{(1)}_{e_m, e_{m+1}} e^{-i\delta_d t} + \rho^{(2)}_{e_m, e_{m+1}} e^{i\delta_d t}$ $\rho_{e_m, e_{m+2}} = \rho^{(1)}_{e_m, e_{m+2}}$ $\rho_{g_m, g_{m+1}} = \rho^{(1)}_{g_m, g_{m+1}} e^{-i\delta_d t} + \rho^{(2)}_{g_m, g_{m+1}} e^{i\delta_d t}$ and $\rho_{g_m, g_{m+2}} = \rho^{(1)}_{g_m, g_{m+2}}$ for all the relevant values of m. Finally each population has one constant term. We can have a series of linear differential equations by substituting the expanded density matrix elements in equation (2.1). After solving these equations, the matrix elements essential for the probe absorption can be derived. Finally, the absorption coefficient is averaged over the longitudinal velocity distribution and finite transit time distribution as follows [23]

$$\alpha = -\frac{3\lambda^2}{2\pi}\frac{N_{\text{at}}}{\Omega_1}\int_0^{t_{\text{av}}}\frac{dt}{t_{\text{av}}}\int_{-\infty}^{\infty}\frac{dv}{\sqrt{\pi}u}\ \text{Im}\left[\sum_{q=\pm1}\sum_{m=-3}^{3} a_q^* C_{3,m}^{4,m+q}\rho^{(1)}_{e_{m+q}, g_m}\right] \tag{2.10}$$

where $N_{at}$ is density of atoms in the cell, $t_{av}$ is the average time crossing a laser beam, and u is the most possible speed in the cell.

## 2.5 Saturated absorption spectroscopy

Saturated absorption spectroscopy (SAS) is frequently used for locking the laser to a specific hyperfine transition. With simple saturated

spectroscopy we can observe the decrease in probe absorption caused by strong pump beam which depletes the population.

Schematic of experimental setup which we used in our experiment is shown in Fig. 2.6

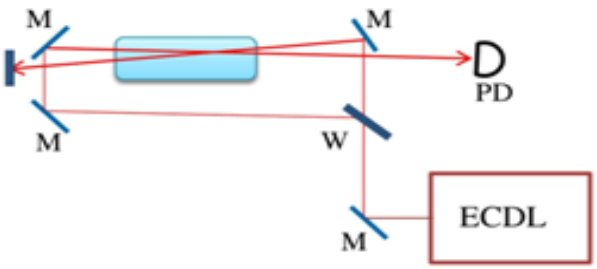


Fig. 2.6 Schematic of experimental setup of saturation absorption spectroscopy

Laser beam from external cavity diode laser (ECDL) is divided into two beams by using window. The transmitted beam, which is stronger and can be used as a pump and the reflected beam from window, is weaker and used as probe. These two counter propagating beam passes through gas cell which contains both rubidium isotopes in natural abundance overlap at the center cell. In off resonance condition when these two beams interact with atoms, one of them will excite the velocity group of $v_z$ and the other will excite the velocity group - $v_z$. When we tuned the laser to on resonance, both pump and probe beams will excite the same zero velocity group $v_z = 0$. As mentioned

the strong pump beam will excite most of the population to the excited state so the intensity of probe will pass through the cell without absorbing by atom. When we detect this probe beam by photodetector, we observe an increase in transmission of probe intensity. This decrease in absorption of probe beam caused by pump beam will result a dip in absorption profile and called as Lamb dip. When laser frequency is exactly similar to atomic transition frequency than one can observe saturated absorption spectroscopy signal. By looking at the spectra of SAS signals of Rb atoms one can observe six probe transmission peaks. Three of them are called principal hyperfine while the others three are known as crossover resonances. The occurrence of these crossover resonances can be explained as follow. As atoms inside the cell are always in random motion and we consider a group of atoms are moving with velocity $v_z$ in opposite direction to the prorogation of pump laser of frequency $\nu_{laser}$. So due to Doppler's effect the red-shifted resonant frequency for pump beam can be written as

$$\nu_{pump} = \nu_{laser}(1- v_z/c) \tag{2.12}$$

As mentioned above that pump and probe laser beams inside the cell are propagating in opposite direction. So at the same time for probe laser beam the blue shifted frequency can be of the form

$$\nu_{probe} = \nu_{laser}(1+ v_z/c) \tag{2.13}$$

by adding Eq. (2.12) and (2.13) we can have equation of the form

$$\nu_{laser} = (\nu_{pump} + \nu_{probe})/2 \quad (2.14)$$

Eq. (2.14) shows that the crossover resonance occurs at the middle of two transitions peaks.

# Chapter 3
# Optical pumping spectroscopy of Rb atoms

## 3.1 Introduction

Compared to non-degenerate three-level systems, degenerate two-level configurations [1-2, 15] are much more complicated and it is more complex to describe pump-probe system due to many sublevel and high order optical and Zeeman coherences. In case of D2 transition line of $^{85}$Rb and $^{87}$Rb atoms there are four closely-spaced excited state levels. The off resonance strong pump beam can cause non resonant excitation from ground level to all possible excited state levels and consequently the probe transmission shows the additional VSOP peaks [19]. In optical pumping mechanism, the Zeeman sub-levels plays vital role in response of light-matter interactions and as a result of this interaction not only there is population redistributions between magnetic sub-levels but also it creates coherence among the ground state Zeeman sublevels.

In pump-probe experiments when atoms are resonant with these two fields, the strong coupling laser beam creates dress states due to AC Stark shift and strong probe laser causes pump absorption dependent on the probe laser so that solution of the two-level system can be derived differently from the case of the weak probe beam. However the coupling laser can cause the populations to redistributes among the states by optical pumping. The population of one state can be optically pumped to another state which

affects the absorptions and transmissions spectrum profile of probe laser beam.

In the DTLS, the polarizations of the pump and probe laser beams play very important role in Zeeman coherences of the ground and excited states, transfer of the coherence from the excited states, contribution to optical coherences between the ground and excited states because the polarizations connect magnetic sublevels of the ground state with those of the excited states. In case of cycling transitions of both isotopes of rubidium atom, the probe transmittance peaks which results from atomic coherence is dominant because of transition selection rule the population of any ground state of cycling transition cannot optically pumped into any other or non- resonant states.

In this chapter we have applied for this solutions to understand the spectra of the EIT-like and EIA including the pump and probe absorption spectra due to adjacent hyperfine levels and velocity groups of the atoms. The observed signal profiles are compared with probe transmission signals calculated from the generalized time-dependent density matrix equations and match well with the calculated signal profiles. Thermal averaging of velocities of atoms in the cell is taken into account and complete analysis of arbitrary polarization change of the probe beam. Then, we have obtained the transition coefficient by averaging the calculated density matrix elements over a Maxwell-Boltzmann velocity distribution.

## 3.2 Experimental setup for same-circular and linear-linear polarization configuration

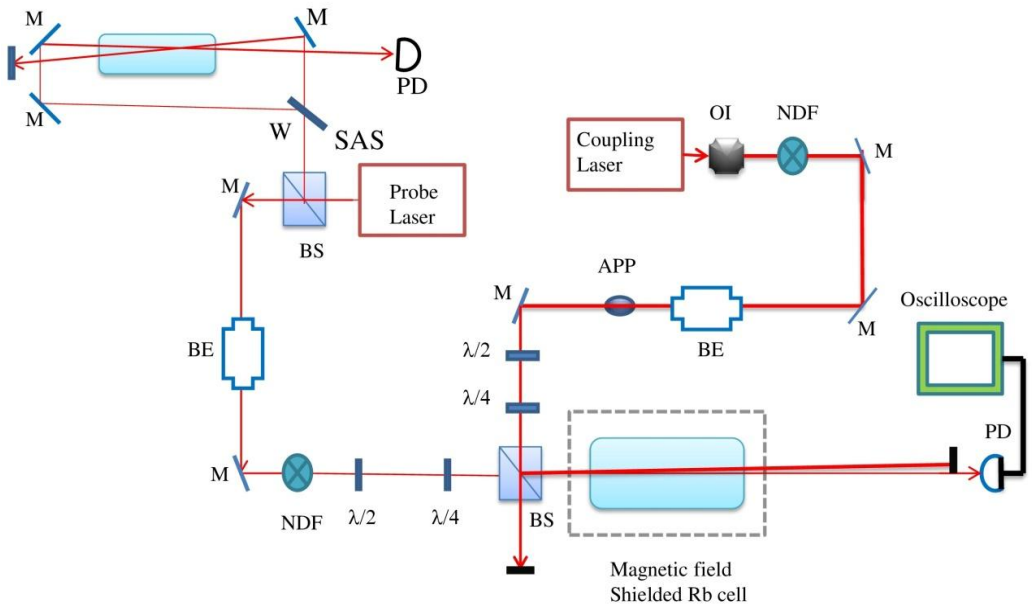


Fig. 3.1 Schematic diagram with two home-made External cavity diode lasers for same-circular and linear and parallel polarizations of both pump and probe beams. Figure keys**:** M-mirror, OI-optical isolator, W-window, APP-aperture, BE-beam expander, λ/2- half wave plate, λ/4-quarter wave plate, NDF- neutral density filter, PBS-polarizing beam splitter, PD-photodiode.

The Experimental setup is described schematically in above Fig. 3.1. Two separate 780 nm homemade external cavity Diode lasers (ECDL) are used for both pump and probe beams. The frequency of probe beam is fixed and locked on $F_g = 3 \rightarrow F_e = 4$ of $^{85}$Rb D2 transition line by using home-made lock-in amplifier. As shown in Fig, the vertically polarized coupling laser

beam after passing through optical isolator is sent into one of the beam expander to expand this beam up to 6 mm in diameter. An aperture is inserted in the path of coupling laser beam which control the size of beam used for experiment. Before mixing with weak probe laser beam at beam splitter (BS) which is placed just before the magnetic field shielded rubidium vapor cell, this coupling beam has to pass through half wave plate (HWP) and quarter wave plate (QWP). A neutral density filter (NDF) and these two plates contribute to control the variations in power and polarizations of coupling laser beam respectively. At BS the transmitted coupling beam is useless and is blocked while the reflected beam is used in cell experiment. Similarly another vertically polarized beam from probe laser is first divided into two parts by using another BS. The reflected beam from this BS is further divided by window to use for saturation absorption spectroscopy (SAS) setup to lock the laser frequency on desire hyperfine transition line. After window 90% of the total power of laser beam is transmitted while the remaining 10% will be reflected. These transmitted and reflected beams are used as pump and probe for SAS setup to observe the spectra. On the other hand the transmitted beam from second BS is sent to another beam expander to expand it up to required diameter. This expanded probe laser beam mixed with coupling beam at BS after passing through HWP and QWP. As mentioned that both lasers beams are vertical polarized but after passing through many optics the polarization state of these beams may be changed up to some extent so that the polarizations of the pump and probe lasers beams are made vertical polarizations just before a BS by using two HWPs once more. This experimental setup can be used for two different polarization

configurations of probe and coupling lasers beams. One of them is linear and parallel case while the other is same-circular polarization configuration For same-circular polarization configurations, two separate QWPs with optics axis angle ε = 45 with respect to y-axis for the pump and probe lasers are used to have same right circular polarizations just before the BS where two beam are combined. Both slightly deviated beams are overlapped well near the center of a magnetic shielded rubidium vapor cell for the pump and probe experiments. At long distance from the cell these two beams are separated and the pump beam is blocked while the probe beam is focused on a photodiode to measure the transmission of the probe beam through the cell. In case of linear and parallel polarization configurations of pump and probe lasers beams, two QWPs before BS for the coupling and probe experiment from the setup with same-circular polarization configuration are removed. In this way both the coupling and probe beams are vertically polarized.

## 3.3 Experimental setup for orthogonal-circular and linear-perpendicular polarizations configuration

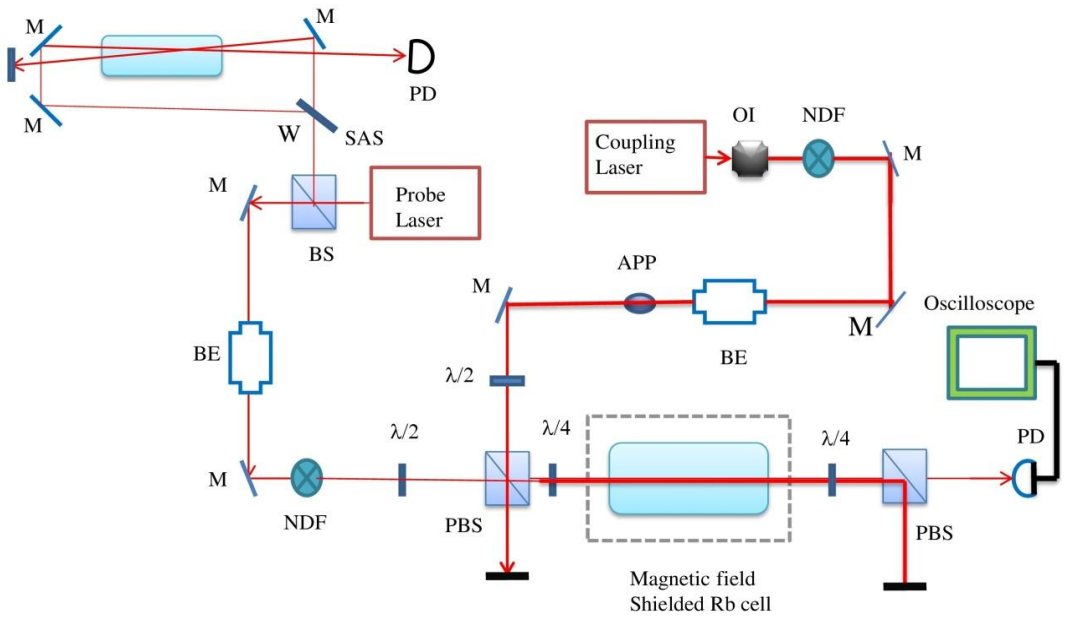


Fig.3.2 Schematic diagram with two home-made External cavity diode lasers for circular- orthogonal and linear - perpendicular polarizations of both pump and probe beams. Figure keys**:** M-mirror, OI-optical isolator, W-window, APP-aperture, BE-beam expander, λ/2- half wave plate, λ/4-quarter wave plate, NDF- neutral density filter, PBS-polarizing beam splitter, PD-photodiode.

By making some modifications in Fig. 3.1 and converting it into Fig. 3.2, we can use this setup for circular and orthogonal polarization configuration of coupling and probe lasers experiment in vapor cell. Further some changes in this setup will able us to use this experimental setup for liner and perpendicular polarization experiment of coupling and probe lasers beams.

For the experimental case of circular and orthogonal polarizations of the coupling and probe beams, one need to replace BS by PBS and inserting two quarter wave plates just before and after Rb vapor cell in Fig. 3.1 Finally one PBS should be inserted before the photodiode. As mentioned both beams are vertically polarized. The polarization state of probe beam is changed to horizontal polarization by changing the optic axis HWP. Now this beam transmits from PBS which is inserted before Rb cell. The vertically polarized coupling beam and horizontally polarized probe beam are mixed at PBS and very well overlapped in the throughout the rubidium vapor cell. When the polarization angle of QWP inserted before cell is set at $\varepsilon$ = -45 degree with respect to y-axis, then This arrangement prepared pump beam as left circularly polarized and at the same time initially horizontally polarized probe beam will be right circularly polarized. These two circular and orthogonal polarized beams interact with randomly moving atoms in the cell and emerged out to second QWP which is set at $\varepsilon$ = - 45 degree with respect to y-axis after the cell makes again the coupling beam as vertical polarized and probe beam horizontal polarized, respectively. When these two well overlapped beams reached at $2^{nd}$ PBS placed after vapor cell, the vertical pump beam reflected at 90 degree and horizontally polarized probe beam is transmitted. The reflected beam is blocked while the transmitted beam is detected by photodiode and monitored by oscilloscope.

In case of linear and perpendicular polarization configuration we need to remove both QWPs from the setup which are inserted before and after rubidium vapor cell. In this situation after $1^{st}$ PBS the coupling beam is vertically polarized while the probe beam is horizontally polarized. When

these two well overlapped beams reached at 2nd PBS after passing through Rb vapor cell, the vertical coupling beam reflected and horizontally polarized probe beam is transmitted. The reflected beam is blocked while the transmitted beam is detected by photodiode. The intensities of both beams were controlled by two separate neutral density filters (NDF).

## 3.4 Circular and orthogonal polarization dependences of the velocity dependent probe transmission signal

We have investigated theoretically and experimentally probe transmission profiles due to thermal velocities of atoms and scanning strong coupling laser frequency from $F_g = 3$ to $F_e = 2, 3, 4$ with weak probe laser resonant on $F_g = 3 \rightarrow F_e = 4$ of $^{85}$Rb atoms with respect to polarization. We have calculated the transmission and absorption spectra of $^{85}$Rb between hyperfine-level $F_g = 3 \rightarrow F_e = 4$ with degenerate magnetic sublevels when polarization coupling beam is changed from right circular polarized to left circularly polarized with fixed probe beam polarization. In DTLS polarization of probe and control lasers fields plays significant role to transfer of population from excited states and consequently variation in absorption and transmission signal profile is observed when the polarization state of control and probe lasers fields were changed. The experimental results matched well with those results which were calculated from density matrix equation. As probe and control lasers co-propagates through cell, detuning for control and probe lasers which atom feel are $\delta_{control} = \delta_c - kv$ and $\delta_{probe} = \delta_p - kv$, respectively where $\delta_c$ and $\delta_p$ are control and probe laser detuning from $F_g = 3 \rightarrow F_e = 4$ resonance line respectively. Fig. 3.3(a) and

(b) shows spectral change between frequency region including $F_e$ = 2, 3, and 4 hyperfine components with reference to fixed laser frequency of $F_g$ = 3 → $F_e$ = 4 and for theoretical calculation and experimental observation, respectively. Here polarizations of control beam are changed from right circular polarization to left circular polarization while the polarization of probe laser is right circularly polarized

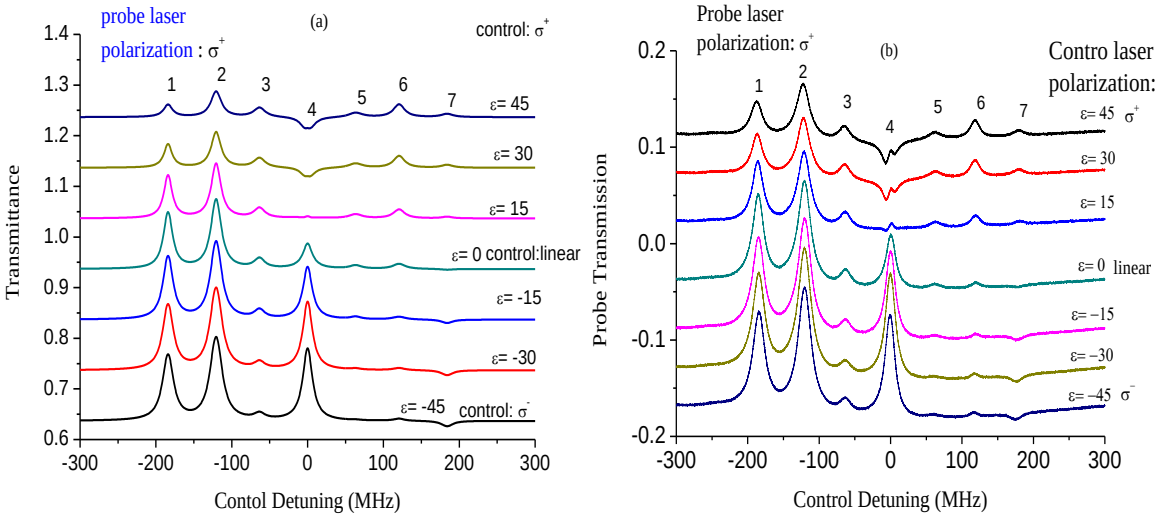


Fig. 3.3 Transmission spectra of $F_g = 3 \rightarrow F_e = 4$ of $^{85}$Rb (a) theoretically calculated from density matrix equation (b) experimentally observed spectra. Probe laser is right circularly polarized and the polarization of control laser is change from right circular polarization to left circular polarization. Shape and size of signal is changed due to redistribution of atomic population for different polarization state of control laser field.

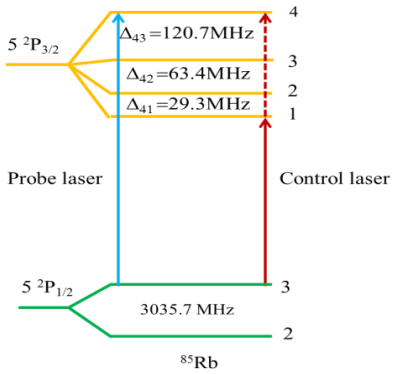


Fig. 3.4 Energy level diagram of $^{85}$Rb showing the hyperfine structure of the $5S_{1/2}$ and $5P_{3/2}$ levels.

Here we describe some detail about occurrence of seven peaks at different frequency domain. As the frequency of probe laser beam is fixed and locked between $F_g$ = 3 and $F_e$= 4 hyperfine of $^{85}$Rb D2 transition line. The pump beam is scanning between ground ($F_g$ = 3) and excited hyperfine components ($F_e$ = 2, 3, 4). As we have selected $F_e$ = 4 as a zero point, then possible velocity groups on resonant to the hyperfine components due to the pump beam can be 0 - kv = 0, $-\Delta_{43}$(= 120.64 MHz), and $-\Delta_{42}$(= 184.041 MHz) as shown in Fig. 3.4 (as pump beam scanning between hyperfine components $F_e$ = 2, 3, 4) ) and possible velocity groups on resonant to the hyperfine components due to probe laser beam scanning can be $\delta_c$- kv = 0, $-\Delta_{43}$(= 120.64 MHz), and $-\Delta_{42}$(= 184.041 MHz). Thus detuning $\delta_c$ which an atom feels for pump and probe laser can be obtained from kv = 0, 120.64 MHz, 184.041 MHz. Thus $\delta_c$ = -184.041 MHz, -120.64 MHz, -63.401 MHz, 0 MHz, 63.401 MHz 120.64 MHz, 184.041 MHz. Thus we observe seven resonances peaks when the pump laser is scanned through hyperfine

components between $F_e$ = 4 and $F_e$ = 2 as shown in Fig. 3.3a (theoretical calculated) and 3.3b (experimentally observed). As mentioned that the polarization of probe beam is fixed at right circular polarization while the polarization of coupling laser is changed from right circular to left circular polarization by changing the angle between optics axis of the quarter wave plate and vertically polarized probe beam with an increment of 15 degree. A vertically polarized coupling beam is passed through quarter wave plate with optic axis angle of +45 degree with respect to y-axis to make it as right circularly polarized coupling beam. Than the optic axis angle (ε) of the quarter waveplate with respect to the y-axis is rotated in anti-clockwise direction by +15 degree. The polarizations of the pump beam at ε = 0 and ε =15 are vertically linear polarization and elliptically polarizations. Finally the polarization of the coupling laser beam becomes left circular polarization at ε = -45. For each polarization of the probe laser beam, transmission signal of the probe beam are measured theoretically and experimentally. In Fig. 3.3 we have seven calculated and observed resonance peaks in between -300 MHz to 300 MHz control laser detuning frequency range. We can see that the signal for cycling transition $F_g$ = 3 to $F_e$ = 4 (fourth peak from left to right in the Fig. 3.3) is significantly changing as the polarization of coupling laser is changes. In case of $\sigma^+$–$\sigma^+$ –polarization (both coupling and probe lasers are right circularly polarized) the doublet structure (EIT-like) can clearly be observed which is the main difference from case of $\sigma^+$–$\sigma^-$ -polarization of probe and coupling lasers in the spectrum. According to transition selection rule $\Delta m_F$ = 0, ±1, the right circularly polarized probe beam is consider to be

taken as $m_F$ = +1 and coupling laser as $m_F$ = -1. In this particular condition, the two photon transition probability is lowest then all other polarization configuration of coupling and probe lasers beams. The atomic populations decay into dark state through optical pumping process by control laser and due to high saturation effect the transmission increase. Similarly if we look at other peaks of the spectrum it can be seen that first and second peaks continuously increasing as the polarization of control laser changes from right circular polarization to left circular polarization. Intensity of third, fifth and sixth peak is gradually decreasing while the 7$^{th}$ peak of the spectrum is totally upside down with orthogonal polarization state of probe and coupling lasers fields due to redistribution of atomic population in magnetic sub levels.

## 3.5 Linear-linear polarization dependences of the velocity dependent probe transmission signal

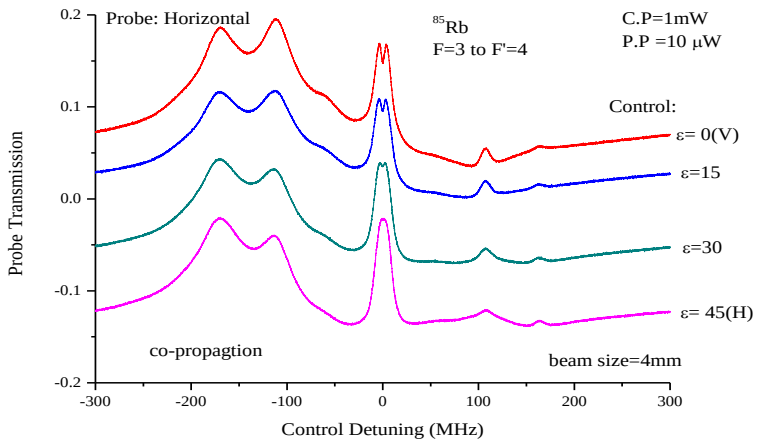


Fig. 3.5 Experimentally obtaind probe beam transmission spectra in case of linear and orthogonal polarization configuraltion.

We have observed experimentally probe transmission profiles due to thermal velocities of atoms in coupling-probe experiment from hyperfine level between the ground $5S_{1/2}$ and excited $5P_{3/2}$ D2 transition line of $^{85}$Rb atom with degenerate magnetic sub-level with respect to changes of polarization of coupling beam We have calculated the transmission and absorption spectra of $^{85}$Rb between hyperfine-level $F_g = 3 \rightarrow F_e = 4$ with degenerate magnetic sublevels when polarization coupling beam is changed from vertically polarized to horizontally polarized by changing the angle between optics axis of the half wave plate and vertically polarized coupling beam with an increment of 15 degree while the polarization of probe laser is fixed as horizontal linear polarized.

As explained earlier in detail the occurrence of probe transmission peaks in case of circular polarization configuration of coupling and probe laser fields. Similarly in case of liner polarization configuration of coupling-probe fields, one can explain these probe transmission peaks exactly similar way. Fig. 3.5 show transmission profile variation with respect to scanning of coupling laser beam between-300MHz to 300 MHz in closed system with zero detuning at $F_g = 3$ and $F_e = 4$ of $^{85}$Rb atom. The probe and coupling powers were kept fixed as 10 μW and 1mW respectively. The probe laser frequency is fixed and locked to transition between $F_g = 3$ ground and $F_e = 4$ excited state while the frequency of control laser is scanning. In case of linear and parallel polarization configuration of coupling and probe laser beams, the level configuration consists of separate two-level system which is connected through spontaneous emission. Each two-level system compose of

a two Zeeman sublevel with equal magnetic quantum number in ground and excited state $m_g = m_e$. A narrow transmission peak in linear and parallel case can be observe as the population transfer due spontaneous emission between pairs of level connected by these fields. As coupling-probe laser cannot form N-type or V-type atomic system in case of linear and parallel polarization configuration, that is why we cannot observe EIA-dip in lowest peak of Fig. 3.5.

In linear-linear configuration, the most interesting and most complex case is linear and orthogonal polarizations of coupling and probe beams. Linear and orthogonal polarization configuration provides almost similar probe transmission signal as in case of circular and orthogonal polarizations of coupling and probe laser because each of linear polarization consist of right and left circular polarizations with more transitions lines in DTLS. In Fig. 3.5 the top most curve show the result for case when coupling and probe laser fields are linear and perpendicular polarized. The main difference between circular-orthogonal and linear-orthogonal case is the optical pumping effect. Optical pumping is linear phenomenon for spontaneous decays and compare to linear polarization configurations the optical pumping effect in circular polarization configuration of coupling and probe laser is much stronger. When the polarization coupling and probe beams are linear and orthogonal, the strong coupling beam will transfer all the atomic populations to Zeeman sub-level through optical pumping mechanism and as result probe transmission decrease down at zero detuning regions. In DTLS polarization of probe and control laser fields plays significant role to transfer of population from excited states and consequently variation in absorption

and transmission signal profile is observed when the polarization state of control and probe lasers fields were changed.

## 3.6 Power dependent probe transmission spectra in case of linear and perpendicular polarizations.

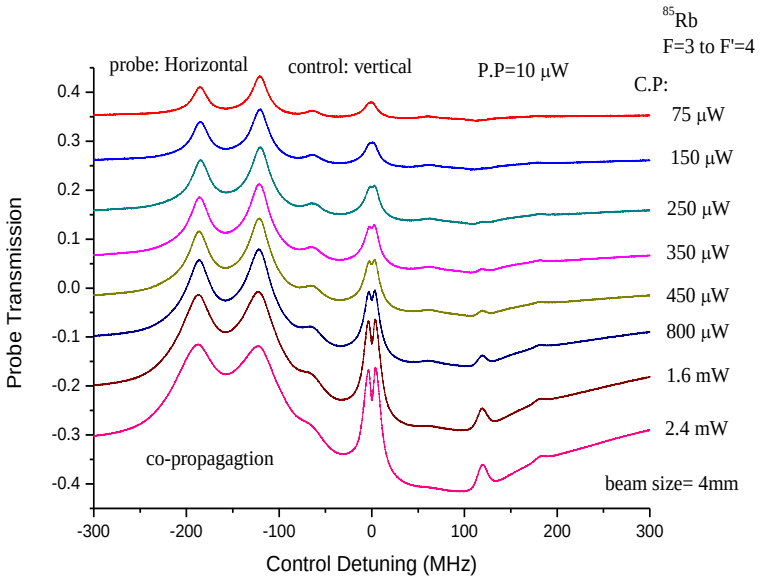


Fig 3.6 Experimentally obtaind coupling power dependent probe transmission spectra in case of linear and orthogonal polarization configuraltion between -300 MHz and 300 MHz.

In Fig. 3.6 we show obtained coupling power dependent transmission spectra of $F_g = 3 \rightarrow F_e = 4$ D2 transition line of $^{85}$Rb atom in rubidium vapor cell. Probe laser is horizontally polarized while the control laser is linear vertically polarized. The intensity of probe laser is fixed at 10 μW while the

intensity of coupling beam is changes from 75 μW to 2.4 mW. Probe laser is locked to $F_g = 3 \rightarrow F_e = 4$ while the coupling laser is scanned through hyperfine $F_g = 2$ and $3 \rightarrow F_e = 1,2,3,4$ of $^{85}$Rb. In linear and perpendicular polarization configuration, all ground state magnetic sub-levels are coupled to strong coupling laser beam and atomic population is distributed among all these ground state sub level. The size of these seven peaks depends upon the power of lasers beam. As shown in Fig. 3.6, when power of coupling laser is very weak, the optical pumping effect is lower and we observe smaller sized transmission spectra. However as power of coupling laser is gradually increased, the transmission peaks become clearer because the intensity of coupling laser is directly related to atomic coherence and in cycling transition one can observe very interesting phenomenon of probe absorption at zero detuning. It is already explained in detail in case of circular-circular polarization configuration that why and how these seven peaks appears when coupling laser scanned between -300 MHz and 300 MHz frequency range. Due to optical pumping effect the shape and size of transmitted peaks are changes due to redistribution of atomic population.

## 3.7 Probe Transmission spectra in an open system

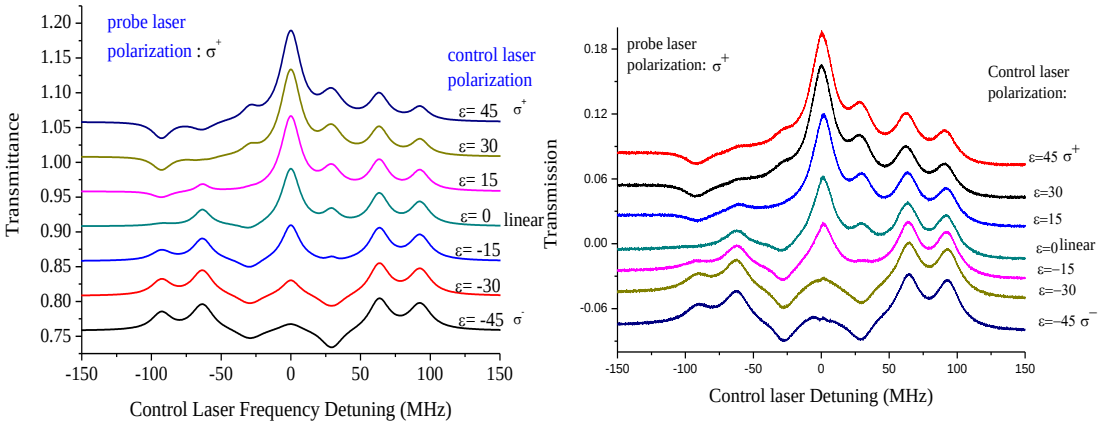


Fig. 3.7 Probe transmission spectra of $F_g = 2 \rightarrow F_e = 3$ of $^{85}$Rb at (a) theoretically calculated from density matrix equation (b) experimentally observed spectra. Probe laser is right circularly polarized and the polarization of control laser is change from right circular polarize to left circularly polarized.

This set of experiment was performed using co-propagating coupling and probe laser beams in an open system of $^{85}$Rb atom D2 line. Theoretically calculated and experimentally observed probe transmission spectra are shown in Fig. 3.7 the intensities of coupling and probe lasers were 90 μW and 9 μW respectively. The frequency of probe laser beam is fixed and locked between $F_g = 2$ and $F_e = 3$ hyperfine of $^{85}$Rb D2 transition line and coupling beam is scanning between ground $F_g = 2$ and excited hyperfine components $F_e = 1, 2, 3$. As probe laser is tuned to hyperfine level $F_g = 2 \rightarrow F_e = 3$ for zero velocity atoms, the transmission of probe laser is increases

when the coupling laser tuned to $F_g = 2 \rightarrow F_e = 1, 2, 3$ also for zero velocity atoms. The additional peaks appears in the spectrum can be explain by Doppler effects. For atoms moving in opposite direction to the propagation direction of laser beam with some particular velocities which correspond to the shifts of 63.4 MHz and 92.7 MHz shown in Fig. 3.4. It is clear that the atoms with velocities which can provide a shift of 63.4 MHz interacting with probe laser beam. The probe laser couple the transition $F_g = 2 \rightarrow F_e = 3$. One can observe the probe transmission peak if the coupling beam is tuned same transition for the same velocity group. This means the peak at 92.7 MHz is not only because of laser interactions with zero velocity atoms but also interaction of atoms in 63.4 MHz shifted velocity group. As coupling and probe laser co-propagates through vapor cell detuning for coupling and probe lasers which atom feel are $\delta_{control} = \delta_c - kv$ and $\delta_{probe} = \delta_p - kv$, respectively where $\delta_c$ and $\delta_p$ are coupling and probe laser detuning from $F_g = 2 \rightarrow F_e = 3$ resonance line respectively. Fig. 3.7(a) and (b) show spectral change between frequency region including $F_e = 1$, 2, and 3 hyperfine components with reference to fixed laser frequency of $F_g = 2 \rightarrow F_e = 3$ and for theoretical calculation and experimental observation, respectively. Because of Doppler's effect, the additional peaks in the spectrum can be observed. From energy level diagram shown in Fig. 3.4, one can predict the exact position of these peaks by looking at frequency shifts due to the Doppler's effect as energy shifts of excited level. As we have taken $F_e = 3$ as a zero point, then possible velocity groups on resonant to the hyperfine components due to the pump beam can be $0 - kv = 0$, $-\Delta_{23}$(= 63.4 MHz), and $-\Delta_{31}$(= 92.7 MHz) as shown

in Fig. 4 (as pump beam scanning between hyperfine components $F_e$ = 1, 2, 3) ) and possible velocity groups on resonant to the hyperfine components due to probe laser beam scanning can be $\delta_c$- kv = 0, -$\Delta_{32}$(= 63.4 MHz), and -$\Delta_{31}$(= 92.7 MHz). Thus detuning $\delta_c$ which an atom feels for pump and probe laser can be obtained from kv = 0, 63.4 MHz, 92.7 MHz. Thus $\delta_c$ = -92.7 MHz, -63.4 MHz, -29.3 MHz, 0 MHz, 29.3 MHz 63.4 MHz, 92.7 MHz. It is observed that the population distribution of among the ground sub-levels are affected by polarization configuration and intensities of laser filed so the magnitude of the transmitted peaks showing different behavior at different polarizations of coupling and probe lasers beams. The experimental results matched very well with those theoretical results which were calculated from density matrix equation.

## 3.8 Probe absorption and transmission spectra in an open system

It has been believed that in open system EIA signal could not be occur. However, Kim *et al*. [30] observed EIA signal in an open system using an orthogonal linear polarization configuration of coupling and probe laser beams with co-propagating beam directions Here we describe the experimentally observed narrow EIA-dip signal in open system of $^{85}$Rb and $^{87}$Rb D1 and D2 transitions line.

The experimentally observed EIA signal in D2 transition line of both isotopes of rubidium atoms for circular and orthogonal polarized coupling and probe lasers with coupling power of 3 mW and probe laser power of 10

μW are shown in Fig. 3.8 (a) and (b).

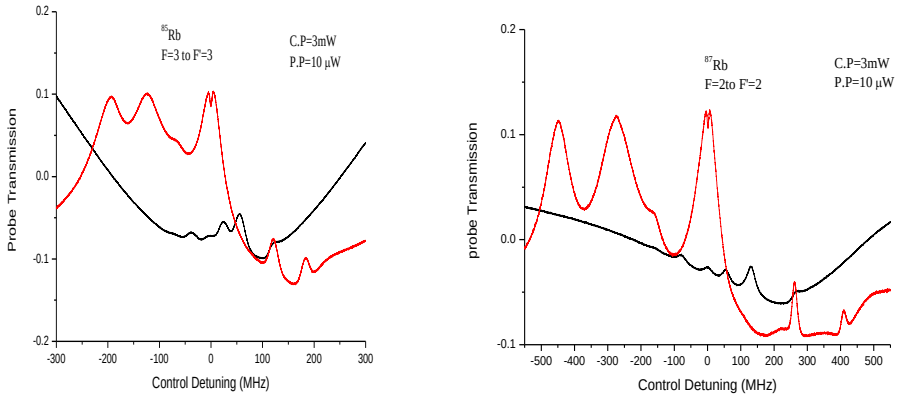


Fig. 3.8: Experimentally observed EIA signal when control laser is right circularly polarized and probe laser is left circularly polarized. The power of control laser is 3 mW while the power of probe beam is 10 μW. (a) Probe laser is locked to $F_g = 3 \rightarrow F_e = 3$ while the coupling laser is scanned through hyperfine $F_g = 2$ and $3 \rightarrow F_e = 1,2,3,4$ of $^{85}$RB (b) probe beam is locked to $F_g = 2 \rightarrow F_e = 2$ and coupling laser is scanned through hyperfine $F_g = 1$ and $2 \rightarrow F_e = 0,1,2,3$ of $^{87}$Rb D2 transition line in an open system. The bottom curve show the SAS signals of respective rubidium isotopes.

By using saturation absorption spectroscopy (SAS), the probe beam is locked to hyperfine components $F_g = 3 \rightarrow F_e = 3$ and scanning of control beam between -300 MHz and +300 MHz between frequency region including $F_g = 2$ and $3 \rightarrow F_e = 1,2,3,4$ of $^{85}$Rb and similarly in case of $^{87}$Rb, probe beam is locked to $F_g = 2 \rightarrow F_e = 2$ and coupling laser is scanned through hyperfine $F_g = 1$ and $2 \rightarrow F_e = 0,1,2,3$. As mentioned [2] that to observe EIA the atomic system must be closed but in case of $F_g = 3 \rightarrow F_e = 3$

of $^{85}$Rb and $F_g = 2 \rightarrow F_e=2$ of $^{87}$Rb atom system are open because of selection rule excited stat atoms can decay back to both of ground state sub levels and does not obey one of the three conditions for observing EIA dip signal so one can expect EIT because control laser is pumping atomic population in to those ground levels which are not coupled to probe laser (dark state) so the number of atoms in original ground state are reducing down. These dark states coupled coherently with control and probe laser fields but the probability of transfer of coherence from excited state to ground state reduced down so we observed decreased EIA dip signal compared with a closed system. The structure near frequency +121MHz, +194 MHz *etc*. in upper trace of Fig. 3.8 (a) and similarly the structure near frequency +267 MHz and +410 MHz in upper trace of Fig. 3.8 (b) are due to velocity selective optical pumping.

## 3.9 Absorption and transmission spectra in D1 line (open system)

In case of D1 line, we obtained EIA signal along with VSOP peaks for all possible allowed optical transitions. Fig. 3.9 show the schematic diagram of energy levels for both isotopes of Rb atom and each isotope separately compose of four allowed transition lines between $5S_{1/2}$ and $5P_{1/2}$ level.

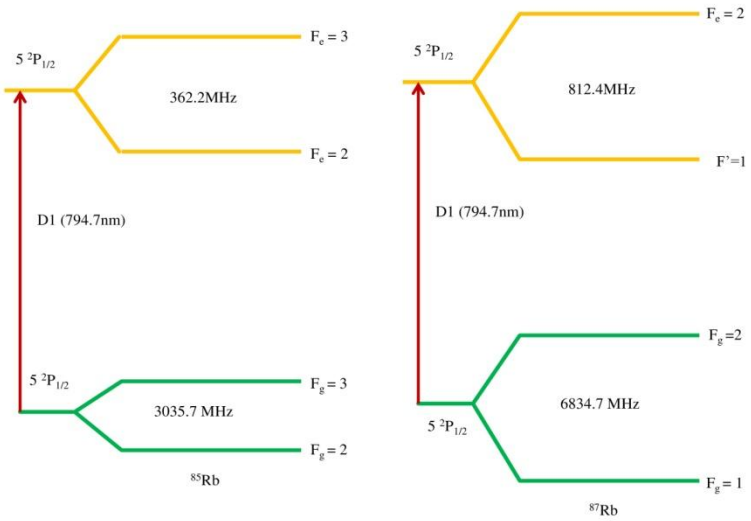


Fig. 3.9 Energy level diagram of $^{85}$Rb and $^{87}$Rb atoms D1 line showing hyperfine structure of the $5S_{1/2}$ and $5P_{1/2}$ level. Energy values are in MHz.

Experimentally observed probe absorption spectra for various values pump power with fixed probe intensity at 30 μW is shown in Fig. 3.10. The probe beam frequency is fixed and locked to the transition between $F_g$ = 2 and $F_e$ = 3 hyperfine D1 transition line of $^{85}$Rb atom while pump beam frequency is scanning around the same transition. Probe laser is horizontally polarized while the control laser is vertically polarized

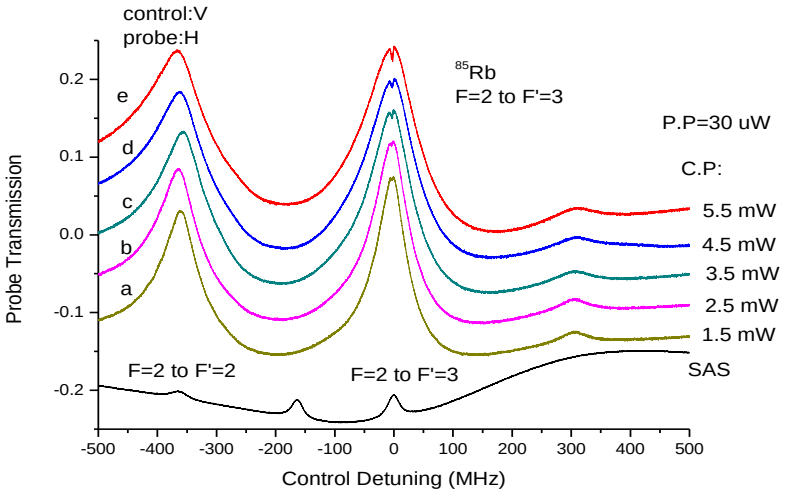


Fig. 3.10 Experimentally observe probe absorption spectra for $F_g = 2$ to $F_e = 3$ D1 transition line of $^{85}$Rb atom for various coupling powers with fixed probe laser power of 30 μW. The bottom curve is SAS signal for calibration.

By looking at the spectra shown in Fig. 3.10, we can observe the transmission peak on left side of EIA-dip signal near -362 MHz which is quite similar separation as shown in Fig. 3.9 between $F_g = 2 \rightarrow F_e = 3$ of $^{85}$Rb atom. This transmission peak is due to velocity selective structure with broad linewidth (FWHM). We could not observed EIA dip-signal up to 1 mW of coupling laser field but as the intensity of coupling field is increased we observe clear EIA signal which stated with 1.5 mW and signal become more clears with high coupling power of 5.5 mW. Compare to closed system much power is needed to observe EIA signal in an open system.

Fig. 3.11 show the absorption spectra observed in open system ($F_g = 3$ to $F_e = 2$) of $^{85}$Rb D1 transition line as a function of pump laser detuning frequency depending upon the intensity of coupling laser field. The pump laser is vertically polarized and probe laser is horizontally polarized. The

probe laser frequency is locked to transition between $F_g = 3$ ground and $F_e = 2$ excited state while the frequency of pump laser is scanning. The intensity of probe laser is fixed to 15 μW and the power of pump laser field is changing from 1mW to 8.5mW with an interval of 1 mW. The bottom curve shows SAS spectrum. We can see two transmittance peaks at $F_g = 3 \rightarrow F_e = 2$ and $F_g = 3 \rightarrow F_e = 3$ respectively, at coupling laser power of 1 mW. These peaks occur when control laser depletes population in open system by optical pumping. Most of the atoms in $F_e = 2$ state decay spontaneously to ground stat $F_g = 3$ and remaining atoms transfer to other ground state $F_g = 2$.

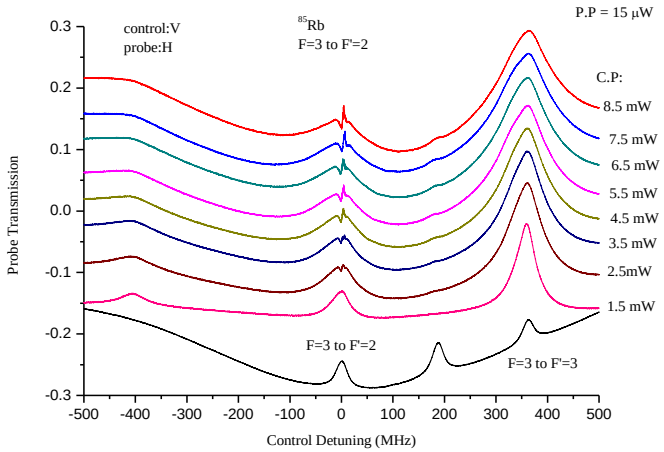


Fig. 3.11 Experimentally obtained probe absorption spectra of $F_g = 3$ to $F_e = 2$ , 3 D1 transition line as a function of control laser frequency while the probe laser frequency is locked to $F_g = 3$ to $F_e = 2$. Probe laser is horizontally polarized while control laser is vertically polarized. The power of probe laser is fixed to 15 μW. The power of control laser is increasing from 1 mW to 8.5 mW. The lowest curve indicates the SAS spectra of D1 line of $^{85}$Rb.

Since this system is an open system and absorption spectra should show transmission because strong coupling laser optically pumped the atomic population to other sub-levels which are not coupled with weak probe laser. Up to 1mW of coupling beam power we only observe the transmission peaks as the power of coupling laser field increases, EIA dip start to appear near 3.5 mW. Furthermore, an increase in control laser power breaks up EIA into two dips and convert it to EIT based on CPT into dark state. But we observe EIA signal although these observed signals are very small compare to those signals which we obtained in a closed atomic system of both isotope of Rb atom. Thus we can say that spectrum shown in Fig. 3.11 is determined by EIT. This conversion of EIA into EIT also been observed by Z. Y-Ting *et al*. [42] in closed system of Cs atoms.

# Chapter 4
# Spectral features of electromagnetically induced absorption in $^{85}$Rb atoms

## 4.1 Introduction

Previously there have been lot of research works related to broad EIA-dip signals based on different parameters like powers of beams, different polarization configuration, beam size, and geometry of the experimental setup *etc*., but thermal averaging effects on spectral features like ultranarrow signals of EIA were not investigated theoretically and experimentally with respect to power of pump beam by many researcher groups. In high power pump limit of circular and orthogonal polarization configuration, thermal averaging effects play decisive role in the splitting of EIA spectra.

In this chapter we provide comprehensive detail of absorption spectra by using newly developed theoretical technique. This technique is used for solving the generalized time dependent density matrix equation to explain the features of absorption spectra without considering phenomenal parameters. This new method unravels EIA spectra with ultra-narrow and split signals based on intensity of pump laser beam in both thermal and stationary atoms. In this chapter we mainly focused on obtained transmission spectra for the case of $F_g = 3 \rightarrow F_e = 4$ cycling transition D2 line of $^{85}$Rb atoms. Pump beam power dependent ultranarrow and split spectral features of EIA in broad subnatural EIA have been investigated. Sensational variations in ultranarrow signals are observed with an increase in pump

power due to thermal average effects. In case of same-circular and circular and orthogonal polarization of pump and probe beams, the EIA signals have ultranarrow EIA features in low power of pump beam. However at high power of pump beam the behavior of EIA signals are different at different polarization states of pump and probe beams. A complete detail of EIA features with respect to pump power in case of same and orthogonal polarization configuration is present in upcoming sections of this chapter. A part from these EIA features we make sure the coherent effect in EIA by investigating the difference between transmission signal with and without coherence terms in density matrix equation such as transfer of coherence or Zeeman coherence. We concluded that the coherence terms of density matrix equation determined the broad dips in normally coherent EIA features instead of incoherent power saturation effects.

Our experimentally observed results in case of two independent lasers for each of pump and probe match well with the calculated features for same and orthogonal polarization configuration except ultra-narrow EIA peak. This is because of lasers linewidth of two independent pump and probe lasers which is approximately equal to 2 MHz.

## 4.2. Calculated absorption spectra from various coupling beam Rabi frequencies

### 4.2.1Theoretical calculated spectra

Probe absorption signals with coherence effects between magnetic sublevels were calculate by using above mentioned technique. Pump-beam Rabi frequencies dependent absorption spectra have been calculated. The coupling beam frequency detuning is fixed at the resonance line while the probe beam frequency is detuned. The results for the stationary atoms ($v = 0$) and Doppler thermal averaged results in case of same polarization configuration are shown in Fig. 4.1(a) and (b) and for orthogonal polarization configuration of pump and probe beams are shown in Fig. 4.1(c) and (d), respectively. In Fig. 4.1, the Rabi frequency of the probe beam is $2\pi$ × 1MHz (hereafter, $2\pi$ is omitted). At low pump Rabi frequencies the ultranarrow EIA spectra are observed in both, same and orthogonal polarization configuration when the stationary atoms are considered which are shown in Fig. 4.1(a) and (c). As the pump Rabi frequency increases, famous Mollow-type three-peaks are observed and shown in Fig. 4.1(a), while four absorption peaks are found in Fig. 4

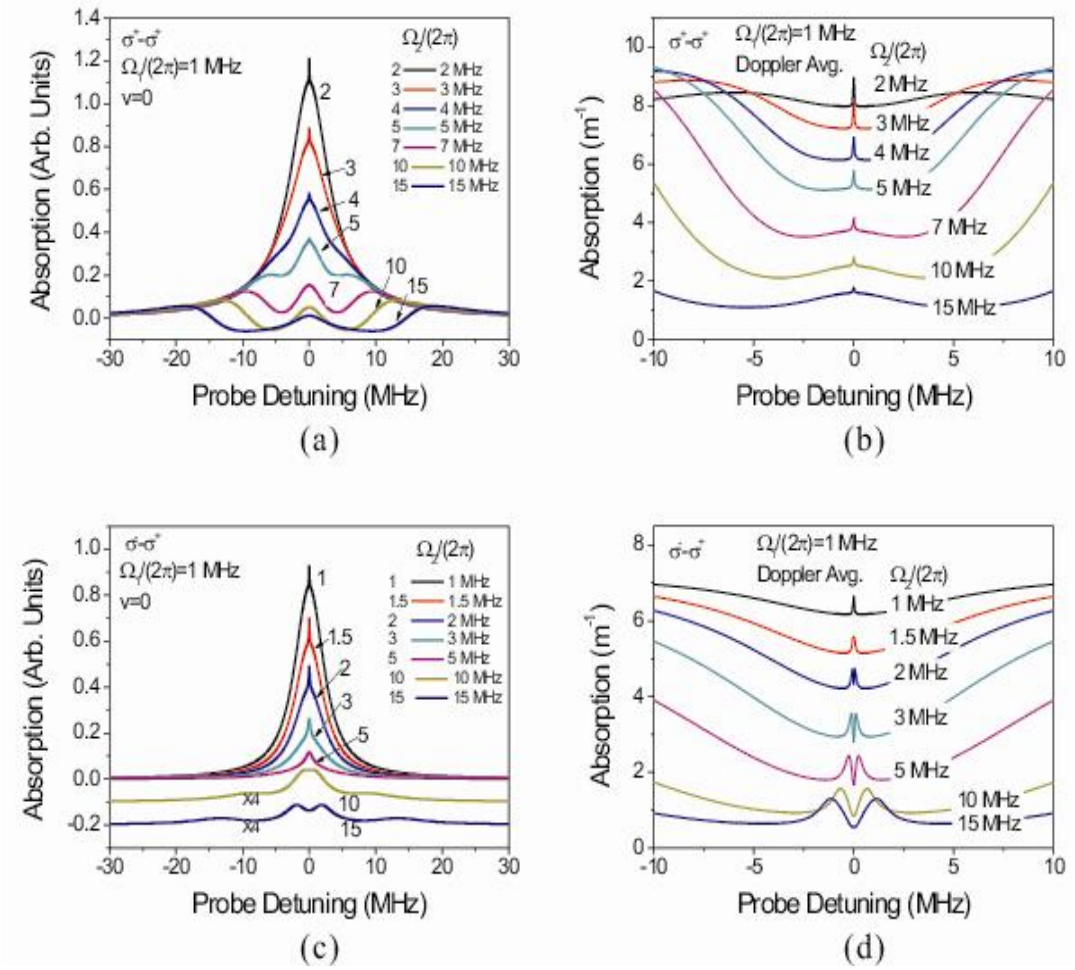


Fig. 4.1 Theoretical probe absorption spectra obtained in the cases of same ($\sigma^+ - \sigma^+$) polarization configuration (a) between −30 and= 30MHz with v = 0, (b) between −10 and 10 MHz with thermal motions of atoms, (c) orthogonal ($\sigma^- - \sigma^+$) polarization configuration between −30 and 30 MHz with v = 0, and (d) between −10 and 10 MHz with thermal motions of atoms, respectively.

Fig. 4.1(d) shows the results of case when thermal average effect is taken into account. It can be seen that as the pump Rabi frequency increases the

ultra-narrow EIA peaks become wider and splitted but still the linewidth of these peaks remains sub-natural. In Fig 4.1(c) the ultra-narrow signals which were observed up to 3 MHz of pump Rabi frequency remain only at 1 MHz of probe Rabi frequency. In case of same polarization combination of pump and probe laser beams, the ultra-narrow peak can be observed at low power of pump beam and even at high power of pump laser this ultra-narrow peak are generated but the magnitude of this ultra- narrow signal become weak as shown in Fig.4.1(b).

To examine various aspects of thermal averaged absorption coefficient for same and orthogonal polarization configuration cases, particular absorption coefficient at v = 0 and ± 5ms$^{-1}$ are calculated as shown in Fig.4.2. As observed in the partial energy level diagrams using a dressed state formalism shown in Fig. 4.2, the resonances of the probe detuning ($d_p$) for the same and orthogonal polarization cases at $d_c = 0$ are given by

$$d_p = 0, \pm \sqrt{(kv)^2 + \Omega_2^2} \tag{4.1}$$

for same polarization,

$$d_p = \pm 1/2[\sqrt{(kv)^2 + \Omega_2^2} + \sqrt{(kv)^2 + 15\Omega_2^2/28}\ ], \quad \pm 1/2[\sqrt{(kv)^2 + \Omega_2^2} - \sqrt{(kv)^2 + 15\Omega_2^2/28}] \tag{4.2}$$

for orthogonal polarization case respectively.

It can be seen in Fig. 3 that separation of dressed state is different. In case of same polarization configuration ultra-narrow peaks can be observed at all pump laser power in thermal averaged absorption spectra. This fact can be

explained and understand in straight forward way: despite the consequences of motion of atoms, there exist a dispersive-shaped resonance at $d_p = 0$ as mentioned in equation (4.1). The slope of this resonance for positive and negative value of atomic velocity is totally opposite to each other which can be seen in Fig. 3(a). The narrow absorptive signal which is shown in Fig 4.2(b) is the consequence of combined velocities effect contributed by individual atom. On the other hand in case of orthogonal polarization configuration, refer to equation (4.2) the atomic velocities dependent four resonances exist. Fig. 4.2(b) show the result of these particular case for v = 0 and $V = \pm 5 ms^{-1}$. After taking thermal averaging effect the two outer resonances result flat signals. Similarly two interior resonances results in two splitted EIA signal centered at $\sim \pm (1 - (15/28)^{1/2})\Omega_2$. So ultra-narrow signal can only be observed at very low power of pump beam and splitted EIA spectral profile at moderate or high pump power.

In Fig. 4.3 we show the results for pump scanning at resonant condition of probe ($d_p = 0$). All the parameters and schemes are just similar as those in Fig. 4.1. The narrow features for zero velocity atoms are similar to those result which are presented in Fig 4.1 due to coherent effect which is commonly depends upon the difference in detuning of pump and probe laser beams. But on the other hand the Mollow-type three resonance peaks due to same polarization

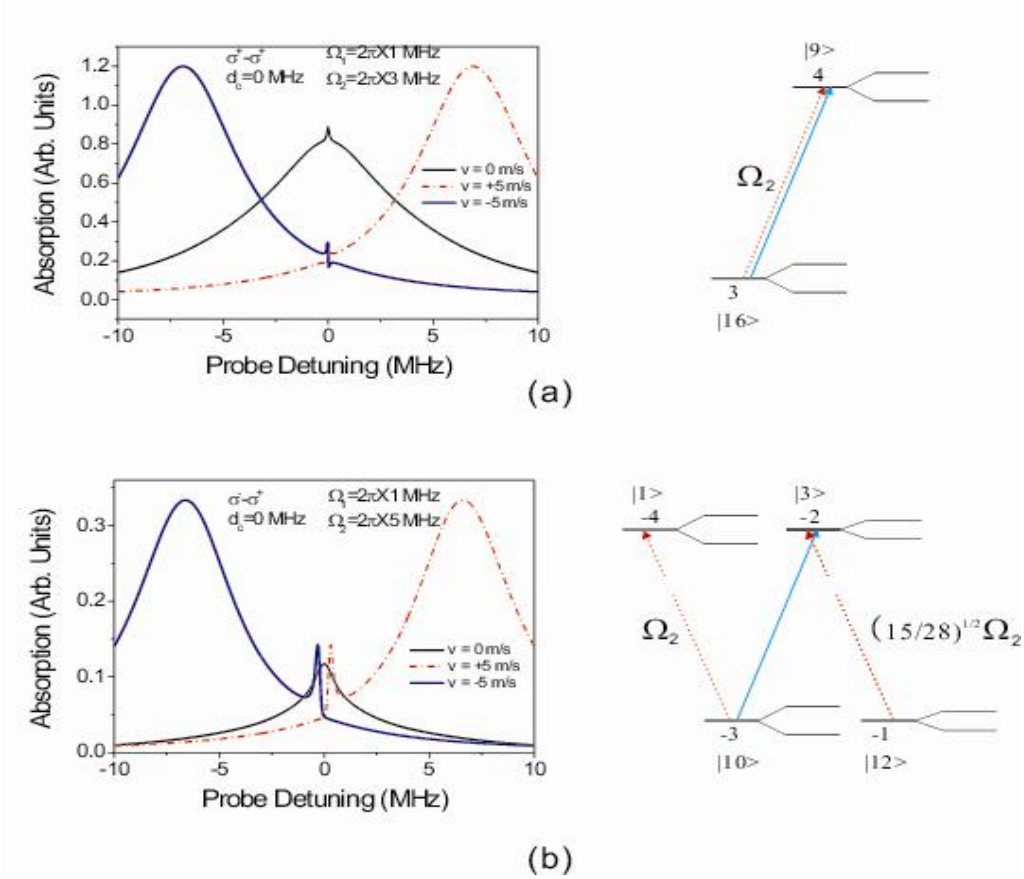


Fig. 4.2 Calculated absorption coefficients for (a) the same and (b) orthogonal polarization cases at v = 0 and ±5 m s−1. Simple dressed state energy level diagrams are also shown to explain the resonances.

and four absorption peaks in case of orthogonal polarization combination are not easily visible. This happened because the exact location of resonance depends upon the Rabi frequency and detuning of pump beam. As pump beam is scanning so there will be variation in its detuning and that is why the resonance become unclear. When thermal averaging effect and small

scanning range are considered then non coherent effects are averaged out so we can observe almost similar absorption spectra shown in Fig. 4.1. At far detuning region, it is mostly observed that the results for two scanning schemes are different.

## 4.3 The origin of the broad sub-natural EIAs

To investigate the origin of broad sub natural EIAs, we solved density matrix equation in such conditions that coherence effect such as Zeeman coherence and transfer of population were not taken into account. Theoretically calculated probe absorption spectra with and without coherence effects between magnetic sub levels are shown in Fig 5. The absorption spectra with coherence effect is represented with solid line and without coherence effect is shown by dash line are observed in case of same ($\sigma^+ - \sigma^{+)}$ and (b) orthogonal ($\sigma^- - \sigma^+$) polarization configurations. For numerical calculation we take the circular laser beam with radius 2mm and Rabi frequencies of 15.7 MHz for pump and 0.94 MHz for probe beam. The method of calculation without considering the coherence effect is called simply rate-equation. As shown in Fig. 4.5, in the results of the rate-equation calculations disregarding coherence effects such as TOC and TDTOP, EIA spectra disappear. So the occurrence of EIA in both case due to coherence effects instead of incoherence effects.

In Fig. 4.4(a), rate-equation calculations were performed by neglecting time-dependent terms in equation (2.4) and terms of $e^{-2i\delta pt}$ and $e^{i\delta pt}$ in

equation (2.5), which result from the nonlinear wave mixing between the pump and probe field. There exists significant difference between the cases when calculating the absorption spectra with and without coherence effects. This mean that the coherence term leads to results in both ultra-narrow absorption signal and broad subnatural EIA signals. In off resonance condition the population oscillation term do not disappear so big difference is exists between two results. even though absolute inequity of the signals due to coherence effects was reported in the case of pure two-level atoms [43, 44], it was not likely to discriminate the signals for the complex levels of $F_g = 3 \rightarrow F_e = 4$ of the $^{85}$Rb-D2 line. In Fig. 4.4(b) the rate equation calculations are carried out by neglecting the Zeeman coherences between the magnetic sublevels in the excited and the ground states. But, the difference between cases with and without coherence effects exists only near zero detuning because the Zeeman coherences established between the magnetic sublevels in the excited state die out in the off resonance situation. Obviously it can be seen that the EIA was take place due to transfer of Zeeman coherence of the excited states.

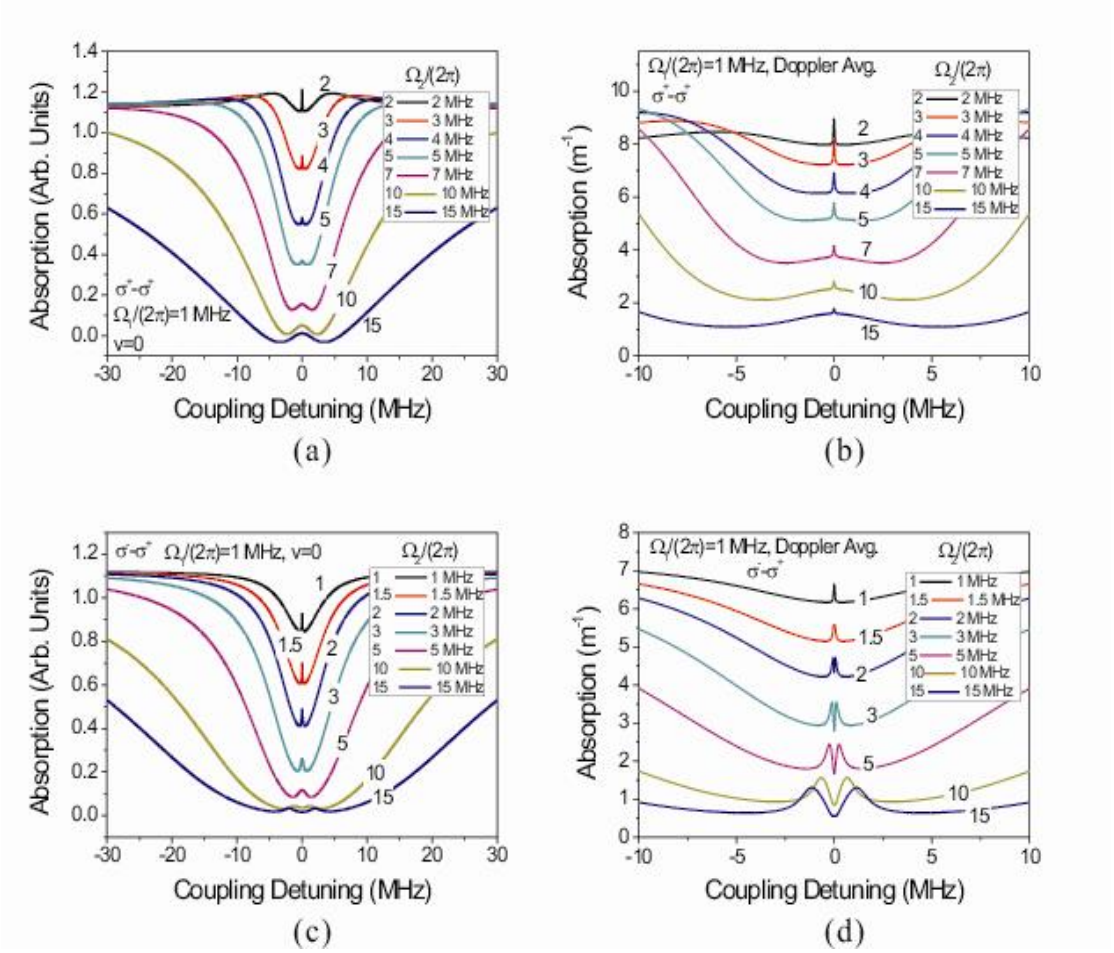


Fig. 4.3 Theoretical probe absorption spectra for the coupling-detuning scanning, obtained in the cases of same ($\sigma^{+} - \sigma^{+}$) polarization configuration (a) for stationary atoms, (b) for thermal atoms, and (c) orthogonal ($\sigma^{-} - \sigma^{+}$) polarization configuration for stationary atoms,(d) for thermal atoms.

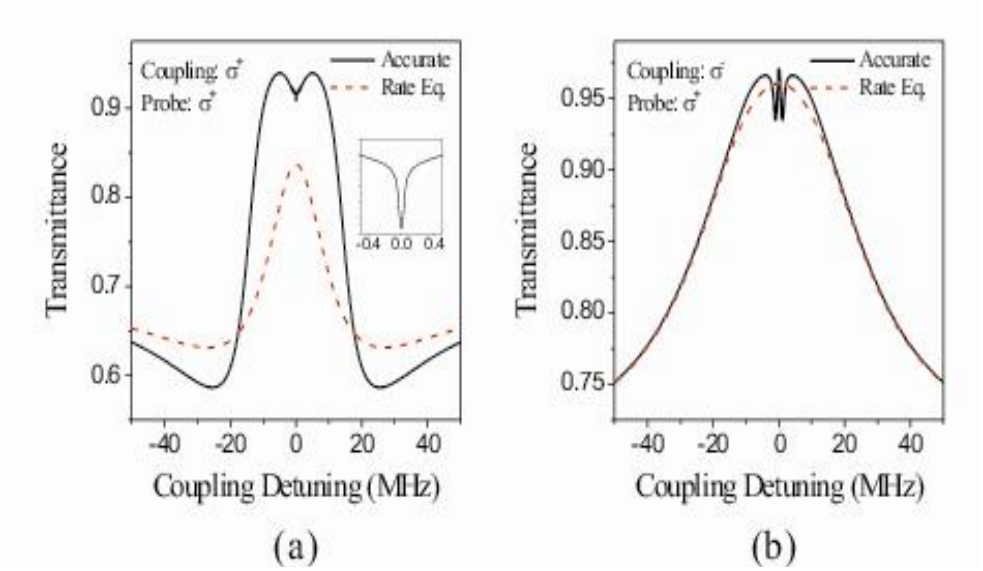


Fig. 4.4 Theoretical probe transmission signals with coherence effects between magnetic sublevels, represented with solid line, and without coherence effects between magnetic sublevels, represented with dashed line, obtained in the cases of (a) same- ($\sigma^+ - \sigma^+$) and (b) orthogonal-($\sigma^- - \sigma^+$) polarization configurations. In the inset of Fig. 4.4 (a) ultra-narrow spectrum is shown.

## 4.5 Explanation of Experimental results.

The experimental setup is described schematically in Fig. 3.1 and also a comprehensive detail of this setup is present in section 3.2. For this particular case of experimental results we used the same experimental setup. The lasers beams with diameter of 4mm and Rabi frequencies of 15.7 MHz for pump and 0.94 MHz for probe are used to observe EIAs absorption spectra. By using saturation absorption spectroscopy (SAS), the probe beam is locked to the hyperfine $F_g = 3 \rightarrow F_e = 4$ transition line while the pump laser is scanned

in wavelength around the same ( $F_g = 3 \rightarrow F_e = 4$) transition.

Fig. 4.5 shows theoretical (upper curve) and experimental (lower curve) probe transmission spectra for the transition $F_g = 3 \rightarrow F_e = 4$ of the $^{85}$Rb-D2 line obtained in the cases of (a) same ($\sigma+ - \sigma+$) and (b) orthogonal ($\sigma- - \sigma+$) polarization configurations of pump and probe beams. For theoretical calculation and experimental observation the spectral features which are shown in Fig. 4.5 have observed when pump beam scanned between frequency range −50 to +50 MHz with respect to the fixed probe-laser frequency of the $F_g = 3 \rightarrow F_e = 4$ transition,

In case of same polarization configuration the pump and probe beams ($\sigma^+ - \sigma^+$) both the lasers excite the same magnetic sublevel between ground and excited states. Thus it is obvious that in this situation pump-probe laser beam cannot form N-type atomic system between magnetic sub-levels so that EIA resonance signal cannot be observed. But there are theoretical predictions for observing EIA signal even in case of same polarization of pump and probe beams due to transfer of population. On the basis of theoretical prediction and calculation we expect not only sub natural EIA signal but also extra ultranarrow EIA signal implanted in broad sub natural EIA. Three different features can be observed in theatrically calculated spectra shown in Fig. 4.5(a). These features like an ultra-narrow EIA, a broad Subnatural EIA, and a very broad probe transmission. All of these signals are enclosed in the Doppler absorption profile. The middle wide probe-transmission spectrum results from pump power-dependent saturation effects and its spectrum increases as the power of pump laser increased. The inset in Fig. 4.5(a) shows stretched spectra of the calculated EIA signal, which shows a spectral

linewidth of ~0.1 MHz. These ultra-narrow and broad sub-natural EIA spectra vanish whenever coherent effect such as TDTOP is eliminated. Asymmetries of the main broad peak in Fig. 4.5 result from overlapping of a closely adjacent spectrum due to power broadening without EIA, which are not shown in Fig. 4.5.

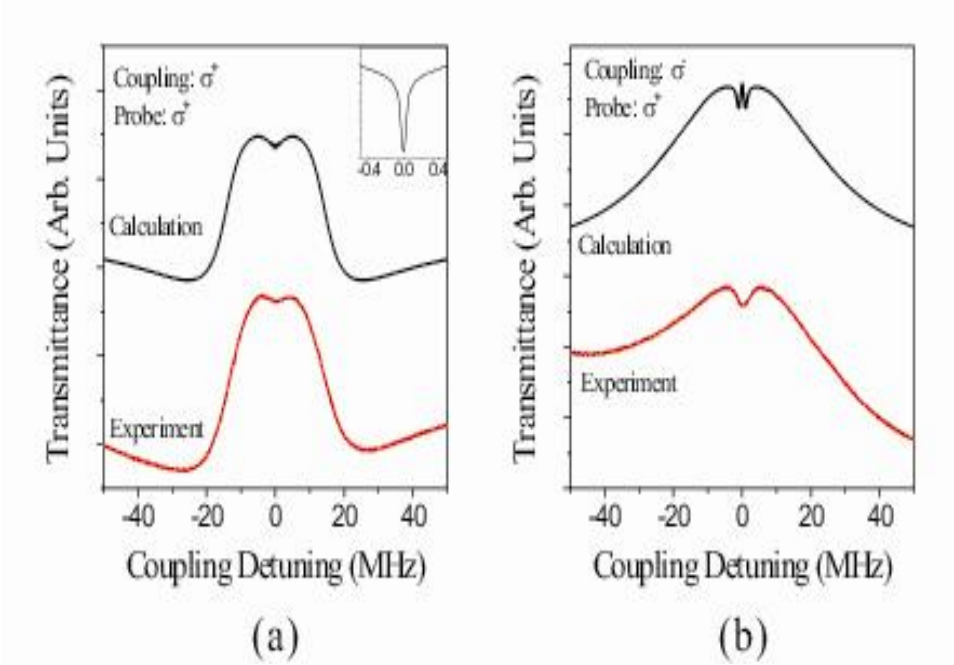


Fig. 4.5 Theoretical (upper trace) and experimental (lower trace) probe transmission spectra obtained in the cases of (a) same ($\sigma+ - \sigma+$) and (b) orthogonal ($\sigma- - \sigma+$) polarization configurations, respectively. The inset in (a) shows expanded portion of ultra-narrow EIA embedded in broad sub-natural EIA obtained from the theoretical calculation.

We mainly concentrate on the middle peak with EIA in the calculation

without considering effects from neighboring peaks. In the theoretical calculation, the effect of neighboring peak on the middle peak is not taken into account so that a symmetric line is observed. The major dissimilarity between theoretical and experimental results is situated at the central part of the spectra, where results from the coherence effects of TDTOP are due to spontaneous decay from upper excited magnetic sublevels for the same polarization configuration.

A.D.W. Gordon *et al*. [43] and V.S. Letokhove *et al*. [44] reported that in the case of a pure two-level system when the decay rate of the upper level is less than that of the lower level due to collisional effects then the additional ultra-narrow line can be observed. They did not consider coherence effects due to interlinking between magnetic Zeeman sublevels. However, EIA is created because of time-dependent oscillating population decays from levels interlinked between magnetic sublevels even in our case, without such collisions as hyperfine-changing collisions in the ground state where the decay rate of the ground state is much slower than those of the excited states. Ultra-narrow EIA signal was not observed in the experiment. The reason that there is no ultra-narrow line in the central part of the spectra is that two different lasers with linewidth of ~1 MHz produce an approximate 2 MHz linewidth difference. Thus, spectral shapes much narrower than the laser linewidth cannot be observed because of the large shared linewidths of the two different lasers. In orthogonal polarization case the observed EIA signal is slightly wider but not much deeper. Experimentally observed linewidth of EIA is 3.8 MHz, which is similar to the theoretically calculated 3.3 MHz. The linewidth of the EIA signal is smaller than the natural linewidth of 6

MHz. At low pump power the EIA signal was not observed. With an increase in pump power the EIA signal steadily increase. Fig. 4.5 (a) and (b) show the agreement between theoretical and experimental transmission signal except for central region. But we performed another experiment by using one laser combined with acousto-optic modulators (AOM) which provided much narrow linewidths of observed EIA spectra so that such ultra-narrow EIA signal has revealed and presented in chapter 5.

The theoretical calculated spectrum in case of orthogonal polarization of pump and probe laser beams shown in Fig. 4.5 (b) consist of two narrow, split EIA signal in upper curve, which splits into two EIAs due to the high power of the pump laser beam. The split EIAs in the central area have a spectral linewidth of ~1 MHz. The experimental spectrum in Fig. 4.5(b) composed of an EIA signal inside the wide probe transmission in the lower curve because of coupling-power saturation. The observed linewidth of EIA is 3.7 MHz, which is similar to the calculated 3.2 MHz without taking into consideration a narrow central peak with a linewidth of 1 MHz. The linewidth of the EIA dip signal is smaller than the natural linewidth of 6 MHz. the experimentally observed spectrum which is compose of an EIA signal. The absence of narrow and split EIA spectra inside the probe transmission is due to pump power saturation effect. As mentioned above that pump and probe laser beam together have broad linewidth so these ultra-narrow and split EIA line could not observed. The increase in pump laser power results in splitting of EIA signals. In case of same polarization combination of pump and probe laser beams, the decrease in pump power does not results in EIA signal. Except central region of spectra strong

agreement between experimental and theoretical transmission spectra is shown in Fig. 4.5 (a) and (b).

# Chapter 5

# Observation of ultra-narrow spectral features of electromanetically induced absopton in two-level system with Zeema multiplet degeneracies of $^{85}$Rb atom

## 5.1 Introduction

Some researcher groups bevlied that there should be existance and splitting of ultranarrow EIA signals based on powers and different polarization combination of pump and probe laser fields. Even at significantly low power of pump beam these ultranarrow signals should have to observe due to time dependent transferof population(TDTOP) in DTLS in case of same polarization combination of pump and probe fields. In closed atomic system the splitting of these ultranarrow signal in case of orthogonal polarization configurtion of pump and probe lasers can occure when the Rabi frequency of pump beam is greater than the decay rate of upper excited state and lower than probe intensity [29].

Uptill now there is no report on experimental obsrevation of such ultranarrow spectral features of EIA signal profile in case of same and orthogonal polarizaition combinations. Althouh an attempt has been made to observe these predicted ultranarrow signals in case of same polarization configurartion by using tow separate lasers sources for pump and probe laser

beams [38] but they did not succed to generate these ultranarrow features. The linewidths of these ultranarrow signal can have in the range of some tens of kilo Hretz (90 to 100 KHz). Useually the lasers systems used for pump-probe experiments have linewidth roughly equal to 1 MHz so in case of two independent laser system experiment the the combined lienwidth of both beam would roughly be equal to 2 MHz which is quite larger than compare to linewidth of predicted ultranarrow signals and we think that this is the main reason that in two laser system of pump- probe experiment no body has generated usch ultranarrow EIA signals.

In this chapter we describe our major experimental breakthrough in which we observe ultra-narrow EIA signals, which were theoretically predicted due to TOP and TOC in cycling transition of DTLS of $^{85}$Rb atoms. The experimentally observed linewidths of EIA signal are less than 100 kHz and much narrower than one predicted in [29]. For this purpose we used two different experimental schemes by using single laser combined with two acousto-optic modulators (AOMs) to investigate theoretical predictions. The experimental ultra-narrow EIA features matched well with simulated spectra obtained by using generalized time-dependent optical Bloch equations.

## 5.2 Experimental Setup

The experimental setup for same circular polarization configuration is shown in Fig. 5.1. We used four different experimental schemes for different polarization combinations of pump and probe laser fields.

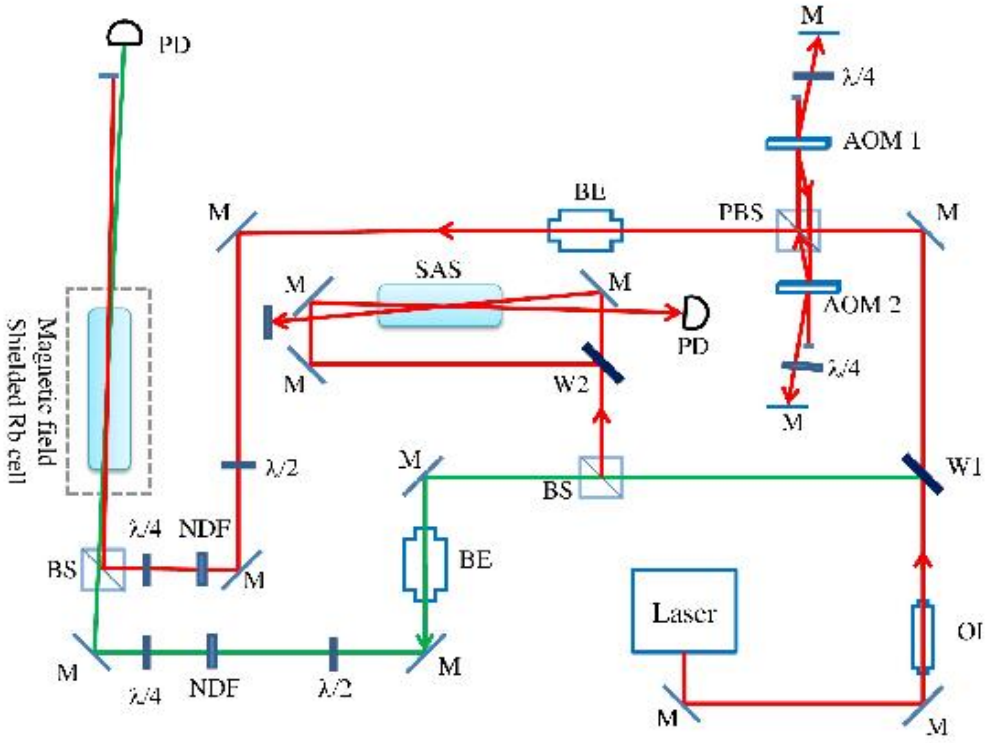


Fig. 5.1 Schematic of the experiment with one laser for both control and probe laser beams. Figure key**:** M-mirror, OI-optical isolator, W-window, AOM-acousto-optic modulator, BE-beam expander, λ/2- half wave plate, λ/4-quarter wave plate, NDF- neutral density filter, PBS-polarizing beamsplitter, PD-photodiode and BS-beam splitter.

A 780 nm homemade external cavity Diode laser (ECDL) is used for both pump and probe beams. The frequency of probe beam is fix and locked on $F_g = 3 \rightarrow F_e = 4$ of $^{85}$Rb D2 transition line by using home-made lock-in amplifier. As shown in Fig, the vertically polarized laser beam is first divided into pump and probe beams by using first window (W1). After window the

reflected beam is further divided into two equal portions by beam splitter (BS). At this point the one part of beam (transmitted) is used as a probe beam for EIA experiment while the other part (reflected) of this beam is used for SAS experiment. The scanning of pump laser frequency is achieved by using two acousto-optic modulators (AOM). The vertically polarized transmitted beam from window (W1) of frequency $\omega_0$ was sent into first AOM1. The AOM will be adjusted to be at Bragg angle such that only first and zero orders beam will be emitted. Here we used the method of double pass of pump beam through AOM1. As zero order beam is not important and there is no more any use of it throughout the experiment that is why we blocked it. To change the polarization state of the first order up-shifted pump beam, this beam passed through quarter wave plate and focused on mirror. Here at this point the pump beam was reflected to trace back the original path passing through all optics and then into AOM1. As the beam has passed through AOM1 twice which results the beam frequency up-shifted to $\omega_0 + 2\omega_1$ , where $\omega_1$ is the central frequency of AOM1. Here the polarization of pump beam has changed from vertical to horizontal polarization because this beam passed twice through quarter wave plate. Now at this stage pump beam can pass through PBS. This doubly up-shifted ($\omega_0 + 2\omega_1$) pump beam was once again sent into second AOM2 for double pass down shift in frequency which results as $\omega_0 + 2\omega_1 - 2\omega_2$ where $\omega_2$ is the central frequency of AOM 2. Again this pump beam passed through $2^{nd}$ quarter wave plate twice so the polarization of this doubly down shifted beam will be vertically polarized just before PBS. Now this beam will be deflected by PBS at 90 degree. Two separate beam expanders were used to expand the pump and probe lasers

beams equal to 4mm in diameter. The polarization of pump and probe lasers beams were made perfectly vertical and horizontal respectively just before first common beam splitter (PBS) by using two half wave plates.

This experimental setup can be used for two different polarization configurations of probe and pump lasers beams. One of them is linear and parallel case while the other is same-circular polarization configuration. As discussed above that pump beam is vertically polarized. Now by using half wave plate, the probe beam was also made as vertically polarized which can be checked by using polarimeter. Two separate quarter wave plates with optics axis angle $\varepsilon = 45$ with respect to y-axis are inserted in front of both pump and probe laser beams just before the BS which prepared the right circular polarized pump and probe lasers beams. Both beams are mixed at BS and well overlapped in the vapor cell. At long distance these two beams are separated. The pump beam is blocked while the probe beam is focused on photodiode.

In case of linear and parallel polarization configurations of pump and probe lasers beams, one need to remove only two quarter wave plate from above setup of same-circular polarization configuration. In this case both the beams are vertically polarized which interacts with atoms in the cell. Similarly this setup can also be used in case of circular and orthogonal polarization configuration as well as linear and perpendicular polarization configuration of pump and probe laser beams by changing the optics axis angle of half wave plate and quarter wave plate. But one can get more batter and narrow EIA signal by making some modification in above experimental setup without disturbing main setup. Replacing BS by PBS and inserting two

quarter wave plates just before and after Rb vapor cell. Finally one PBS should be inserted before the photodiode. In this way when vertically polarized control and horizontally polarized probe beams are mixed at first PBS then these two beams look like to be one beam because of very well overlapping. First of all these two beams passed through first quarter wave plate. When the polarization angle of quarter wave plate is set at ε = -45 degree with respect to y-axis, then This arrangement prepared pump beam as left circularly polarized and at the same time initially horizontally polarized probe beam will be right circularly polarized. These two circular and orthogonal pump and probe lasers beams interact with Rb atoms in the cell. Now placing another quarter wave plate after cell at ε =- 45 degree with respect to y-axis will make again control beam as vertical polarized and probe bean as horizontal polarized. These two beams can be separated by placing another PBS after Rb cell. This PBS reflects the vertically polarized pump beam and allow horizontally polarized probe beam to transmit. The transmitted probe beam is detected by photo diode.

Similarly in case of linear and perpendicular polarization configuration we need to remove both quarter wave plates from the setup. In this situation after $1^{st}$ PBS the control beam is vertically polarized while the probe beam is horizontally polarized. When these two well overlapped beams reached at $2^{nd}$ PBS after passing through Rb vapor cell, the vertical pump beam reflected at 90 degree and horizontally polarized probe beam is transmitted. The reflected beam is blocked while the transmitted beam is detected by photodiode.

A ramping voltage of $125mV_{pp}$ (peak to peak) which allow the pump beam

to detune in the range of 5MHz. The intensities of both beams were controlled by two separate neutral density filters (NDF). Maximum power of control beam which is used in this experiment was 1mW while the power of probe beam used here between 10 and 20 μW.

## 5.3 Experimental results

In this part of thesis we explain the theoretical calculated and experimentally observed ultra-narrow EIA signals which are obtained by using experimental setup shown in figure 5.1.

### 5.3.1 Circular polarization case

In case of same circular polarization combination of pump and probe laser fields, the theoretically calculated and experimentally observed probe absorption spectra are shown in Fig 5.2 (a) and (b) respectively. The absorption spectra from the cycling transition line in DTLS of thermal $^{85}$Rb atoms were obtained between -2 MHz and 2 M Hz. To investigate the spectral variations in probe absorption spectra, we changed the power of pump laser beam while the power of probe beam was fixed at constant value

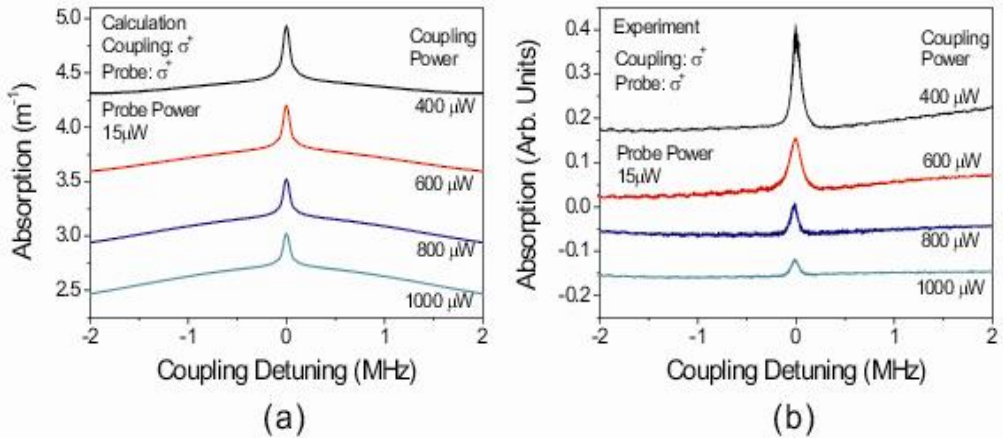


Fig. 5.2 (a) Theoretical and (b) experimental EIA spectra in the case of same circular polarizations of the probe and coupling beams with respect to the changes of pump powers.

Compare to natural linewidth of upper state which is 6.1M Hz the observe linewidth is much narrow. Doppler broadening, laser line linewidth, laser power, decay rate *etc*. are some factors which can affect the linewidth of EIA signal. The experimentally measured linewidth of EIA signal at pump power of 400 μW is approximately equal to 90 kHz while the theoretically calculated linewidth is equal to 87 kHz which show the higher degree of matches between observed and calculated linewidth. Much narrower linewidth of EIA signal can be produced by using laser with linewidth narrow than our case. This EIA spectrum is not split differently from orthogonal circular and linear cases, which the EIA signals are split and broadened when the coupling powers are increased moderately and because of thermal averaging effects there is no splitting in spectra with strong power of pump beam. In case of same polarization of pump and probe beams, there

have been some theoretically predictions about such EIA spectra but no one reported this type of observation in case of same polarization. Only one experimental observation [38] was reported with same polarization configuration but they could not able to produce such ultra-narrow EIA signal and most probably it happened due to high power of pump laser and combined linewidth of two independent lasers sources.

As shown in Fig. 5.2 when the powers of the pump beam increase, the strengths of the EIA signal are decreasing. As explained in detail in chapter 4 the ultra-narrow EIA signal for a stationary atom exists at lower coupling beam power and diminishes with the increased pump beam power. This ultra-narrow signal remains for thermal atoms and also another factor can cause to produce narrow EIA signal. In this case at zero detuning of pump beam the resonance exist irrespective of atomic velocity. Since the slope of the resonance at positive and negative value of the velocity is precisely opposite, a narrow absorption signal can be observed. This effect can only support to produce narrow signal when the power of pump beam is high. That is why the intensity of whole EIA signals decreases as the power of pump beam increases.

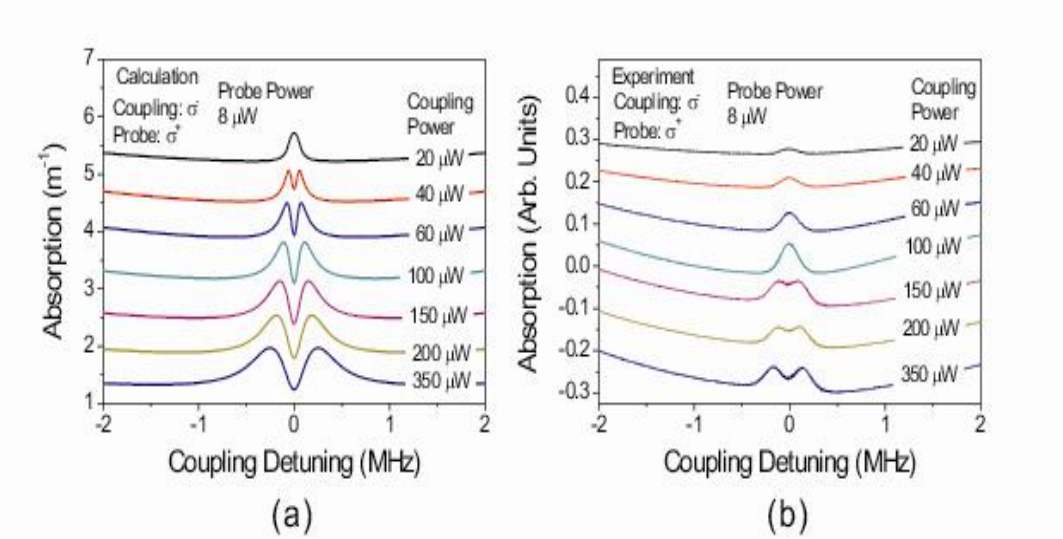


Fig. 5.3 (a) Theoretical and (b) experimental EIA spectra in the case of orthogonal circular polarizations of the probe and coupling beams with respect to the changes of pump powers.

The theoretical calculated and experimentally observed probe absorption spectra between -2 MHz and 2 MHz in case of circular and orthogonal polarization configuration are shown in Fig 5.3 (a) and (b) respectively. Based on theoretical prediction the splitting of EIA signal into two at even sufficient low power of pump beam is due to thermal averaging effect. In chapter 4 as we discussed in detail that in cold atomic case the splitting of EIA signal could not be observed. In splitting of EIA signal the power of pump laser play vital role due to TOC effects. Compare to linear and perpendicular polarization case the splitting in circular and orthogonal case of polarization occur at relatively low power of pump beam. The author of reference [48] also described that TOC effect in case of linear and

perpendicular polarization combination of pump and probe laser can take place in higher pump power than decay rat of upper excited state. The strong pump power can generate Mollow-triplet [59] type splitting lines. But so far there is no any report to observe these ultranarrow splitted resonances due to TOC which provide the linewidth below 100 kHz instead of very wide feature due to power of pump laser. In chapter 4 we have explained the thermal averaging effects on splitting of line due to pump powers between same and perpendicular circular polarization cases by using dressed state formalism. We could not observe the splitting at the central region of resonance line in case of same circular polarization of both beams because absorption resonances due to positive and negative atomic velocities cancel each other. On the other hand at central region in case of orthogonal polarization of pump and probe beams, the ultranarrow split EIA signals exist at $\sim\pm[1-(15/28)^{1/2}]\,\Omega_2$. From these theoretical and experimental investigation and discussion we understand that power dependences of the spectral profiles in the orthogonal- and same- polarization configurations in thermal state are pretty dissimilar from those in cold state. Because of wider linewidth of laser being used in experiment the experimentally observed spectra shown in Fig 5.3 (b) in lower power of pump beam are not splitted well as in case of theoretical calculation shown in Fig. 5.3(a).

## 5.4 Linear polarization cases.

Now we explain our next experimental results which were performed in case of linear polarized of pump and probe beams. The optical pumping effect in linear polarization case is weaker as compare to circular polarization case. As linearly polarized pump beam can cause to exist the atomic

populations at magnetic sub-levels so the theoretical calculation in linear polarization cases are more tedious and complex as compare to circular polarization case. The comparison between calculated and experimentally observed probe spectra in case of same-linear polarization combinations are shown in Fig. 5.4 (a) and (b) respectively

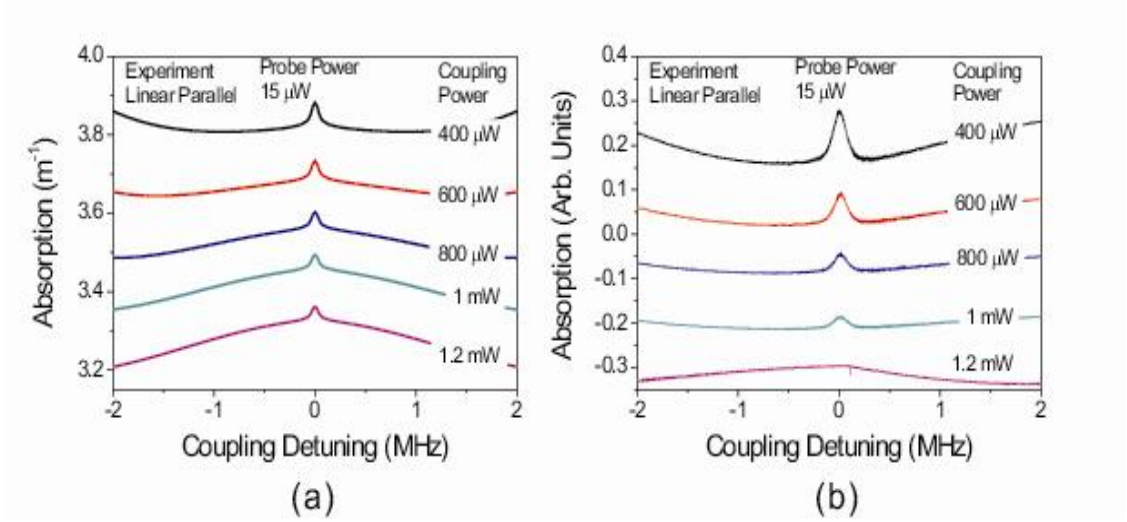


Fig. 5.4 (a) Theoretical and (b) experimental EIA spectra in the case of same linear polarizations of the probe and coupling beams with respect to the changes of pump laser powers.

The observed linewidth of ultra-narrow signals in case of linear polarization is 150 kHz. In case of same polarization, it is interesting to have similar spectra between linear and circular polarization configuration because these two schemes primarily identical except for different transitions strength and population accumulation in circular polarization case. The pump and probe beams tuned to the same transition line and TOP play important role in

generating EIA signals in both cases.

It can be seen from Fig 5.4 (b) that the magnitudes of observed signals are decreasing with the increases of pump powers which show quite similar behavior as in case of same-circular polarization and above 1 mW, the experimental EIA signal disappear. May be in all previous experimental works different researcher groups used high powers of pump and probe lasers in case of same polarization configuration and concluded that in same polarization case N or V-type connection cannot be formed so occurrence of EIA in this case is not possible.

The comparison between theoretically calculated and experimentally observed spectra in case of linear and orthogonal polarization combinations are shown in Fig. 5.5 respectively. With an increase in pump power the subnatural ultranarrow EIA signal become wider and then split into two near 2 mW theoretically as shown in Fig. 5.5 (a) but in case of circular and orthogonal case this splitting start relatively very low power of pump beam. Up to 1 mW we can observe well matched theoretical calculated and experimental observed spectra shown in Fig. 5.5 (a) and (b). Due to some experimental limitations we could not increase the power of pump beam more than 1mW and that is why we could not observe the splitting in experimental spectra which is shown in theoretical calculated one.

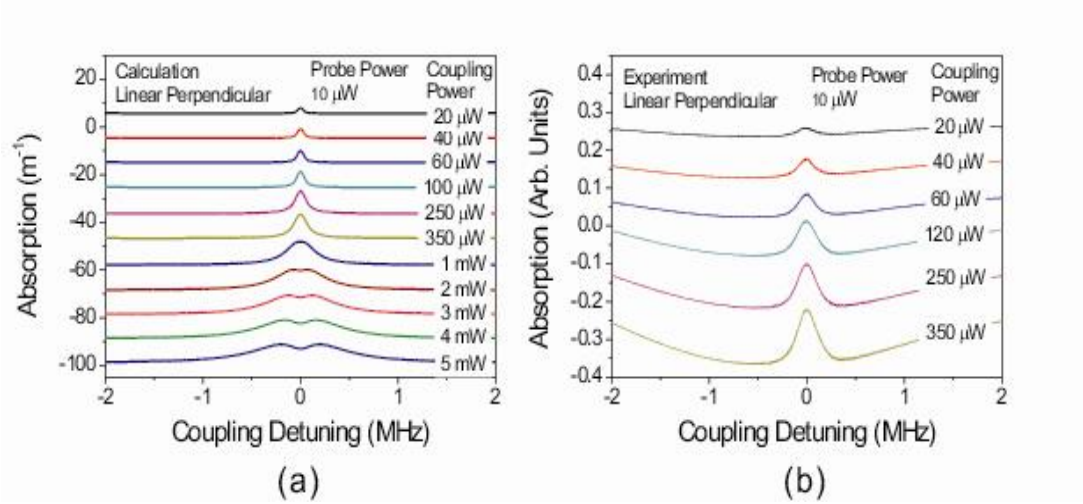


Fig. 5.5 (a) Theoretical and (b) experimental EIA spectra in the case of orthogonal linear polarization configuration with respect to the changes of pump powers.

Compare to circular and orthogonal polarization, the splitting power of pump beam is very high in linear and perpendicular polarization case because the separation of the dressed state for a magnetic sublevel is not quite different from that for closest magnetic sublevel. The separations between the resonances for a stationary atom in the orthogonal linear scheme are 0.024 $\Omega_2$, 0.077 $\Omega_2$, 0.15 $\Omega_2$, and 0.5 $\Omega_2$, while the separation in the orthogonal circular scheme is 0.27 $\Omega_2$. Therefore, we need approximately 10 times larger Rabi frequency in linear scheme than in circular scheme in order to see a similar spacing between the two absorption peaks.

# Chapter 6

## Conclusions

Based on different polarizations combinations, powers and direction of pump and probe laser fields we have shown the variations in probe transmission spectra from hyperfine levels between ground $5S_{1/2}$ and excited $5P_{1/2}$ D2 line of Rb atoms at room temperature using degenerate two-level atomic system. Various polarization dependent profiles in absorption and transmission signal with EIT-like and EIA signal have been observed. We calculate EIA spectra by solving time-dependent full density matrix equations for the transition $F_g = 3 \rightarrow F_e = 4$ of the $^{85}$Rb-D2 line. Compared to the existing calculating methods more accurate EIA spectra can be produced since our method does not employ any phenomenological constants and is based on temporal solutions of the density matrix elements. From this new theoretical method, EIA spectra with ultra-narrow linewidths embedded in broad sub-natural EIA, in the case of the same and orthogonal circular-polarization configurations of coupling and probe lasers have been obtained theoretically.

Thermal averaging effects on spectral features such as additional ultra-narrow and split spectral profiles of EIA embedded in broad sub-natural EIA have been investigated with respect to powers of coupling beam. The EIA signals have ultra-narrow EIA signals in low powers of coupling and probe laser beams in both same- and orthogonal-polarization configurations irrespective of thermal averaging of the EIA signals. However, the ultra-narrow EIA signals from high powers of coupling laser beams in the same-

polarization configuration have disappeared and still remained in the ultra-narrow state in zero velocity and thermal averaging cases, respectively. The ultra-narrow EIA signals in the orthogonal-polarization configuration from high powers of coupling laser beam have disappeared and split into two in zero velocity and thermal averaging cases, respectively. Origins of the existence of ultra-narrow EIA spectra and splitting of the ultra-narrow EIA spectra under high power and thermal averaging have been revealed. The observed EIA spectral profiles of probe transmission for the case of same- and orthogonal-polarization configurations of coupling and probe laser beams match well with the calculated spectral profiles of probe transmission. We also confirm coherent effects in EIAs by checking the differences between probe-transmission profiles with and without coherence terms of density matrix elements in the density matrix equations, which elucidates in detail the EIA spectral-line profiles according to laser detuning.

We observe strange behaviors of observed EIA signals depending on circular and linear polarizations and power variations of the coupling and probe lasers. The EIA signals with sub-natural linewidth of ~ 90 kHz even in the cases of same circular and linear polarization configuration have been obtained for the first time to the best of our knowledge. Ultra-narrow splittings of EIA spectra with the increase of the laser powers in the case of orthogonal polarization were obtained. EIA signal was decreased in the case of same polarization case with the increase of coupling powers due to TOP. In weak coupling power limit of orthogonal polarization configurations, thermal averaging effects plays major role in the splitting of the EIA spectra while in strong coupling power, Mollow triplet-like mechanism due to strong

power bring into broad split feature. The experimental ultra-narrow EIA features using one laser combined with an AOM match well with simulated spectra obtained by using generalized time-dependent optical Bloch equations.

# References

[1] A. M. Akulshin, S. Barreiro and A. Lezama, "Electromagnetically induced absorption and transparency due to resonant two-field excitation of quasi degenerate levels in Rb vapor," Phys. Rev. A **57**, 2996-3002 (1998).

[2] A. Lezama, S. Barreiro and A. M. Akulshin, "Electromagnetically induced absorption," Phys. Rev. A **59**, 4732 -4735 (1999).

[3] H. Failache, P. Valente, G. Ban, V. Lorent and A. Lezama, " inhibition of electromagnetically induced absorption due to excited-state decoherence in vapor cell," Phys. Rev. A **67**, 043810-043817 (2003).

[4] I. B. Aroya and G. Eisenstein, "Observation of large contrast electromagnetically induced absorption resonance due to population transfer in a three level Λ-system interacting with three separate electromagnetic fields," Opt. Express **19**, 9956-9961(2011).

[5] S. R. Chanu, K. Pandey and V. Natarajan, "Conversion between electromagnetically induced transparency and absorption in a three-level lambda system," Euro. Phys. Lett. **98**, 44009-44015 (2012).

[6] X. Yang, J. Sheng and M. Xiao, "Electromagnetically induced absorption via incoherent collisions," Phys. Rev. A **84**, 043837-043842 (2011).

[7] H. J. Kim and H. S. Moon, "Electromagnetically induced absorption with sub-kHz spectral width in a paraffin-coated Rb vapor cell," Opt. Express **19**, 168-173 (2011).

[8] F. Fleischhauer, A. Imamoglu and J. P. Marangos, "Electromagnetically induced transparency: Optics in coherent media," Rev. Mod. Phys. **77**,

633-673 (2005)

[9] Y. Wu and X. Yang, "Highly efficient four-wave mixing in double-Λ system in ultraslow propagation regime," Phys. Rev. A **70**, 053818-053823 (2004).

[10] Y. Wu and X. Yang, "Electromagnetically induced transparency in V-, Λ-, and cascade-type schemes beyond steady-state analysis," Phys. Rev. A **71**, 053806 – 053813 (2005)

[11] M. D. Lukin, "Trapping and manipulating photon states in atomic ensembles," Rev. Mod. Phys. **75**, 457-472(2003).

[12] K. HaAmmerer, A. S. Sørensen and E. S. Polzik, "Quantum interface between light and atomic ensembles," Rev. Mod. Phys. **82**, 1041 - 1093(2010)

[13] A. M. Akulshin, A. Cimmino, A. I. Sidorov, P. Hannaford and G. I. Opat, "Light propagation in an atomic medium with steep and sign-reversible dispersion," Phys. Rev. A **67**, 011801(R) -011805(R) (2003).

[14] A. Lezama, A. M. Akulshin, A. I. Sidorov and P. Hannaford, "Storage and retrieval of light pulses in atomic media with "slow" and "fast" light," Phys. Rev. A **73**, 033806- 033810(2006).

[15] S. R. Chanu, A. K. Singh, B. Brun, K. Pandey and V. Natarajan, "Subnatural linewidth in strongly-driven degenerate two-level system," Opt. Commun. **284**, 4957-4960 ( 2011).

[16] J. Dimitrijević, A. Krmpot, M. Mijailović, D. Arsenović, B. Panić, Z. Grujić and B. M. Jelenković, "Role of transverse magnetic fields in electromagnetically induced absorption for elliptically polarized light," Phys. Rev. A **77**, 013814-013826 (2008).

[17] F. Renzoni, C. Zimmermann, P. Verkerk and E. Arimondo, "Enhanced absorption Hanle effect on the $F_g = F \rightarrow F_e = F + 1$ closed transitions," J. Opt. B: Quantum Semiclass. Opt. **3** S7-14 **(**2001).

[18] S. M. Iftiquar**,** G. R. Karve , and V. Natarajan, "Subnatural linewidth for probe absorption in an electromagnetically induced transparency mediumdue to Doppler averaging," Phys. Rev. A **77,** 063807- 063812 (2008).

[19] M.M. Hossain, S. Mitra, B. Ray, and P.N. Ghosh, "Double EIT and enhanced EIT signal in a combination of Λ- and V-type system of Rb-$D_2$ transition," J. Phys B: At. Mol. Opt. Phys. **103**, 117-122 (2010).

[20] S. R. Chanu, K. Pandey, and V. Natarajan, "Conversion between electromagnetically induced transparency and absorption in a three-level lambda system," EPL **98**, 44009-44015 (2012).

[21] H. J. Lee and H. S. Moon, "Intensity correlation and anti-correlation in electromagnetically induced absorption," Opt. Express **21**, 2414-2422 (2013).

[22] X. Yang, J. Sheng, and M. Xiao, "Electromagnetically induced absorption via incoherent collisions," Phys. Rev. A **84**, 043837-043841 (2011).

[23] H. U. Rehman, M. Adnan, H.-R. Noh, and J. T. Kim, "Spectral features of electromagnetically induced absorption in $^{85}$Rb atom," J. Phys. B. **48**, 115502-115511 (2015).

[24] R. Drampyan, S. Pustelny, and W. Gawlik, "Electromagnetically induced transparency versus nonlinear Faraday effect: Coherent control of light-beam polarization," Phys. Rev. A **80,** 033815-033824 (2009).

[25] Z. J. Ming, Z. Y. Ting, H. Tao, X. L.Tuan and J. S. Tang, "Observation of EIA in closed and open cesium atomic system," Chin. Phys.soc. **14,** 725-728 (2005)

[26] P. M. Anisimov, J. P. Dowling, and B. C. Sanders, "Objectively Discerning Autler-Townes Splitting from Electromagnetically induced transparency," Phys. Rev. Lett. **107**, 163604-63608 (2012).

[27] C. Andreeva, S. Cartaleva, Y. Dancheva, V. Biancalana, A. Burchianti, C. Marinelli, E. Mariotti and L. Moi, "Coherent spectroscopy of degenerate two-level systems in Cs," Phys. Rev. A **66**, 012502-012514 (2002).

[28] A. Lezama, S. Barreiro, A. Lipsich and A. M. Akulshin, "Coherent two-field spectroscopy of degenerate two-level systems," Phys. Rev. A **61**, 013801-013812 (1999).

[29] T. Zigdon, A. D. W-Gordon, and H. Friedmann, "Pump-probe spectroscopy in degenerate two-level atoms with arbitrarily strong fields," Phys. Rev. A **77**, 033836- 033846 (2008).

[30] S. K. Kim, H. S. Moon, K. Kim and J. B. Kim, "Observation of electromagnetically induced absorption in open systems regardless of angular momentum," Phys. Rev. A **68**, 06813-06818 (2003).

[31] H. S. Chou and J. Evers, "Dressed-atom multiphoton analysis of anomalous electromagnetically induced absorption,"Phys. Rev. Lett.

**104**, 213602- 213604 (2010).

[32] A. Lezama, G. C. Cardoso and J. R. Tabosa, "Polarization dependence of four-wave mixing in a degenerate two-level system," Phys. Rev. A **63**, 013805-013812 (2000).

[33] A. Akulshin, M. Singh, A. sidrovo and P. Hannaford, "steep atomic dispersion induce induced by velocity-selective optical pumping," Opt. Exp. **29**, 15463-15468 (2008).

[34] C. Goren, A. D. W. Gordon, M. Rosenbluh and H. Friedmann, "Atomic four-level N system," Phys. Rev. A **69**, 053818-053828 (2004).

[35] A. Lezama, S. Barreiro, and A. M. Akulshin, "Electromagnetically induced absorption," Phys. Rev. A 59, 4732-4735 (1999).

[36] D. V. Brazhnikov. A. M. Tumaikin, and V. I. Yudin "Electromagnetically induced absorption and tranperency in magneto optical resonances in ellipitically polarized field," Opt. Sco. Am. B **22**, 010057-010064(2005).

[37] M. Kwon, K. Kim, H. D. Park, and J. B. Kim, "Dependence of EIA spectra on mutual coherence between pump and probe fields in Cs atomic vapors," J. Kor. Phys. Soc. **40**, 452-455 (2002).

[38] A. Lipsich, S. Barreiro, A. M. Akulshin, and A. Lezama, "Absorption spectra of driven degenerate two-level atomic systems," Phys. Rev. A **61**, 053803-053813 (2000).

[39] Y. C. Chen, I. A. Yu, "*The coherence induced phenomena in cold atom,"* (Tsinghua University,) 2002

[40] K. J. Boller, A. Imamoglu and S. E. Harris, " Observation of

electromagnetically induced transparency, “ Phys. Rev. Lett. **66**, 2593-2596 (1991).

[41] K. Dahl, L. S. Molella, R.H. Rinkleff, and K. Danzmann, “Switching from “absorption within transparency” to “transparency within transparency” in an electromagnetically induced absorption dominated transition,” Opt. Lett. **33** (9), 983-985 (2008).

[42] Z. Y. Ting, Z. J. Ming, X. L. Tuan, Y. W. Bao and J. S.Tang, “Electromagnetically induced absorption and transparency spectra of degenerate tow-level system with a strong coupling field in Cs vapor,” Chin. Phys. Lett. **21**, 76-78 (2004).

[43] A. D. W-Gordon and H. Friedmann ,“Ultranarrow extraresonant antiholes in pump–probe spectroscopy induced by inelastic collisions,” Opt. Lett. **14**, 390 -392 (1989).

[44] V. S. Letokhov and V. P. Chebotayev,” Nonlinear Laser Spectroscopy”, (Springer Series in Optical Sciences) **4**, 80-83 (1977).

[45] A. V. Taichenachev, A. M. Tumaikin, and V. I. Yudin, “Electromagnetically induced absorption in a four-state system,” Phys. Rev. A **61**, 011802-011806 (1999).

[46] C. Goren, A. D. W-Gordon, M. Rosenbluh, and H. Friedmann, “Electromagnetically induced absorption due to transfer of population in degenerate two-level system,” Phys. Rev. A **70**, 043814-043822 (2004).

[47] C. Goren, A. D. W. Gordon, M. Rosenbluh and H. Friedmann, "Electromagnetically induced absorption due to transfer of coherence and to transfer of population," Phys. Rev. A **67**, 033807-033815 (2003).

[48] T. Zigdon, A. D. Wilson-Gordon, and H. Friedmann, "Absorption spectra for strong pump and probe in atomic beam of cesium atoms," Phys. Rev. A **80**, 033825-033834 (2009).

[49] H. S. Moon, L. Lee, and J. B. Kim, "Double resonance optical pumping effects in electromagnetically induced transparency," Opt. Express **16**, 12163-12167 (2008).

[50] C. G. Aminoff, M. Pinard, "Velocity selective optical pumping" J. Physique **43**, 263-277 (1982).

[51] S. J. Park, H.S. Lee, H. Cho, and J. D. Park,"velocity selective optical pumping spectroscopy of 87Rb D2 line by using two co-propagating laser beams," J. Kor. Phys. Soc. **33,** 281-287 (1998).

[52] S.Chakrabarti, A. Pradhan, B. Ray and P. N. Ghosh. "Velocity selective optical pumping effects and electromagnetically induced transparency for D2 transitions in rubidium," J. Phys. B: At. Mol. Opt. Phys. **38** 4321-4327 (2005).

[53] S. Chakrabarti, B. Ray and P. N. Ghosh. "Velocity selective optical pumping effects with counter and co-propagating laser radiation for D2 line of rubidium," Eur. Phys. J. D. **42**, 359-368 (2007).

[54] A. J. Krmpot, M.D. Rabasvic, and B.M. Jelenkovic, "Optical pumping

spectroscopy of Rb vapor with co-propagating laser beams: line identification by a simple theoretical model," J. Phys. B: At Mol. Opt. Phys. **43,** 135402-135409 (2010).

[55] S. Mitra, M.M Hossain, B. Ray, P. N Ghosh, S Cartaleva, D. Slavov, "Coherent laser spectroscopy of rubidium atoms," Laser phys. Application SPIE.**7747**, 77470-77479 (2011).

[56] D. Bhattacharyya, A. Bandyopadhyay, S. Chakrabarti, B. Ray, P. N. Ghosh, "Velocity dependent pump-probe spectroscopy for a five-level system: An application to Rb D2 transitions," Chem. Phys. Lett **440**, 24-30 (2007).

[57] S. Chakrabarti, A. Pradhan, A. Bandyopadhyay, A. Ray, B. Ray, N. Kar, P.N. Ghosh, "Velocity-selective resonance dips in the probe absorption spectra of Rb D2 transitions induced by a pump laser," Chem. Phys. Lett. **399**, 120-124 (2004**).**

[58] A. Krasteva, B. Ray, D. Slavov, P. Todorov, P. N. Ghosh, S. Mitra, and S, Cartaleva, "Observation and theoretical simulation of electromagnetically induced transparency and enhanced velocity selective optical pumping in cesium vapor in a micrometric thickness optical cell," J. Phys. B: At Mol. Opt. Phys. **47,** 175004 -175016 (2014).

[59] B. R. Mollow, "Stimulated Emission and Absorption near Resonance for Driven Systems," Phys. Rev. A **5**, 2217-2222 (1972).

[60] H. R. Noh and W. Jhe,"Semi classical theory of sub-Doppler forces in an asymmetric magneto-optical trap with unequal laser detuning," Phys.

Rev. A **75**, 053411-053420 (2007).

[61] J. Sagle, R. K. Namiotka and J. Huennekens, "Measurement and modelling of intensity dependent absorption and transit relaxation on the cesium D1 line," J. Phys. B: At. Mol. Opt. Phys. **29**, 2629-2643 (1996).

[62] F. Renzoni, W. Maichen, E. Windholz and E. Arimondo, "Coherent population trapping with losses observed on the Hanle effect of the D1 sodium line," Phys. Rev. A **55,** 3710-3718 (1997).

# Acknowledgements

Completing this work has been one of the biggest challenges of my life and I must say that I cannot have got through this without helps of every single person which I mention below. I would like to take this opportunity to pay thanks to all these people who have helped me and given me encourage in making this thesis possible.

First of all I would like to express my gratitude and deep appreciation to my advisor, professor Jin-Tae Kim for his matchless support, valuable discussion, and guidance during all stages of my Ph.D studies.

I would like to thank my parents for their constant support especially to my mother who passed away during my PhD study. I am very thankful to my brothers, Shajahan and Aziz ur Rehman for their support and encouragement. Besides all these I am very thankful to my beloved wife for her efforts with my little loving daughter Rida Fatima in my absence and I really appreciate her efforts. It has been a great opportunity for me to do my research in the laser application lab, Chosun University in Korea. During this study I have really enjoyed the group meetings and discussions with my advisor professor Jin-Tae Kim, Muhammad Adnan, and Muhammad Mohsin Qureshi to boost up my knowledge about atomic physics and laser spectroscopy.

I have received the enormous support from professor Heung-Ryoul Noh in Chonnam National University in Korea and I also express my gratitude to him. It was great pleasures for me to do work with previous and present students in a dark laboratory under the supervision of my advisor.

Finally I would like to thank my professors in Pakistan Dr. Muhammad

Khalid and Dr. Noor Abas Din for their engorgements and supports.